STRUCTURAL ANALYSIS OF THE PERDIDO FOLD BELT: TIMING, EVOLUTION, AND STRUCTURAL STYLE

A Thesis

by

TROY DALE WALLER, II

Submitted to the Office of Graduate Studies of
Texas A&M University
in partial fulfillment of the requirements for the degree of

MASTER OF SCIENCE

May 2007

Major Subject: Geology

STRUCTURAL ANALYSIS OF THE PERDIDO FOLD BELT: TIMING, EVOLUTION, AND STRUCTURAL STYLE

A Thesis

by

TROY DALE WALLER, II

Submitted to the Office of Graduate Studies of
Texas A&M University
in partial fulfillment of the requirements for the degree of

MASTER OF SCIENCE

Approved by:

Chair of Committee,	John H. Spang
Committee Members,	Arnold H. Bouma
	Walter B. Ayers
Head of Department,	John H. Spang

May 2007

Major Subject: Geology

ABSTRACT

Structural Analysis of the Perdido Fold Belt: Timing, Evolution, and Structural Style. (May 2007)

Troy Dale Waller, II, B.S., Texas A&M University

Chair of Advisory Committee: Dr. John H. Spang

The Perdido fold belt is the compressional toe of the complex system of detached structures in the western Gulf of Mexico. Located in the Alaminos Canyon protraction area in ultra deep-water, this extensive fold belt has the potential to accommodate large amounts of hydrocarbons. These folds detach upon Jurassic-age Louann salt, and are northeast-southwest trending and symmetrical to asymmetrical. The lower units in these folds are comprised of mostly carbonates and limy carbonate mud, whereas the upper portion consist of fine grained and muddy siliciclastics which are typical of turbidite and other typical deep water deposits. 2-D, prestacked, depth-migrated seismic data (TGS Phase 45) was interpreted in conjunction with Hess Corporation to determine the geometry and timing of the folds outboard of the allochthonous Sigsbee salt nappe. The interpretation of the seismic data consisted of evaluating the folds by mapping age-dated reflections and kink-band boundaries (fold axial surfaces), along with creating isochores and dip maps. Through the development of new geometric model building of excess areas, which identifies material being added to the cores of the anticlines, along with the extensive seismic interpretation, the Perdido fold belt is identified to have originated in the west as early as the early Paleocene, with some continual fold growth to near present

day. The folds in the Perdido fold belt continue to form eastward into the basin, up to the basinward limit of the autochthonous Louann salt. Also, it has been determined that the geometries and structural styles of the folds are partially dependent on the type of sediment or rock type in place. The lower portions consisting of the carbonates give shallower dipping fold axial surfaces, whereas the upper portions (siliciclastics) provide more steeply dipping fold axial surfaces.

DEDICATION

To my parents Troy D. and Becky Waller,

my wonderful wife Nichole,

and my high school geology teacher, Mrs. Jenny Perry

ACKNOWLEDGMENTS

First I would like to thank Nichole Waller, my wife and my best friend. The speedy completion of this thesis would not have been possible without all of your love, understanding, support and encouragement. I would also like to thank both my parents, Troy and Becky, along with my in-laws Brent and Paula Wade for all of their love and support throughout this endeavor.

I would also like to express my gratitude to my advisory committee: Drs. John Spang (chair), Arnold Bouma (member) and Walt Ayers (member). I truly appreciate all of the feedback throughout the different stages of this work. I would like to sincerely thank my chair Dr. John Spang for his constant support and genuine interest in my research. Through his actions and teachings, he taught me that sometimes you have to step up and work hard in life for things that matter to you.

Many thanks to Bill Kilsdonk, Pam Parks, and Jim McCarthy at Hess Corporation for not only the financial support during the summers of 2005 and 2006, but also for the availability of the seismic data set used in this thesis. Bill Kilsdonk took time to mentor me, and provide very influential insights into this work. Also, I would like to thank TGS for allowing me to use their Phase 45 2-D seismic data in this thesis.

I again would like to thank the teachers and professors that have encouraged me to pursue my interest in Geology. I thank Mrs. Jenny Perry, who was the first to ignite this curiosity in me. It is rare to find a teacher that cares about her students and loves the subjects that she teaches as much as she does. It is very much appreciated! Dr. Tom Olszewski for his passion and enthusiasm for teaching which has inspired me to want more. Dr. Michael Heaney for his free spirit and willingness to help me learn whether in the field or during studies of West Texas tepee structures. Drs. Fred and Judi Chester, who genuinely cared about my well-being and encouraged me to think deeper and harder. And again, I would like to thank Dr. John Spang, who introduced me to the realm of structural geology, which has become the interest and focus of my geologic studies.

Additional financial support for my graduate studies were generously provided by Chevron and Michel T. Halbouty fellowships, along with teaching assistantships, all through the Department of Geology and Geophysics at Texas A&M University. I also received valuable funding from the Tom Hillin scholarship through the College of Geosciences at Texas A&M University.

I would also like to acknowledge all of my friends and colleagues, both students and faculty in the Center for Tectonophysics. The office staff of the Department of Geology and Geophysics has also provided assistance that is much appreciated.

TABLE OF CONTENTS

LIST OF TABLES

Page

LIST OF FIGURES

Page

Page

Page

CHAPTER I

INTRODUCTION

BACKGROUND

Study Area

The study area examined is part of the Perdido fold belt (PFB), located in the Alaminos Canyon protraction area, which is in the ultra deep-water of the northwestern Gulf of Mexico (Figure 1). The Perdido fold belt is partially located in Mexican waters; therefore, only data of the U.S. portion of the fold belt could be studied. The Perdido fold belt is in approximately 6,000 to 9,000 ft (2,000 to 3,000 m) water depth, at the U.S./Mexico border and nearly due south of Houston and Galveston, Texas. In the study area, the PFB consists of eight compressional, salt-cored, kink-style, detachment folds overlaying Jurassic age Louann salt. All of the folds examined in this study are outboard of the allochthonous salt sheets of the Sigsbee salt nappe (Figure 2). Due to poor seismic resolution, the folds under the salt canopies cannot be resolved. In general, the folds strike northeast-southwest, with some variations, and are symmetric to asymmetric. In addition, there are three fold features that are more domal in nature and will require further investigation outside the scope of this thesis.

This thesis follows the style and format of the AAPG Bulletin.

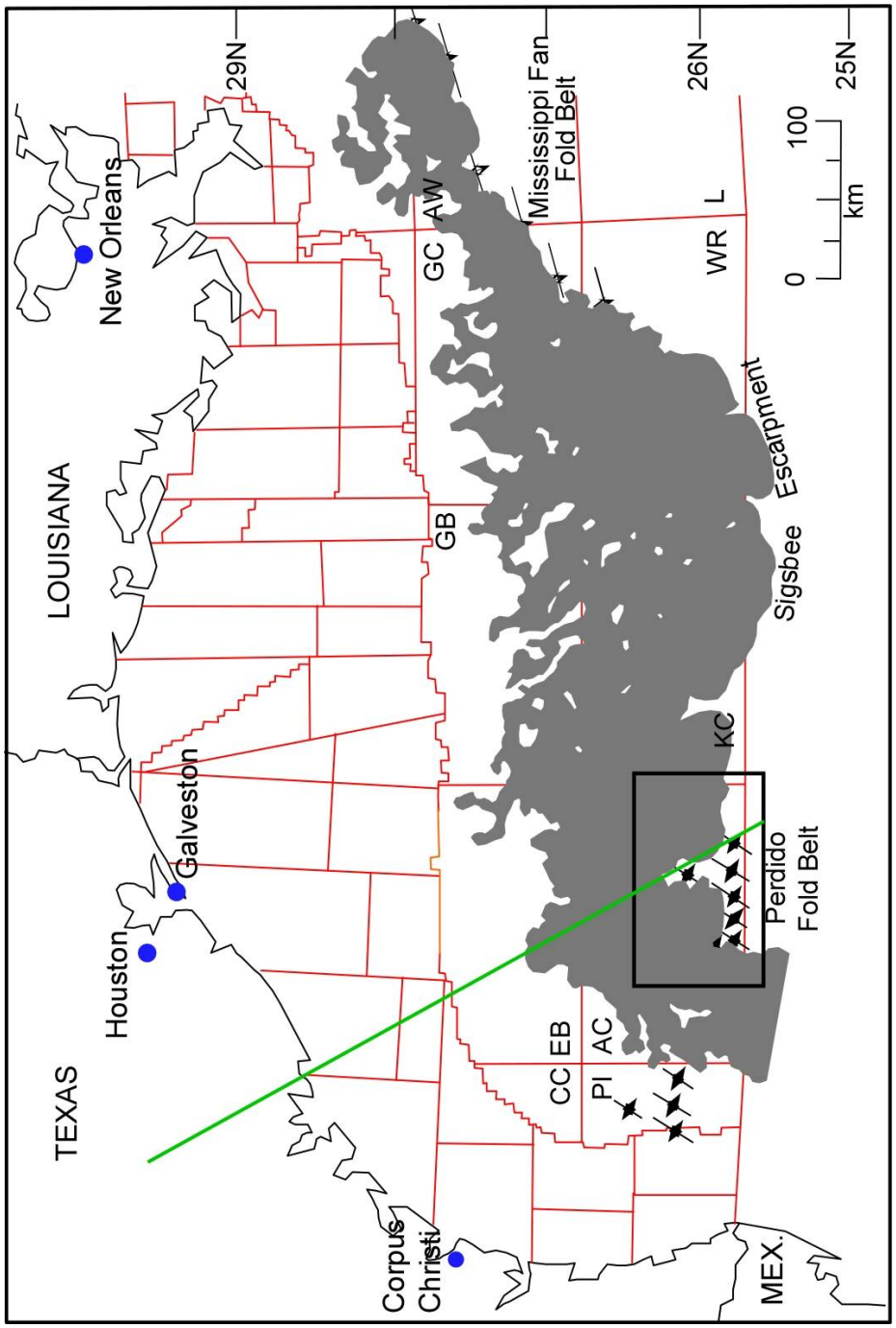

Figure 1: Regional view of Gulf of Mexico. Outlined is the coast of Texas and Louisiana. In red is shown the boundaries of the protraction areas. The general extent of the allochthonous salt is shown in dark gray. Perdido Fold belt study area is outlined with a box. AC=Alaminos Canyon; AW=Atwater Valley; CC=Corpus Christi; EB=East Breaks; GB=Garden Banks; GC=Greens Canyon; KC=Keathly Canyon; L=Lund; PI=Port Isabel; WR=Walker Ridge. Modified from Trudgill et al. (1999). Cross sectional line (in green) used in figure 9.

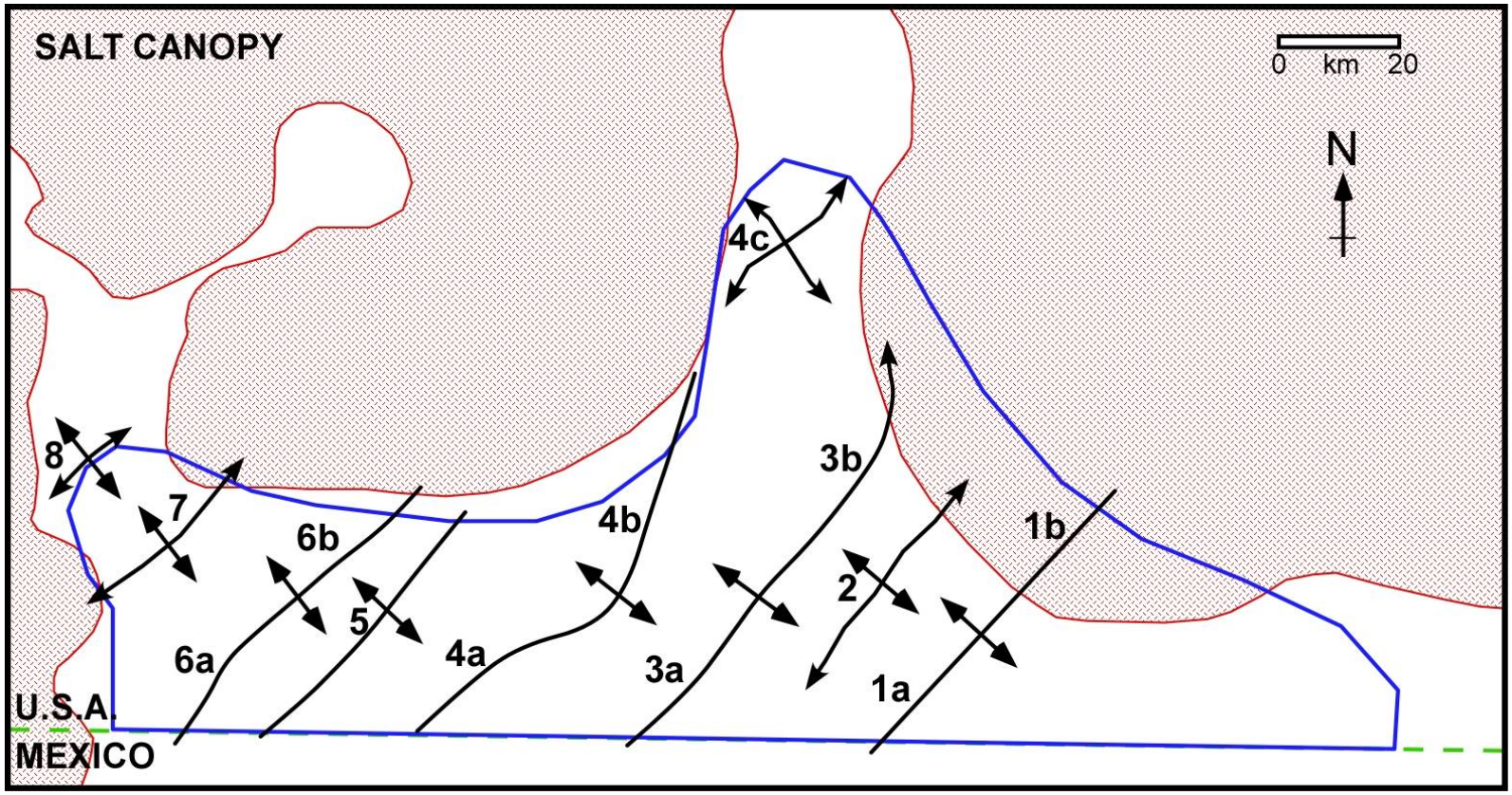

Figure 2: Study area close-up showing fold axis/culminations and nomenclature. The PFB is located in the SE corner of the Alaminos Canyon protraction area. Red-hashed polygons represent the canopy of the Sigsbee salt nappe. The border between U.S.A. and Mexico is shown with a green dashed line. The blue outline represents the area in which TGS Phase 45 2-D psdm data was interpreted for this thesis. Locations of the folds are represented with the black lines. Individual folds within the train are numbered, with fold culminations indicated by lower case letters. Fold nomenclature follows that of Camerlo and Benson, 2006.

Motivation

Fold closures on the fold culminations within the PFB area exceed 55,000 acres, making them some of the largest anticlines in a proven hydrocarbon province in North America (Camerlo and Benson, 2006). With increasing petroleum prices, the ability to explore for and produce hydrocarbons in ultra deep-water wells has become economically feasible. Several wildcat wells have been drilled in the study area, with some success. At this point, most of this well data is still proprietary. The purpose of this study is to illuminate the problems, geometries, mechanisms and timing associated with the formation of these folds.

Data Base

The seismic data were interpretated during the summer of 2006, while the author was employed by Hess Corporation. During that time, computer workstations were used to integrate and interpret the data. Schlumberger's IESX Geoframe® software was used to interpret and manipulate seismic data, and well-log information was examined on both Linux and UNIX operating systems.

Seismic data are owned by TGS-NOPEC, all images of the data have been reproduced with their written permission. The data used in this study is a 2-D prestacked depth-migrated data set (TGS Phase 45) that was chosen because these lines are regionally longer than the lines of available 3-D data sets. These longer lines show multiple structures and will ultimately aid in the structural analysis of these folds. The seismic

grid used is oriented northwest-southeast (inlines) and northeast-southwest (crosslines). The twenty-seven inlines used are oriented nearly parallel to dip (approximately 518 miles/834 km total), and the 30 crosslines are oriented near parallel to strike (approximately 507 miles/817 km total). These data represent all of the 2-D seismic lines available in the study area (Figure 3). The approximate total length of seismic lines interpreted is 1,026 miles (1,651 km). All line numbers and shotpoint references were removed from the displays, along with all depth markers. An approximate horizontal and vertical scale is provided on all seismic displays.

Research Objective

Initially, the seismic interpretation was manipulated to produce depth-structure maps, dip maps along with isopach maps, all of which aid in the interpretation of the overall fold histories. This study takes the seismically imaged and interpreted data of the Perdido fold belt, and applies excess area to depth of detachment calculation techniques developed by Epard, Groshong, Mitra, Spang and many others to determine timing and evolution of the structural styles. Additionally, following the techniques of Groshong and Epard (1994), the requisite strain and line length changes of the interpreted horizons are evaluated.

PREVIOUS STUDIES

To date in the western hemisphere, the Gulf of Mexico (GOM) has become one of the

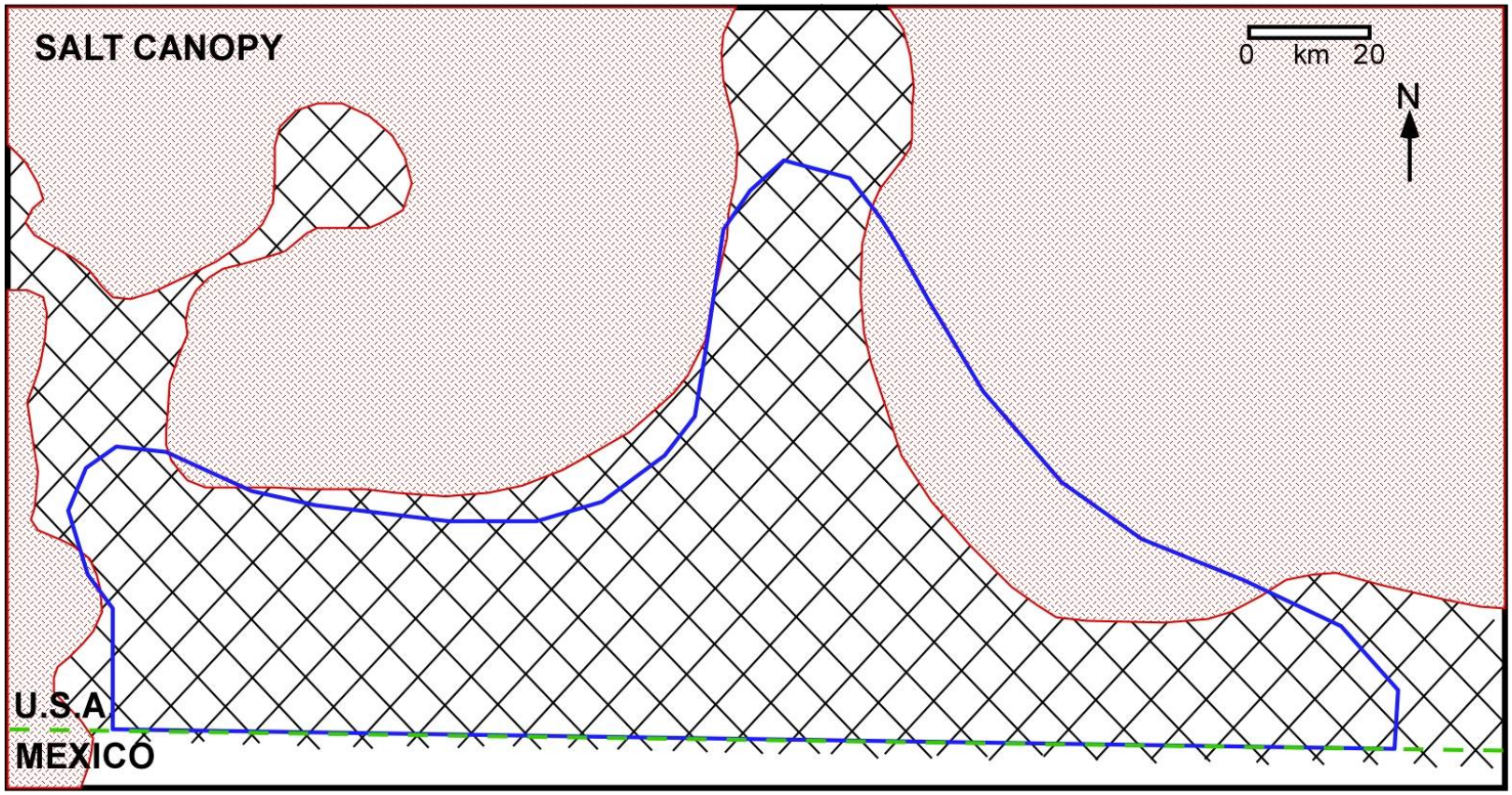

Figure 3: TGS Phase 45 2-D psdm seismic data set availability. Black grid represents the location of the seismic lines available in the interpretation of this thesis. Shading represents the present day location of allochthonous salt.

most important petroleum provinces, and recently the finding of hydrocarbons in the ultra-deep water has enhanced interest in this area. The PFB is located in the northwestern GOM, which has been studied extensively both sedimentologically and structurally (Hazzard et al., 1947; Jackson and Seni, 1983; Salvador, 1987; Worrall and Snelson, 1989; Huh et al., 1996; Watkins and Buffler, 1996; Watkins et al., 1996; Winker, 2004; and many others). With the advent of newer methods of acquisition and processing of seismic data, the resolution of the structures in the study area has become much clearer.

Many previous workers have discussed the structural style of the PFB (Trudgill et al., 1995, 1999; Fiduk et al., 1997, 1999; Fiduk, 1999; Spang, 1999; Camerlo and Benson, 2001, 2006; Mitra, 2002; Rowan et al., 2004; and many others). Comprehensive studies of the PFB are relatively young, dating back to only about the last ten years, although limited information can be found as old as Bryant et al. (1968), who first discovered the PFB by observing a series of linear submarine ridges at the seafloor when completing bathymetric profiles. Since this time, several different geologic and geometric models have been presented for the origin of the PFB.

Based upon seismic, gravity and other data sets, Trudgill et al. (1999) determined that the PFB overlies rifted transitional crust characterized by northeast-southwest-trending basement highs and northwest-southeast transverse structures (transfer faults), also described by Huh et al. (1996). These transfer faults not only affect the amount of

original salt in place, but additionally offsets synrift basins and fault trends and also effect the nature of faulting (Huh et al., 1996). This original basement geometry could also affect the geometry of the autochthonous salt that was deposited. Trudgill et al. (1999) define the folds as symmetrical to asymmetrical anticlines that trend northeast-southwest, with concentric folds usually bounded on both flanks by steep reverse faults, and are a minimum of 31 miles (50 km) in length in the US part of the fold belt. The fold belt continues into Mexican waters at least 62 miles (100 kilometer). The issue of the folds being bounded on the flanks by reverse faults is a current topic of debate. This research supports the work of Camerlo and Benson (2001, 2006), where the authors give adequate geophysical support for unfaulted, steeply dipping fold limbs rather than high angle reverse faults. The steeply dipping, unfaulted fold limbs can be easily resolved at these great depths using modern seismic techniques (Camerlo and Benson, 2006; and this study).

Tectonic and sedimentation history

The following is an overview of the tectonic and sedimentation history of the area based upon the works of previous authors.

Mesozoic Era

The Gulf of Mexico basin developed during the Mesozoic when North America separated from South America (Late Triassic-Early Jurassic) during the breakup of the supercontinent Pangea. At this time, there was extensive rifting and crustal attenuation,

during which time there were terrestrial synrift deposits known as the Triassic Eagle Mills Formation (Worrall and Snelson, 1989). Salvador (1987) defined these sediments to be red, reddish-brown, purplish, greenish-gray or mottled shales, mudstones and siltstones with lesser amounts of sandstones and conglomerates. These thick non-marine sequences formed along linear trends related to rift basins. Salvador (1987) also has listed occurrences of volcanic activity, such as diabase, basalt dikes and sills (Figures 4A, 4B). This package of sediments filled tensionally deformed grabens, half grabens and rift valleys. Alluvial fans originated from the top of the uplifted (horst) blocks.

Late Triassic to Late Jurassic (? – 161 Ma): Synrift Deposits

Worrall and Snelson (1989) also define the late Triassic to mid Jurassic as a time of broad regional subsidence with associated widespread marine incursions, which deposited a thick layer of evaporates. This is the time of the deposition of the Louann salt (Callovian) that is interpreted to core the anticlines in the Perdido fold belt (Trudgill et al., 1999). Hazzard et al. (1947) defined the salt to be halite with minor amounts of anhydrite. The original estimated salt thickness in the East Texas province, as inferred by Jackson and Seni (1983), is between 5,000 ft (1,500 m) and 7,000 ft (2,100 m). Differing amounts of original salt in place could vary due to the Matagorda transfer fault described by Huh et al. (1996). This transfer fault probably formed along preexisting shear zones (transform faults) during rift-stage extension (Huh et al., 1996). The depositional limit of the Louann is found immediately basinward of the PFB, thus acting as a sort of pin, which limits the basinward translation of overlying sediments. After the

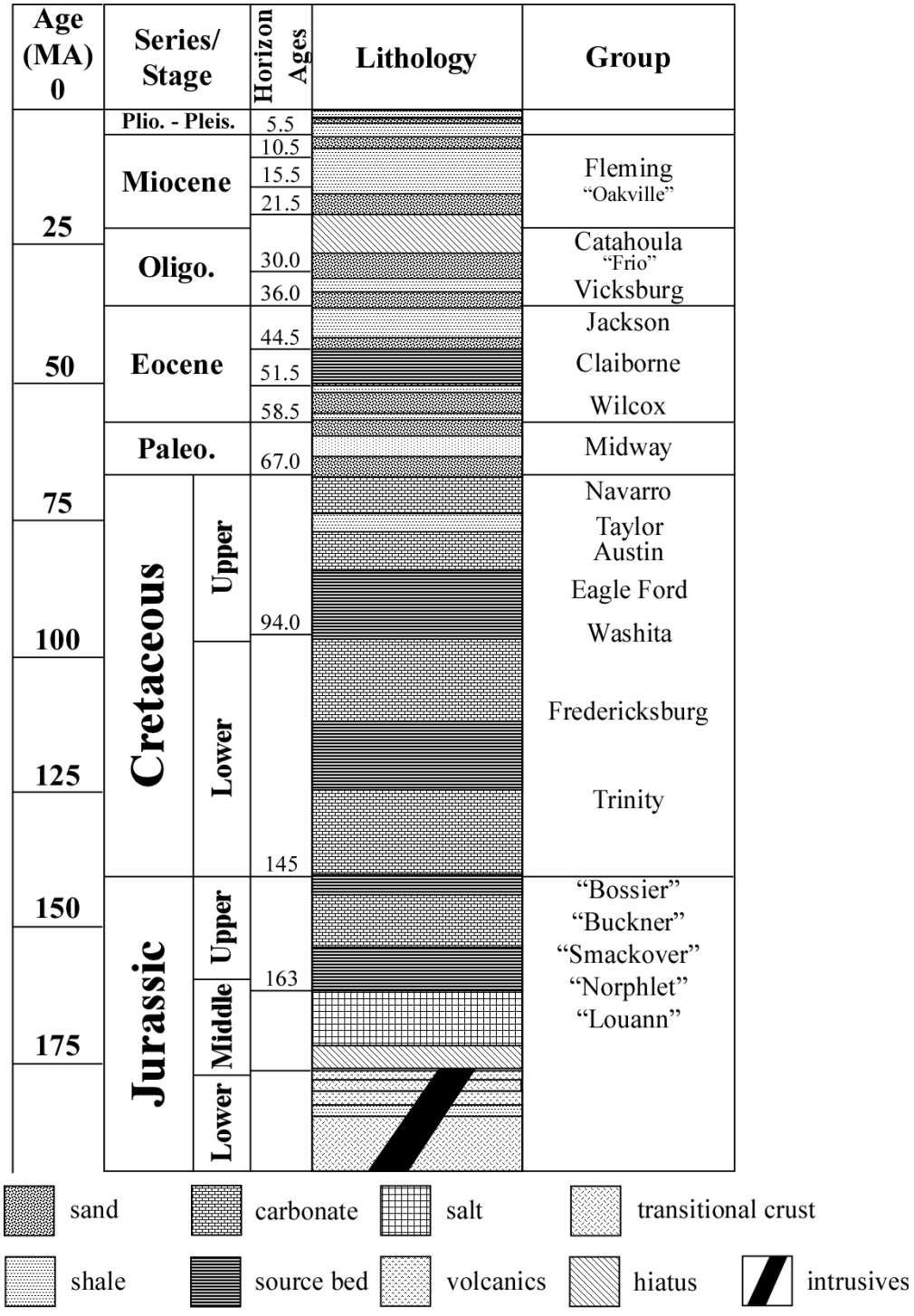

Figure 4A: Generalized stratigraphic column representing the Perdido fold belt. This shows the approximate ages and locations of the above mentioned groups. Modified from Worrall and Snelson (1989); Fiduk et al. (1999).

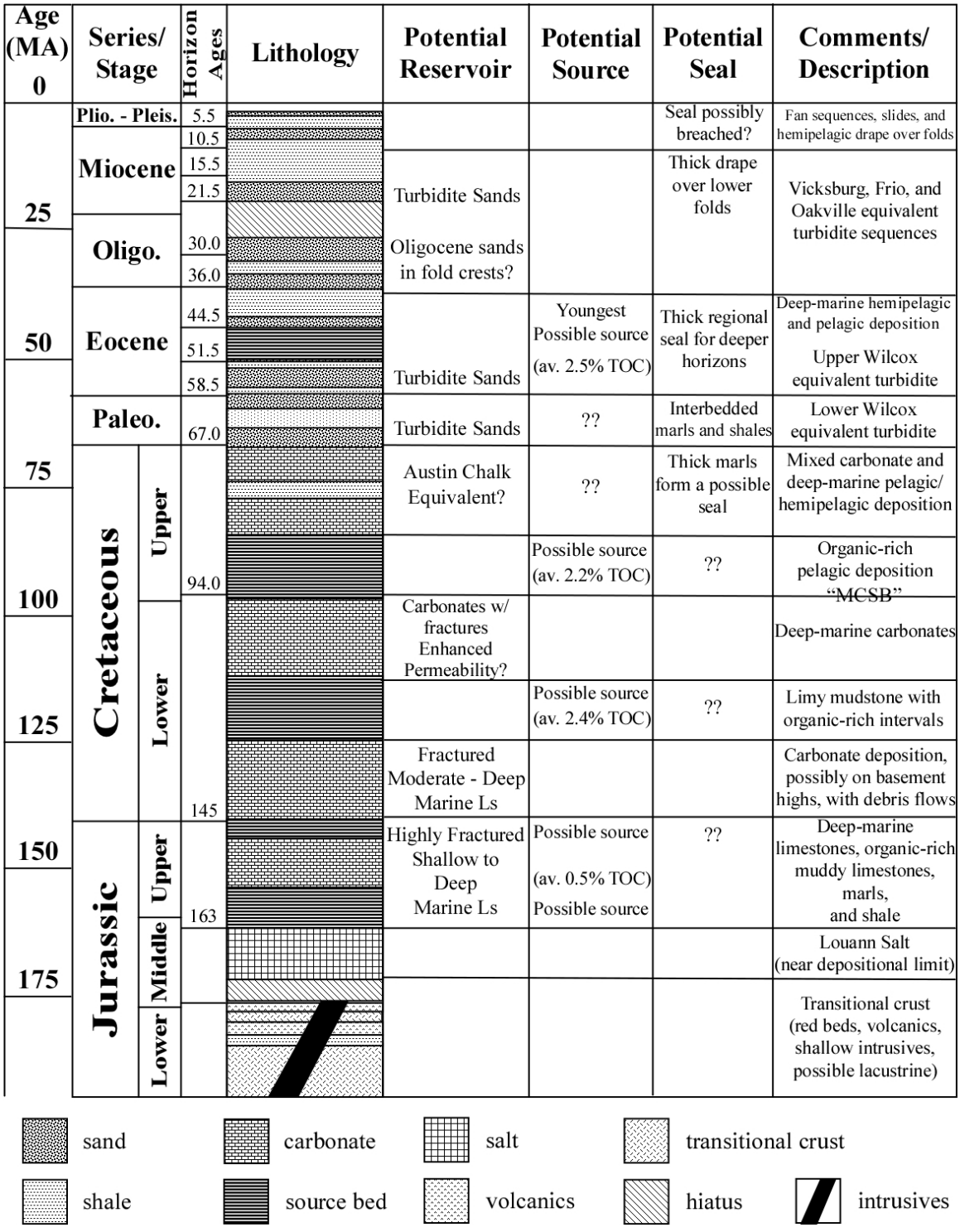

Figure 4B: Stratigraphic column showing areas of potential reservoir, seal and source rocks in the Perdido fold belt area. Modified from Fiduk et al. (1999).

deposition of the Louann salt, aeolian sands composed of quartzose sandstone, red beds and conglomerates of the Norphlet Formation were deposited (Worrall and Snelson, 1989).

Late Jurassic and Cretaceous (161 – 65 Ma): Pregrowth Strata

Through the latest Jurassic (Tithonian), the Gulf of Mexico was open to the Pacific Ocean through Central Mexico. During the late Jurassic, the Yucatan Peninsula reached its present position and ceased movement, forming the boundaries of the GOM basin. Rifting also ceased, and the Gulf of Mexico Basin underwent a period of tectonic stability with persistent subsidence of the entire basin, with substantially more subsidence in the central area (Salvador, 1987). Winker (2004) labels the latest Jurassic deposits (Tithonian) as being a source rock. Worrall and Snelson (1989) show that during the late Jurassic through the earliest Cretaceous, there was deposition of mostly marine sediments, consisting of carbonates (Smackover) and updip evaporite deposits (Buckner) followed by progradation of terrigenous clastics (Cotton Valley and Hosston).

By late Jurassic, the central gulf was approximately 6,500 ft (2 km) deep or greater (Winker and Buffler, 1988). In the earliest Cretaceous, a broad seaway was formed due to continued subsidence of the gulf, and the central gulf became an increasingly deep water environment (Fiduk et al., 1997). Winker and Buffler (1988) estimate that the central gulf was approximately between 13,100 and 14,800 ft (4 to 4.5 km) deep, with the PFB area somewhat shallower by that time due to sedimentation.

Worrall and Snelson (1989) define two major shelf margin reef cycles during the early (Sligo) and middle Cretaceous (Stuart City). The Sabine Uplift is also interpreted as being in part responsible for modifying the Mesozoic shelf of the northern Gulf, separating it into what are now termed the East Texas and Northern Louisiana salt structure provinces. By late Cretaceous, the central Gulf basin was approximately 13,100-16,400 ft (4-5 km) deep (Winker and Buffler, 1988). Watkins and Buffler (1996) note that moderate sedimentation rates occur at this time, with sediments in the center of the basin being largely carbonates and shales. During the late Cretaceous, there was widespread drowning of reefs and associated extensive sedimentation of chalks, marls and shales, following some broad upwarping of the shelf region, local intrusives and the development of a post “Mid-Cretaceous” unconformity. The stratigraphic column, in ascending order, Woodbine, Eagle Ford, Austin, Taylor and Navarro groups make up the classic upper Cretaceous (Gulfian) western gulf coast strata (Worrall and Snelson, 1989). Presumably, deep water equivalents are found in the PFB. Winker (2004) classifies source rocks in the late Cretaceous (upper Cenomanian), which is under the Midway formation of the early Paleocene.

The seismic reflectors observed in the Mesozoic age rocks are parallel and laterally continuous, implying uniform and uninterrupted deposition of these carbonate sediments.

Cenozoic Era

The Cenozoic is a time of widespread sedimentation. The GOM sedimentary basin was fed by sediments from the west, northwest and north from a complex system of shifting alluvial source areas which variously provided coastal deposits along migrating, typically unstable, faulted shelf margins (Worrall and Snelson, 1989). Winker (1982) and Worrall and Snelson (1989) define the early Paleocene as a time of flooding of the older Cretaceous carbonate margins by the stable supply of the basal, siliciclastic, mud-dominated progradational shelf margin systems (Midway). Feng and Buffler (1996) define three major lateral shifts, generally from west to east, of shelf margin depocenters, which may have been related to changes of the Mississippi River system.

Paleocene (65 – 54.7 Ma): Pregrowth Strata

The Paleocene stratum observed in the seismic thins from west to east, supporting the interpretation that the alluvial sediments were supplied from the coast into the deep basin. The shelf of the northwestern GOM shows point-loads, down building and other phenomena caused by the shifting alluvial sources (Worrall and Snelson, 1989). Figures 5-7 show the varieties of depositional locations and relevant amounts of sediment from the late Paleocene to the Holocene. Winker (1982) indicates that during the late Paleocene, the Houston embayment allowed the first large influx of sandy sediment to enter the northwestern gulf (lower Wilcox), flooding the Cretaceous carbonate margins (Figure 5). The Paleocene marks the end of carbonate-dominated facies and the

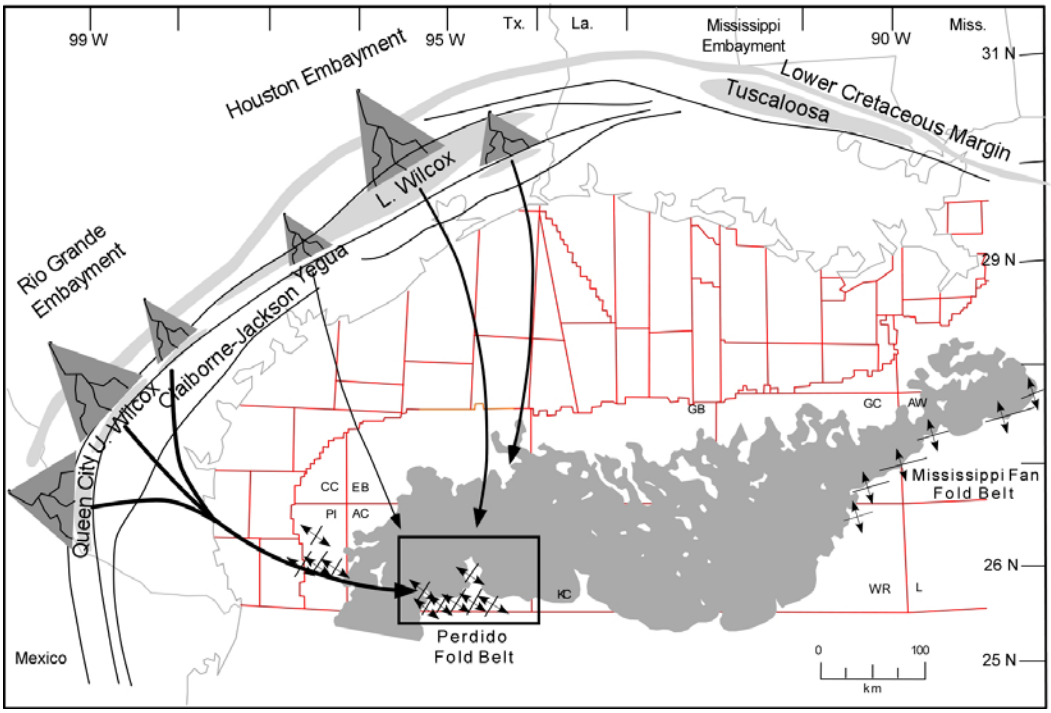

Figure 5: Paleogeographic map for the Cenozoic, northern Gulf of Mexico, showing the location of major marginal-marine siliciclastic depocenters in relation to the Perdido fold belt. Arrows show likely pathway from depocenter to the Perdido area; arrow thicknesses indicate relative sediment contribution. See stratigraphic column compiled by Feng and Buffler (1996) in Figure 8 for specific ages of different depocenters. Present-day allochthonous salt distribution and offshore lease areas are shown to orient the reader. Major shelf-margin depocenters of the lower and upper Wilcox are basinward of the Lower Cretaceous margin in the Houston and Rio Grande Embayments, respectively. (Fiduk et al., 1999).

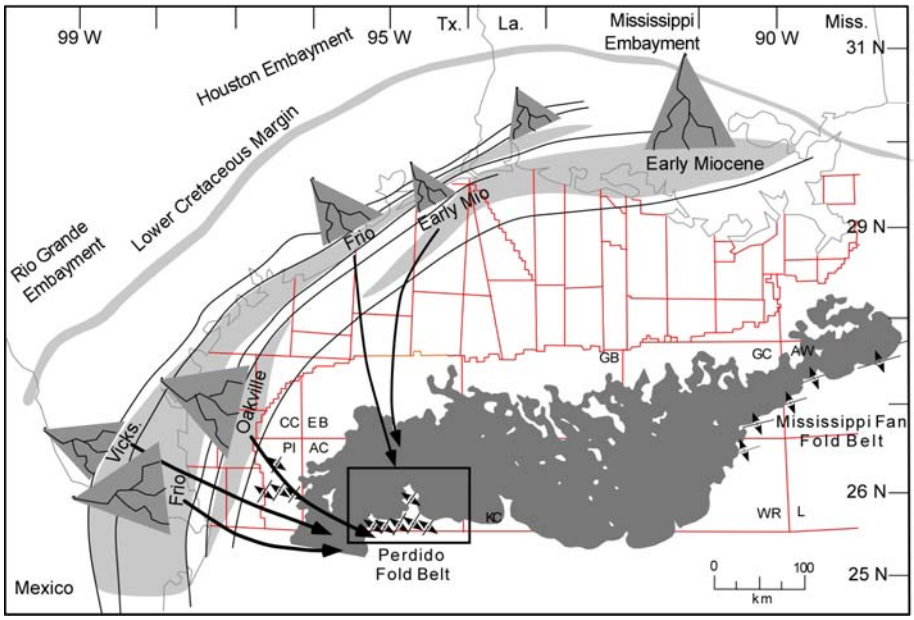

Figure 6: Paleogeographic map for the Oligocene-early Miocene. The Rio Grande embayment was the main axis of sediment influx during this time. By the early Miocene, the shelf margin in the Rio Grande embayment had prograded more than 150 km. (Fiduk et al., 1999).

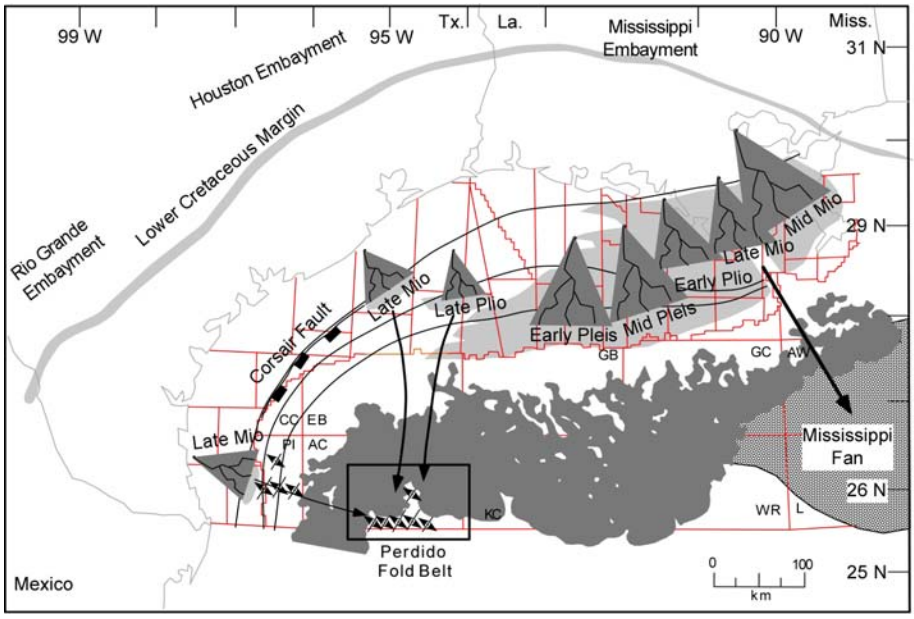

Figure 7: Paleogeographic map for the Middle Miocene-Holocene. Major depocenters now occur in the Mississippi Embayment. From the middle Miocene-Holocene, the Louisiana shelf margin prograded more than 150 km. Most sediment reaching deep water beyond the Sigsbee Escarpment was directed toward the Mississippi Fan. Only minor depocenters in the Houston and Rio Grande embayments were in position to shed sediments toward the Perdido fold belt. (Fiduk et al., 1999).

beginning of siliciclastic-dominated deposition.

Eocene (54.7 – 33.7 Ma): Pregrowth Strata

Sediment was redirected to the Rio Grande Embayment by the early Eocene, where unstable progradation of the upper Wilcox and Queen City deltaic systems and depocenters are characterized by growth faulting, as well as by development of major submarine canyons. These sediments were deposited as turbidite sandstones with channel and lobe geometries in large basin-floor fans (Worrall and Snelson, 1989; Winker, 2004). Winker (1982) defined the middle to late Eocene (Claiborne and Jackson) to show regressive sequences, with the exception of the Yegua formation in East Texas where unstable progradational conditions of the Houston Embayment, associated with salt withdrawal, prevailed (Figure 5). One of the main reasons for the introduction of siliciclastics during this time was the activation of the Laramide orogeny (late Cretaceous-middle Eocene) that uplifted the southern Rocky Mountains and the Sierra Madre Oriental of Mexico.

Oligocene to Early Miocene (33.7 – 15.6 Ma): Growth Strata

The Oligocene marks a time of noticeable growth strata and is presumed to be the time of fold initiation. In the sediments predating the Oligocene, there was a general trend of thinning to the east. However, when examining seismic reflectors of Oligocene stratum, there is a definite reversal, showing an eastward-thickening trend. Oligocene strata are non-existent over the fold crests and thicken in the synclines and basinward in the

abyssal plain. The Oligocene strata were also observed in seismic as the first significant onlapping reflectors. Winker (1982) and Galloway (1989) both define the Oligocene interval as a time of high sediment influx. The Vicksburg Formation was a sandy depositional body that prograded through the Rio Grande embayment during the early Oligocene, and the Vicksburg formation is followed by progradations of the Frio formation in the middle Oligocene in both the Houston and Rio Grande embayments (Galloway, 1989). Sand bodies found in the PFB area are presumed to be the deepwater turbidite equivalents of the shallow-water Vicksburg and Frio formations (Figure 6). Due to the high influx of sediment during this time, the south Texas shelf prograded more than 60 miles (100 km) basinward, which put these depocenters much closer to the PFB than that during the Paleocene and Eocene times (Fiduk et al., 1999)

Early to Middle Miocene (15.6 – 11 Ma): Postgrowth Strata

Miocene stratum represents a time of cessation of growth in the PFB. The early Miocene corresponds to the last major sandy influx of sediment to the area. During that time, the Oakville depocenter provided equivalent sediment out of the Rio Grande embayment to the PFB. During the early to middle Miocene, the primary depocenters migrated eastward to the Mississippi embayment due to the uplift of the Western Interior (Winker, 1982). Most sediment from the interior bypassed the PFB and was diverted to the Mississippi fan.

Middle Miocene to Present (11 Ma – Present): Reactivation Strata?

By the middle Miocene through Holocene time, most sediment was being deflected into what is now the Mississippi Fan, with little amounts of sediment reaching the PFB area. Figure 7 shows the major contributors of sediment to the PFB during this time. None of the major depocenters directly deposited sediments to the PFB, but the Alaminos Canyon was probably a great conduit to collect and transport sediment to this region. Fiduk et al. (1999) divide the middle Miocene to present day sediments into two large-scale wedges. The older wedge (10.5 – 5.5 Ma) thickens to the east, whereas the younger (5.5 – sea floor) thickens to the west. Consequently, the seismic profiles show this sediment to completely bury folds 1 and 2 (using the naming convention of Camerlo and Benson, 2006) but still show some amount of bathymetric expression on the sea floor of the remaining 6 folds.

Figure 8 shows the eustatic sea level changes as defined by Haq et al. (1987), along with the related depositional episodes as defined by Galloway (1989), sequence chronostratigraphy as defined by Feng and Buffler (1996) and the deep Gulf basin sequences, all of which were compiled by Feng and Buffler (1996). Figure 8 shows chronologically the times and bearings of depositional episodes to the PFB.

Sigsbee Escarpment

Worrall and Snelson (1989) consider the Sigsbee escarpment at the base of the Louisiana slope to consist of salt that is, at least locally, “overthrusting” sediment of the abyssal

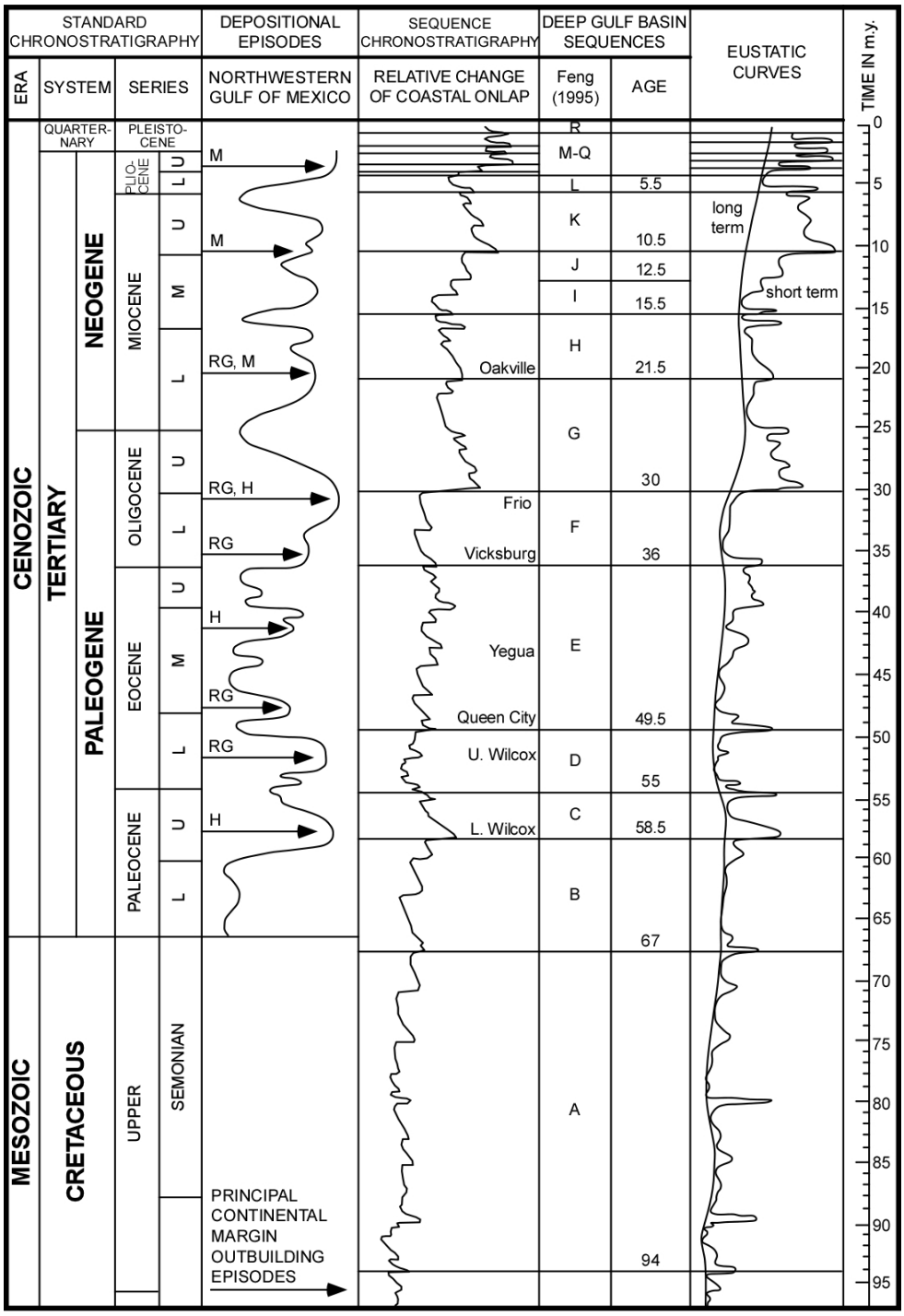

Figure 8: Chronostratigraphic correlation chart for deep Gulf of Mexico seismic sequences, middle Cretaceous through Cenozoic. Coastal on-lap and eustatic sea level curves from Haq et al. (1987), and major transgressions and regressions (depositional episodes) from Galloway (1989). RG=Rio Grande Embayment, H=Houston Embayment, M=Mississippi Embayment. See Figures 5-7 for locations of depocenters. (Feng and Buffler, 1996)

plan at least 6 miles (10 km). They also acknowledge that the wedge of allochthonous salt thickens northward to over 17,000 ft (5.2 km). The base of the allochthonous salt dips northward, and truncates successively older strata. The massive salt "overthrust" has been moving slowly to the south, likely since at least late Eocene time. The Sigsbee escarpment has mostly "down-building" mechanisms rather than diapirism, piercement or "up-building" structures. There are also many tens of kilometers of up-dip Miocene extension off the Texas coast, not seen in the Perdido fold belt. The excess extension could have been taken up in either the Port Isabel fold belt, located west of the PFB, along with influences of salt deformation. Winker (2004), along with Fiduk et al. (1997), Trudgill et al. (1999) and many others believe that the main episode of gravity-driven, salt-detachment folding in the PFB occurred in early Oligocene to early Miocene time. This folding episode was preceded by an early phase of slow structural growth during the early Cenozoic. The folding episode was then followed by a late Cenozoic phase of salt inflation and fold reinitiating in the proximal fold belt.

Growth Faults

Watkins et al. (1996) note that growth faults detach into (or above) underlying mobile substrates (low shear-strength sediments) in the northern GOM, which are either salt or geopressured shales. The down dip movement of the hanging wall block creates extension at the head of the fault and compression at the toe (Watkins et al., 1996). With changing depocenters mostly from delta deposits throughout the Cenozoic, the continental shelf was subjected to varying point loads. Worrall and Snelson (1989) note

that the style of growth faults, caused from the point loads of prograding deltas, are fundamentally different between many of the Cenozoic shelf margins of Louisiana and Texas. These different types are grouped into two distinct styles: the Texas style and the Louisiana style. The Texas style is comprised of very long fault systems, with a basinward dip and a strike parallel to the present coast. These are not generally associated with near-surface salt piercements, although a few salt structures are present. This is a result of either 1) gravity sliding caused by rapid sedimentary loading of prodelta shales near the shelf margin, and/or 2) differential shale compaction. It is also attributed to long, linear, strand plain – barrier island depositional systems that loaded the salt in this region through the most of Tertiary time. The Louisiana style is a much shorter, more arcuate-shaped fault system that dips landward as well as basinward. It is spatially associated with abundant near-surface salt bodies. Strong evidence supports that this systems origin is due to salt movement by sediment loading. It is also attributed to sedimentation predominantly from deltaic systems, which load salt in an uneven, shifting point- or line-load fashion, producing a complex set of arcuate faults and mini-basins, with much remnant salt left behind (Worrall and Snelson, 1989). Winker et al. (1996) conclude that faults detaching into salt are of short-to-moderate (<100 km) length, whereas faults detaching into geopressured shale tend to be much longer with lengths in some instances of >1000 km. They also note that the arcuate faults (mainly those detaching into salt) reflect the arcuate edges of the salt sheets and/or thickness variations.

Previous Reconstructions and Analysis

Many studies and reconstructions have been conducted to better describe the structural properties of the PFB area (e.g. Mount et al., 1990; Peel et al., 1995; Trudgill et al., 1999; Camerlo and Benson 2001, 2006; Mitra, 2002; and many others). Trudgill et al. (1999) discuss in their paper six main conclusions:

1) The PFB is characterized by northeast-southwest-trending, subparallel, concentric box folds bounded on one or both flanks by high angle reverse faults. Folding involves strata of late Jurassic-Eocene age. Trudgill et al. did mention that the reverse faults could have developed as a response to tightening of the fold structures.
2) The fold structures are salt-cored detachment folds, in contrast to other suggestions that they were fault-bend fold structures.
3) The middle Jurassic Louann salt had an original thickness of 0 to 10,000 ft (0 – 3 km), the thickness being controlled by basement structural shapes. They also suggest that one reason the western folds are elevated above basin regional is due to thick salt inflation from the west.
4) Main phase of deformation takes place during the early Oligocene (36-30 Ma) followed by a minor phase that affected the back-limbs of some of the folds between 15.5 and 10.5 Ma. There was also a late stage of regional uplift (5.5 Ma to present day), which may have been caused by movement of the Louann salt due to loading by the advancing and overriding of the Sigsbee salt nappe.

5) The PFB marks the down dip limit of a complex linked system of gravitational spreading of the Paleogene passive margin. The loading and extension to the northwest of the fold belt are not balanced by the 3 – 6 miles (5 – 10 km) shortening within the PFB. Most of the extension was accommodated by extrusion and lateral transport of extensive salt canopies and by folding in the Port Isabel fold belt. This can be seen in a structural cross section (Figure 9) from the Texas coastline to the Sigsbee abyssal plain (Worrall and Snelson, 1989).
6) Although there are similarities between the PFB and the Mississippi Fan fold belts, they are not contemporaneous. Locations of both fold belts are found in Figure 1.

Trudgill et al. (1999) note that minor pop-up folds occasionally were observed on the flanks of larger folds. These minor folds have been considered as individual fold culminations (Camerlo and Benson, 2006). Additionally, even smaller folds are observed in the synclines of some folds. The stratigraphic locations of these smaller folds are in the areas of the Jackson and Anahuac equivalent shales, and their significance will be discussed in a later chapter (Chapter III, Observations).

With the advancement of technology and resulting improved data sets, some of these conclusions have been modified by Camerlo and Benson (2001, 2006). In Trudgill et al. (1999), longer and older vintages (acquired between 1977 and 1988) of 2-D proprietary and speculative regional seismic lines were used. This was followed by Camerlo and

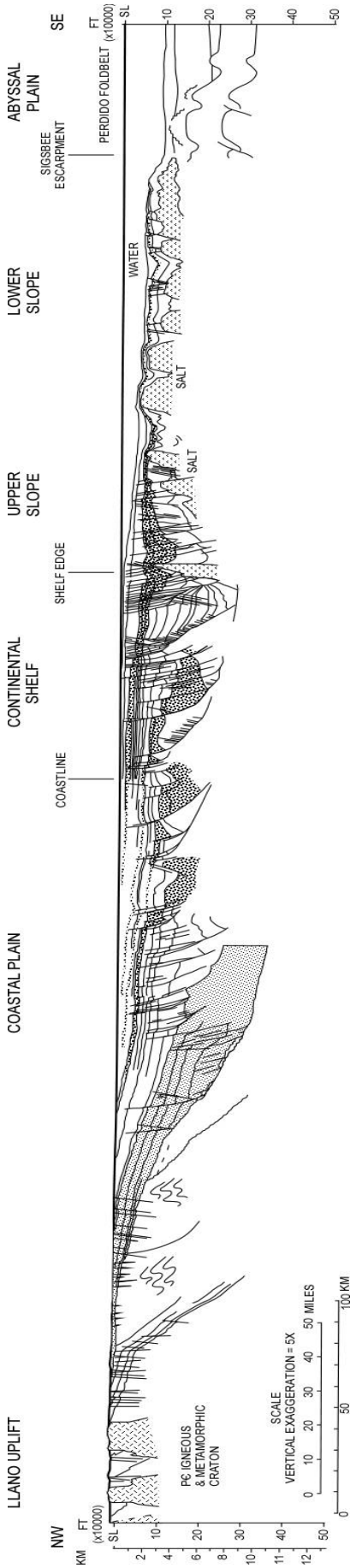

Figure 9: Structural cross section across Texas continental margin into the deep water Gulf of Mexico. Vertical exaggeration = 5x. Location of cross section can be found on Figure 1. Modified from Worrall and Snelson, 1989.

Benson using newer (acquired in 1998) 3-D seismic data. In their papers, the authors extended the fold naming convention of Trudgill et al. (1999) to include more folds, labeling them folds 1 through 8 (Figure 2). Previously only five folds (1-5) had been described. Camerlo and Benson also challenge some of the conclusions of Trudgill et al. (1999) citing discrepancies due to significant noise in the seismic data. Camerlo and Benson (2001, 2006) interpret the structures of the PFB to be contractional folds primarily unassociated with high-angle reverse faulting, and that large-scale reverse faults that are continuous enough to create effective traps are not present.

Camerlo and Benson (2001) initially introduced the notion that older vintages of seismic data are responsible for some of the conclusions that were previously made by other workers. After examining newer 3-D data, they interpret the low reflectivity bands as tabular folded zones of discrete steeply dipping layers known as kink-bands. The low reflectivity of the kink-bands is the result of low signal to noise ratio within the bands and stack attenuation of the steeply dipping events from post-stack time migration. They used the low amplitude seismic response within the bands to define and emphasize the kink-bands. They also found that the finite width of the bands does not support an interpretation of the zones as faults. Those authors realized that as seismic imagining efforts improve, small-scale faulting is likely to be imaged in these high-dip structures, however, the small faults would be second-order structures and would lack folds above the hypothetical faults. They also note that the tabular nature of the bands, the bending of the reflections into the zone at both inner and outer kink planes, as well as offsets

normally occurring in the middle of the band, and not as a single plane, argues against interpretation of the low reflectivity bands as fault shadows.

Camerlo and Benson (2001) discuss the geophysical reasoning behind their interpretations. They use geophysical data to support their ideas, such as vertical seismic sections that are commonly interpreted with large vertical exaggeration causing steeply dipping strata within the kink-band to thin markedly and appear sheared or cut by a fault. They also suggest that seismic stacking velocities are smooth functions that cut across sharp steep structures and result in incorrect positioning of events after migration that appear as fault offsets. They also note that the precision of velocity analysis decreases with depth resulting in the inability to resolve dip and proper migration swing, potentially smoothing sharp kink boundaries and over migrating events through boundaries. Diffractions across kink-planes will result in apparent offsets, and raypath problems through tight synclines which will cause additional imaging problems.

Camerlo and Benson (2001) concluded that:

1) The PFB is a fold dominated contractional belt wherein shortening was accommodated by the formation of open detachment folds and kink-folds, as opposed to the previously proposed models of an imbricate fault-bend fold model (Mount et al., 1990) and the high-angle, reverse faulted detachment fold (Trudgill et al, 1999; Rowan et al., 2000).

2) Thrusting and reverse faulting are relatively minor second-order structures and are not believed to have been significant deformation mechanisms during formation of the fold belt.
3) Early open detachment folding began with limited salt flow to anticlinal cores from fold synclines. The limited volume of ductile salt inhibited continued fold formation by this mechanism, and consequently kink-folding began. Later salt inflation and contraction resulted in resumption of open detachment folding.

In this case, on seismic data the kink bands are poorly imaged zones of low signal-to-noise ratio and low reflectivity. Camerlo and Benson (2006) point out that these seismic artifacts result from problems related to steep dips, primarily a bias of amplitude and the sensitivity of positioning and coherence of dipping events to migration velocity.

CHAPTER II

METHODS

SEISMIC INTERPRETATION

Initially, a set of horizons were interpreted in the 2-D (TGS Phase 45) data set, which was tied to limited proprietary well log data. The following horizons that were interpreted (Figure 10) are outboard of the allochthonous salt sheets and the Sigsbee salt nappe (location of allochthonous salt, Figure 1):

-Sea Floor (Present day)

-Top Pliocene (2.85 Ma)

-Top Miocene (5.8 Ma)

-Top Middle Miocene (11.0 Ma)

-Unconformity

-Top Lower (early) Miocene (15.6 Ma)

-Top Oligocene (23.8 Ma)

-Top Eocene (33.7 Ma)

-Top Paleocene (54.7 Ma)

-Top Early Paleocene (60.9 Ma)

-Top Cretaceous (65.0 Ma)

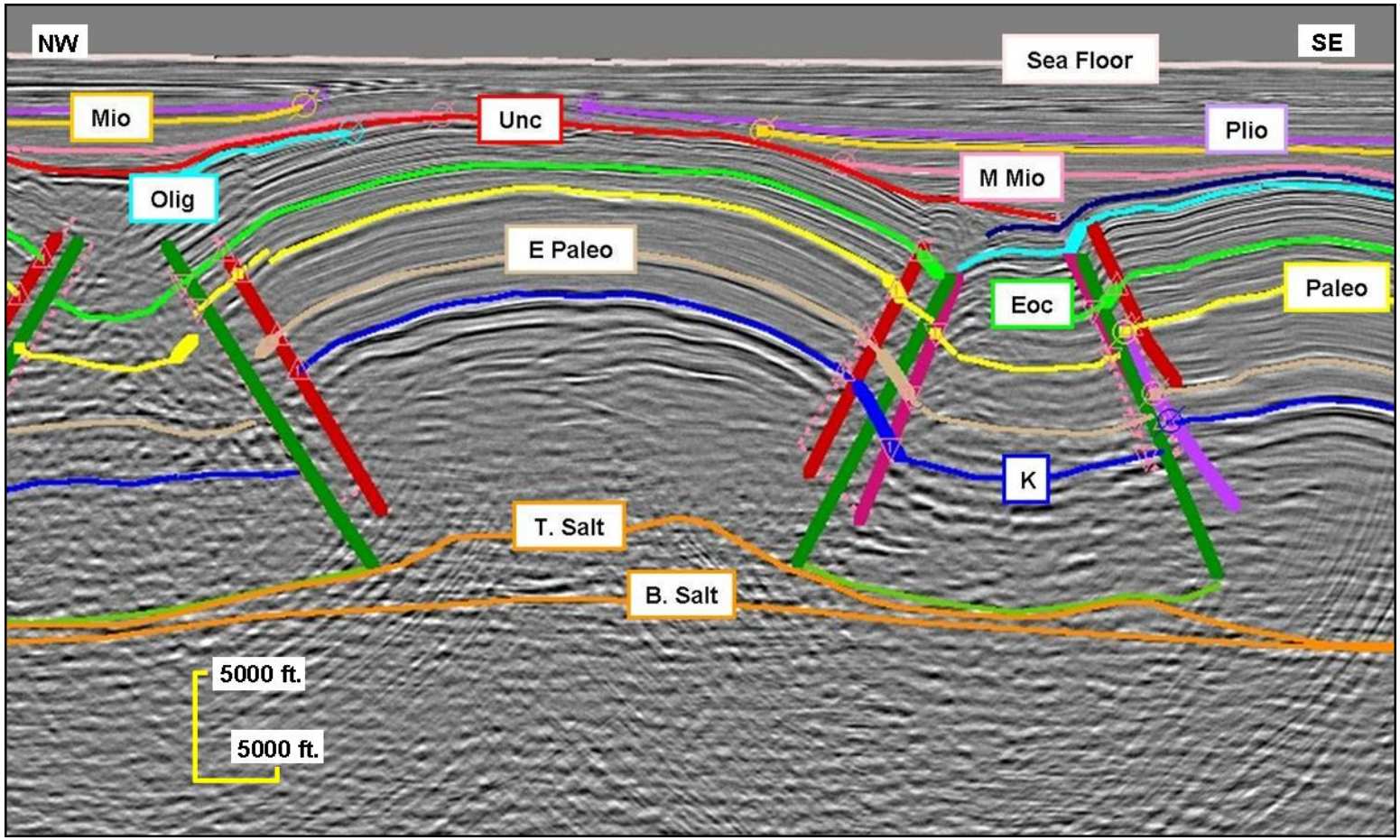

Figure 10: Seismic profile showing interpreted horizons. The main horizons are labeled: B. Salt=Bottom Salt; T. Salt=Top Salt; K=Top Cretaceous; E Paleo=Top Early Paleocene; Paleo=Top Paleocene; Eoc=Top Eocene; Olig=Top Oligocene; Unc=Unconformity; M Mio=Top Middle Miocene; Mio=Top Miocene; Plio=Top Pliocene; Sea Floor=Sea Bottom. Seismic data are owned by TGS-NOPEC, all images of the data have been reproduced with their written permission.

After approximately 1,026 miles (1,651 km) of seismic lines were interpreted, grids were then created over the entire area to interpolate the areas between the interpretations. The final product is a depth-structure, color grid map. These depth-structure grid maps were used to examine timing in detail, and to look at how the fold system evolved with time.

Timing evaluations were accomplished by creating isochore maps to show varying sediment thicknesses by subtracting one depth-structure grid map from another. Presumably, these are isopachs in nature, but low angle dips (such as regional) and compaction were not accounted for. Steep dips, such as areas with kink band geometries were excluded (Figure 11). To better constrain timing and deformation, the unconformities were examined. Along with the depth-structure, color grid maps and isochore maps mentioned above, dip maps were created over the area on most of the above mentioned horizons, which also gives a good map view of the deformation (Figure 12).

All structure forming faults were mapped, along with mapping the kink bands bounding every fold. Timing was better constrained by examining the sequence of folding (faulting if apparent) and the fold/fault propagation and interaction.

The folds in this study (Figure 2) follow the naming convention found in the literature (i.e. Folds 1-8) with fold culminations marked with lower case letters (Camerlo and Benson, 2006, modified from Trudgill et al., 1999).

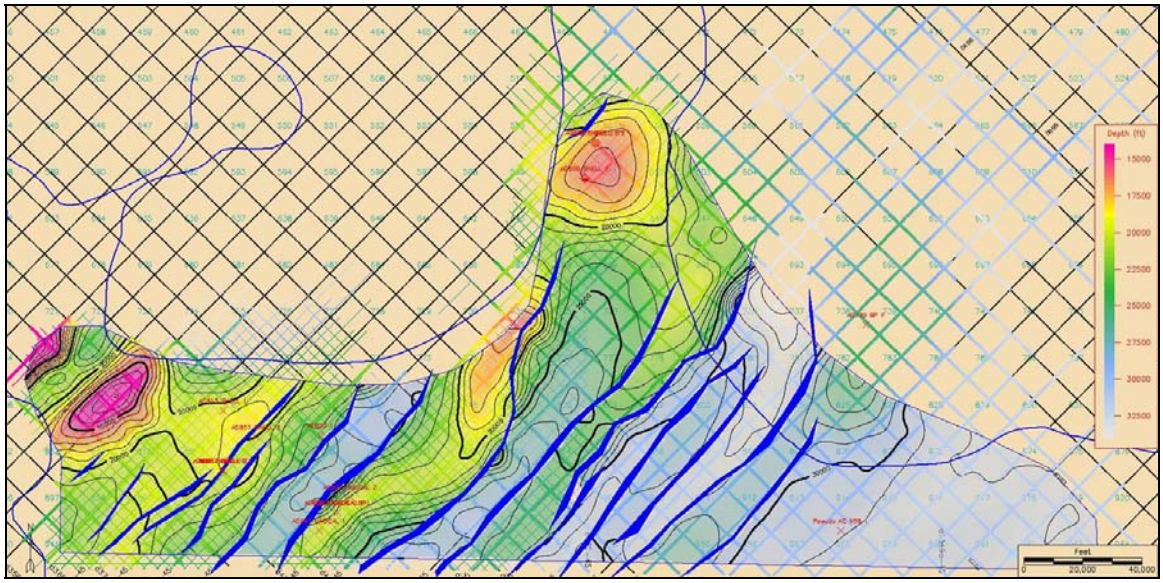

Figure 11: Depth structure map of the top of the Cretaceous horizon. Warm colors (red) are high (shallow), cool colors (blue) are low (deep). Dark blue jagged lines represent the locations of the kink bands on the flanks of the folds – these kink bands were used as boundaries when contouring. Maps based upon TGS seismic data.

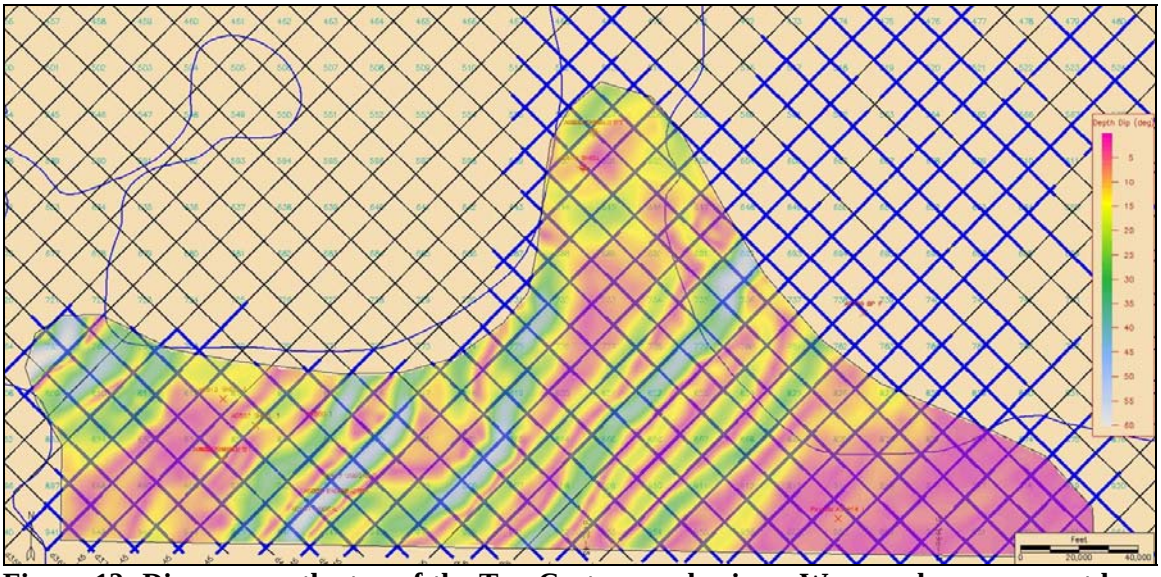

Figure 12: Dip map on the top of the Top Cretaceous horizon. Warm colors represent low dips (pink= 0°-5°, green= 25°-35°) and cool colors represent steep dips (blue= 40°-50°, white= 60°). The kink band locations can be easily seen here as blue and white colors (high dips). Maps based upon TGS seismic data.

It is also useful to consider two end member models: mechanical folding by Davies and Fletcher (1990), which shows folds geometries as shear stress is varied (for the purpose of this study, presume little to no shear stress) to create symmetric folds, and a salt flow model presented by Wiltschko and Chapple (1977).

In relation to salt, I considered the affect that salt thickness has on the folds. Examinations of the seismic show an example of “pop-down” structures that make up a new model in this thesis. It is a possibility that the differences of the High and Low Perdido could be caused by the western most folds partially being elevated above regional by material added underneath the anticline from the buried pop-down structures that are bottomed out against the basement rock. This is in contrast to that of Trudgill et al. (1999) who proposed that the difference is caused by massive salt inflation on the western side. These pop-down structures are synclines that have “fallen” or moved down in an absolute sense into the salt until they bottom out at the base of the mobile salt (or basement rock). With further shortening, the anticlines begin to ride up and over these synclines.

GEOMETRIC MODELS

Excess Area vs. Depth to Detachment Models

A number of mechanical and theoretical models have been produced in order to better understand detachment folds (Wiltschko and Chapple, 1977; Dahlstrom, 1990; Davies

and Fletcher, 1990; Epard and Groshong, 1993, 1995; Spang, 1999; Mitra, 2002, and many others). Epard and Groshong (1993) cite R. T. Chamberlain's 1910 paper which was the first to report on balanced cross-sections that used the measurement of excess area to find the depth to detachment (Figure 13). Chamberlain, in his paper defines two equations that could effectively be used to determine the excess area:

$$S = Dh, \tag{1}$$

where D equals shortening displacement, h is units above the detachment to the top of the formation, and S is the excess area above regional. It is also shown that Chamberlain assumed that bed length remained constant throughout deformation, so that

$$D = L_0 - W, \tag{2}$$

where L_0 is the original bed length and W is the straight line or final bed length (Figure 13). When equation (1) is solved for h and replacing D by equation (2), it gives

$$h = S / (L_0 - W). \tag{3}$$

Epard and Groshong (1993) point out that equation (3) was used by Chamberlain to estimate the depth to detachment for the thin-skinned Appalachian fold and thrust belt. Although Chamberlain's methods in general will be used in the calculations, his original theory failed for several reasons, which are based on the five assumptions presented by Epard and Groshong (1993). If these five assumptions are not satisfied, then problems will arise. The assumptions are:

1) No material is assumed to enter or leave the ends of the cross section.

2) Bed length is assumed to be constant.

3) The area is assumed to be constant within the cross section. Equations (1) and (2)

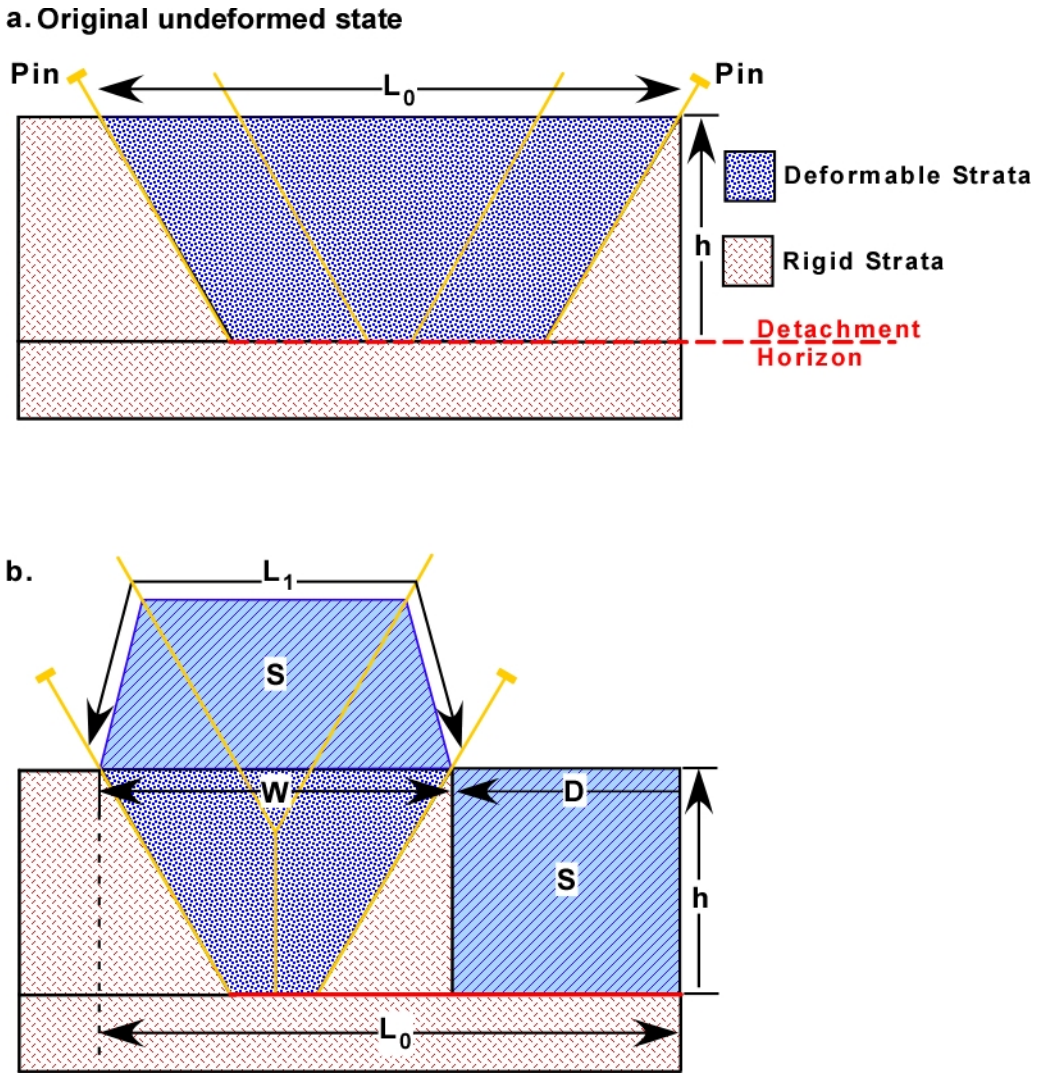

Figure 13: Illustration for the case of calculating depth to detachment from excess area from a single layer as originally proposed by R. T. Chamberlain (1910). A few modifications have been made to make this represent a box-style detachment fold, similar to the models proposed in this thesis. Part (a.) shows original undeformed strata. Red hash marks (granite symbol) represent rigid strata, and blue dotted (sandstone) areas represent deformable strata. Part (b.) represents the deformed state of the fold. S = Excess Area; W = Width of the fold; L_0 = Original length (W+D); L_1= Final bed length; D = Displacement; h = Depth to detachment. Modified from Epard and Groshong (1993) and Groshong and Epard (1994).

could be invalid if area is gained or lost.

4) The original regional elevation of a bed is assumed to be known. Most often, regional is set at the base of the deepest syncline. However, this does not recognize the potential of thinning or thickening of sediments below or in the syncline. If this is not taken into account, equation (1) will become invalid. In the data set used in this thesis, the synclines move absolutely down; therefore, regional is set to that of the presumed undeformed or "rail-road track" sediments in the abyssal plain basinward of the last fold (fold 1).
5) The reference horizon and the lower detachment are assumed to be parallel to one another, which mean that there is no tilting of the folds (i.e. the wave-train of folds).

Epard and Groshong (1993) proposed a new method that uses the excess areas of multiple horizons (Figure 14). This, in return, requires no bed length measurements, thus eliminating Chamberlains equation for displacement as it relates to bed lengths, along with the many assumptions associated with it

For the purposes of this thesis, a generalization will be made so that equation (1) will apply to the structures of interest. Epard and Groshong (1993) point out that this equation has one known variable (S) and two unknowns (D and h), therefore requiring two equations to obtain a unique solution. The solution can be found on a graph that represents the excess area, S, as a function of depth to detachment, h (Figure 14). Epard

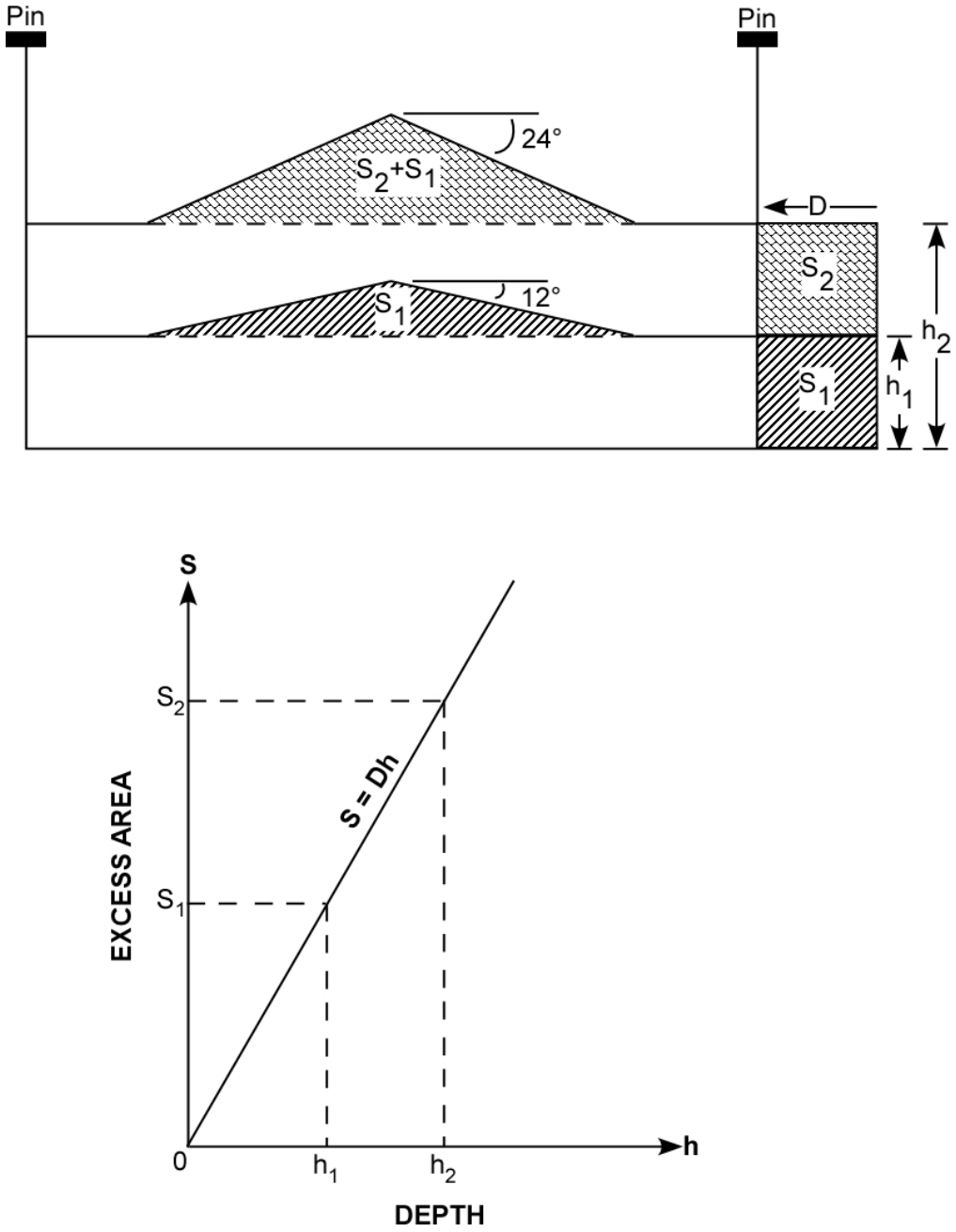

Figure 14: Excess area at two levels in an area-constant anticline when depth to detachment is known. The diagram is plotting excess area vs. depth to detachment. The slope of the line (D) represents the displacement on the detachment. In the lower level, area is added equivalent to that lost at that level by displacement. The upper level has area added under the anticline equal to that of the first level plus the area lost by displacement in the second level. In this simple model, observe how the limb dips increase as you move up section. Modified from Epard and Groshong, 1993.

and Groshong (1993) show that on this graph, equation (1) is a straight line that has two important properties: it passes through the origin, and the value of the slope of this line is D, the displacement. In this thesis, the displacement is not explicitly known, so for this case, we will use the procedure outlined below, from Epard and Groshong (1993). The true depth to detachment can be inferred from some seismic profiles, but is not in order to eliminate any data bias.

When neither the displacement nor the depth to detachment is known, the measurements of elevation, h, are made from an arbitrary reference horizon. In order for this technique to work, the geologic data has to be good enough to measure excess area in a minimum of two levels (Figure 15). These measurements give a general equation so that

$$S = Dh + S_a. \quad (4)$$

The inference from this is that if the line goes through the origin ($S_a = 0$), as in Figure 14, then the arbitrary reference level that was picked is the same as the true detachment horizon. Conversely, if the line does not pass through the origin (Figure 15), the arbitrary horizon is not the true detachment level. By examining the graph, the true detachment horizon can be determined by looking at the difference between the origin and the point of intersection with the h axis (Figure 15). Therefore, if the point of intersection is in the positive portion of the depth axis, the true detachment horizon is above the reference horizon the marked amount of units. If the point of intersection is in the negative portion, it is below the true detachment horizon the marked amount of units.

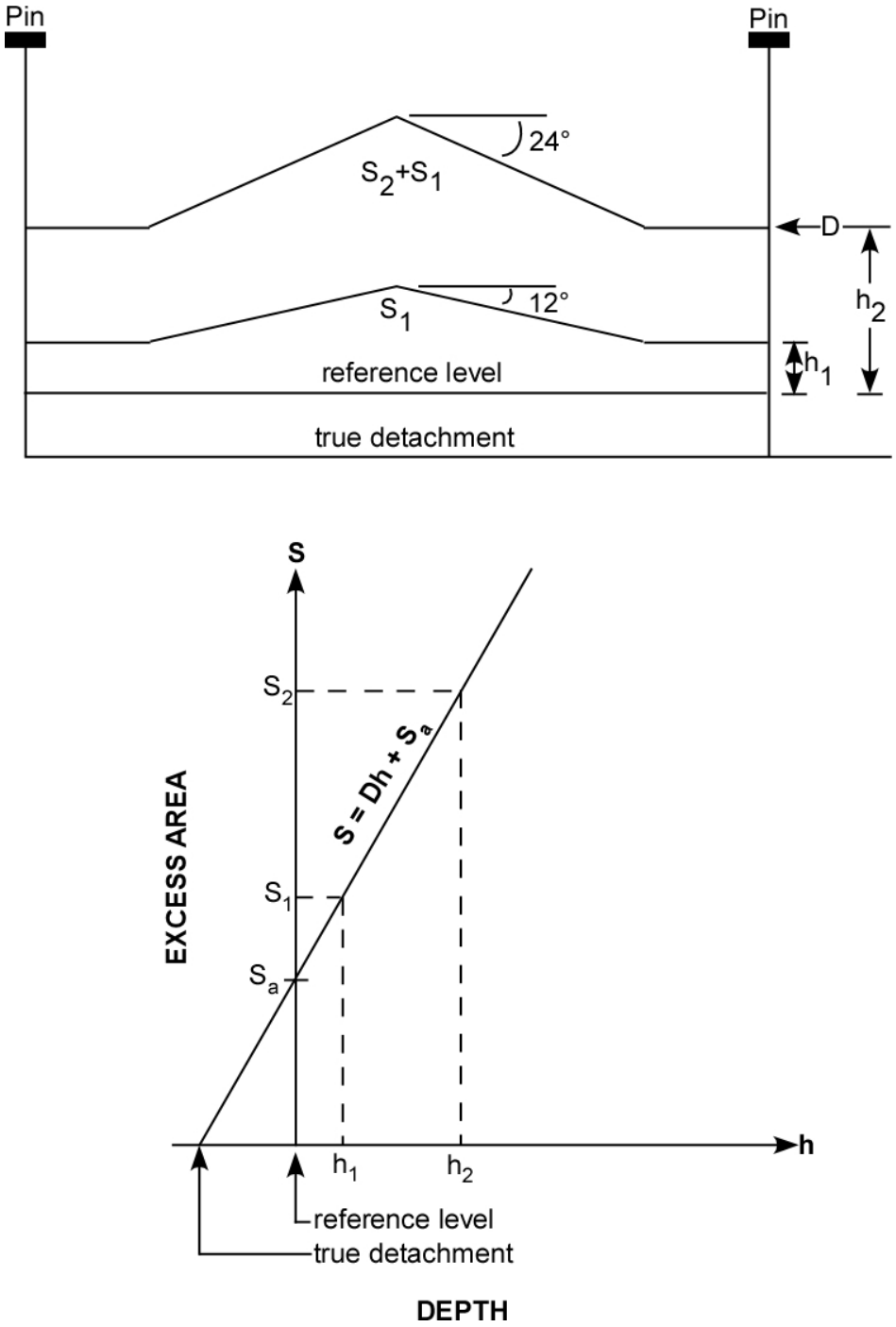

Figure 15: Excess area at two levels in an area-constant anticline when depth to detachment is unknown. In the cross section, measurements are made from an arbitrary reference horizon. The diagram is plotting excess area vs. depth to detachment. The slope of the line (D) represents the displacement on the detachment. The depth intercept of the line (excess area = 0) is the depth of the detachment below the reference level. Modified from Epard and Groshong, 1993.

In a generic model, when dealing with either a wave train or a single fold, a positive slope indicates pre-growth sedimentation (Figure 15). Accompanying this will also be a negative sloping line, which represents growth sedimentation. For growth sediments, the area (or excess area) above regional goes down as you go up stratigraphically, and the excess area goes to zero at the top of the growth sediments when folding stops. The intersection of these two lines represents the onset of folding, and this location is determined by the location of this intersection relative to the depth axis on the plot. The point location where the positively sloping line intersects the horizontal, or depth (h) axis should be the true detachment horizon, and the location where the negative sloping line intersects the horizontal, or depth (h) axis should be the height above the arbitrary detachment horizon where folding ceases. In addition, the total displacement can be found from the slope of the excess area curve (line) for pre-growth sediments.

Geometric Models: This Study

In models that have been presented by Epard, Groshong, Mitra, Spang, and others, the geometric models represent “perfect” data, with a single anticline, syncline or a perfectly deformed fold pair or wave-train. However, in nature, rocks commonly do not behave “perfectly” nor is the data (interpreted seismic reflections) perfect. When looking at a complex wave-train such as the PFB, it is difficult to determine which if any syncline-anticline pair to evaluate. The questions arise: Which pairs are important? Do I consider the entire wave train? Do I work with anticlines and synclines separately? After doing some preliminary work, the latter procedure has been chosen.

The models developed for this thesis follow the methods of Epard and Groshong (1993), as previously described. Figure 16 shows the generic model for a “classic” box-style detachment fold.

The deformable rock (salt, carbonate and sandstone symbols) is that found between the hinge pin lines and above the detachment horizon. All other rock is considered rigid and undeformable (granite symbol). The observation made in figure 16 is that with a prescribed amount of displacement, the lower layer only sees the effect of the amount of material that has been displaced within its boundaries (area A in Figure 16b). The layer above it sees not only the amount displaced within its boundaries (area B in Figure 16b), but also that of the layer below it (area A+B), and so forth up section. The dips of the fold limbs increase as you move up the section. Also, there is observed a prescribed amount of line length shortening or elongating. To the left of the figures, the amount of shortening (negative values) or elongating (positive values) is marked. The bottom most layer shortens the most, and that amounts decreases as you move up section, until at some point, the excess area causes the original line lengths to begin to elongate. Additionally, in figure 16, the amount of amplitude gained by the upper most layer is observed to increase more rapidly as the amount of displacement is increased. Figure 17 is used to model an anticline that is formed by only area being added to its core equal to that displaced by a “falling” adjacent syncline with no shortening between the fixed anticlinal axial surfaces. In this anticline every stratigraphic level sees the same amount

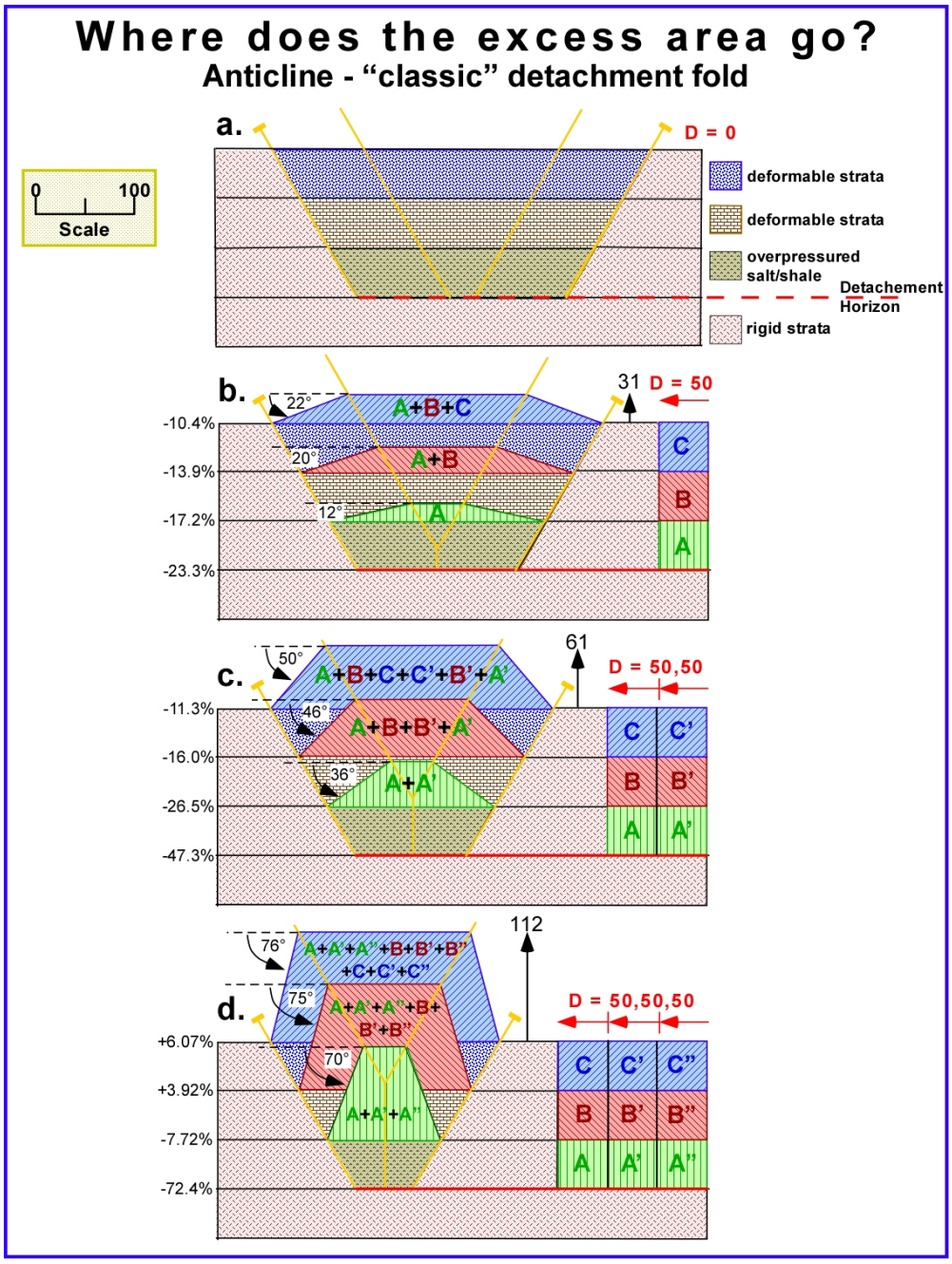

Figure 16: Excess area models showing the deformation of a classic box-style detachment fold. The excess area is the amount of material that has moved up pass regional. Part (a) shows the original undeformed state. Part (b) shows the area added to each layer by 50 units of displacement. The dips of the layers increase up section, and the line lines are shortened more down section. Parts (c) and (d) show similar results. The layer parallel strain (labeled in percent) is marked to the left of each diagram. The line at the base of material a (green) never folds and therefore, it will always shorten. Somewhere between parts (c) and (d), the line lengths have begun to elongate, denoted with a positive value. Also, the changes in fold amplitude are marked.

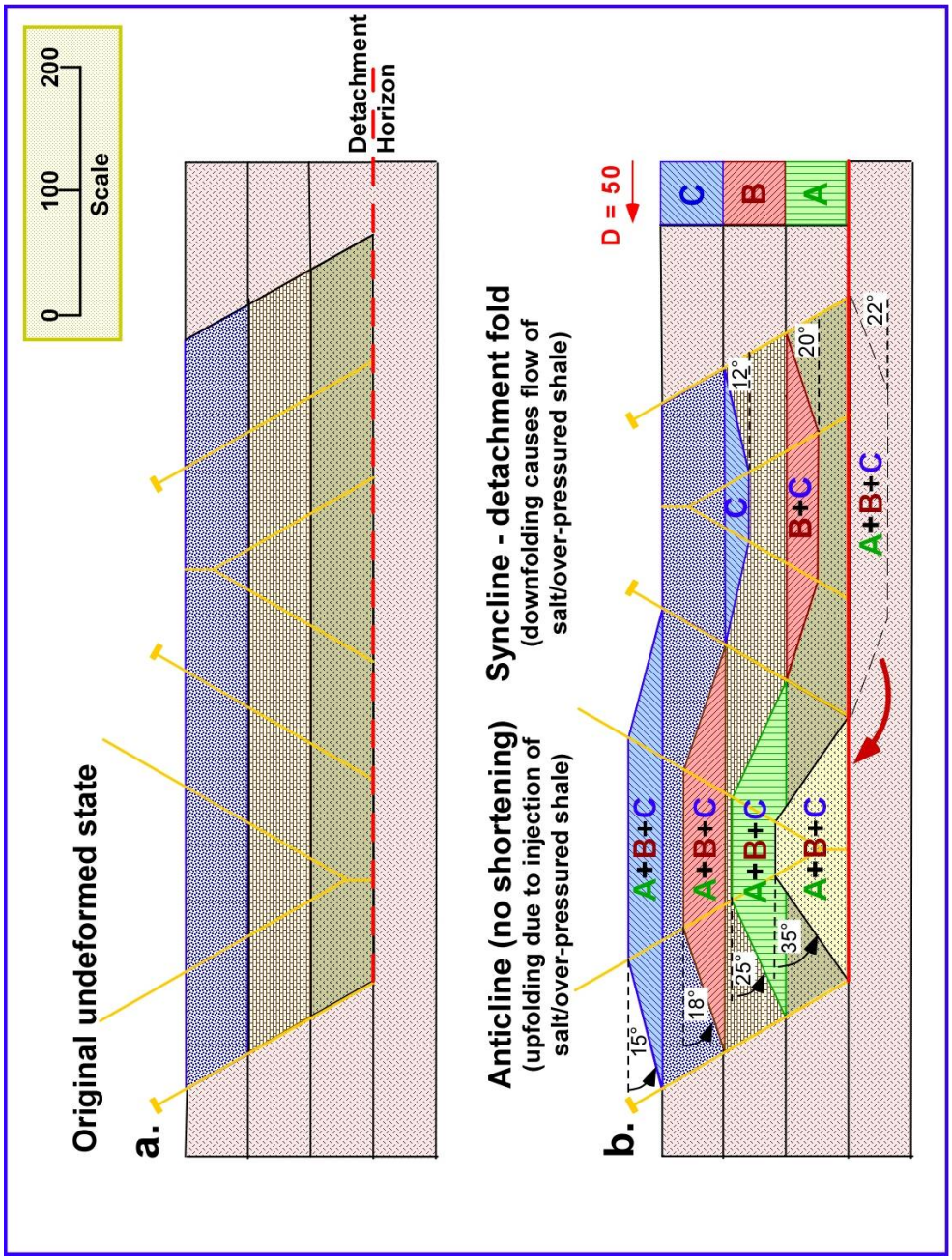

Figure 17: Excess area model showing the deformation of upfolding due to injection of salt. Diagram (a) shows the undeformed state of the rocks, and is followed by diagram (b), which shows the growth of the anticline by injection of the overpressured salt/shale which is displaced from under the falling syncline. Since the axial limbs diverge and the same amount of material is added to each layer, the dips on the fold axial limbs decrease up-section.

of area added. Since the anticlinal axial surfaces diverge, the dips decrease as you move up section. Figure 18 is a model that combines the previous two, compression along with salt injection from an adjacent “falling” syncline. Here, the observation is made that all stratigraphic layers see the same amount of area added by the salt injection, and each layer sees the amount of excess area from the level below it, along with its excess area due to the shortening of the anticline. The results of figures 16-18 are graphed on figure 19. In this figure, there are three different sets of data points: one representing the excess areas of an anticline with influences of both compression and salt injection from a neighboring syncline, another represents an anticline with only salt injection, and the third set of data points represents a syncline that has been modified by compression. On the graph, it is shown that the intersection of the anticline curves and the syncline curve is located at the correct depth to detachment; however, the excess area that is represented is the amount of material that has migrated from below the syncline into the neighboring anticlines core. In natural folds, we would normally use the intersection where the excess area goes to zero to locate the level of the detachment horizon. However, when the excess area curves for the anticline and syncline intersect at a positive area, the positive excess area is the amount added to the anticline and removed from the syncline.

Another important aspect of these models is that of the growth sediments. Figure 16 is modified to show a scenario were constant over-fill growth sediments are added at each stage of deformation (Figures 20, 21). Figure 20 represents three different stages: the first were there is no displacement (a.), the second is the over-fill added after 50 units of

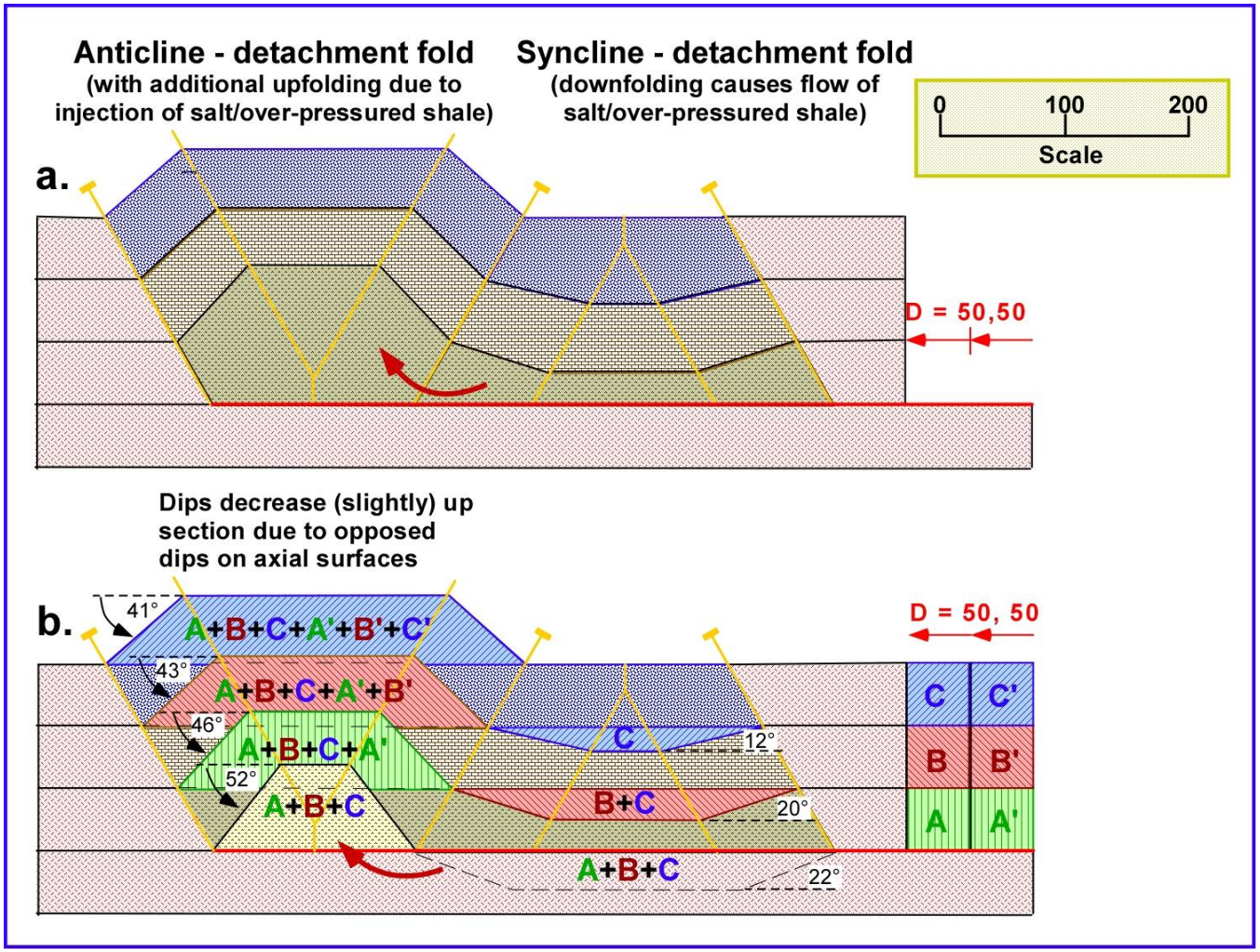

Figure 18: Excess area models showing the deformation of a classic box-style detachment fold with influences from salt injection. Deformation of the anticline in this figure is the result of both compression and injection of overpressured salt/shale. The dips on the fold axial limbs decrease slightly up-section.

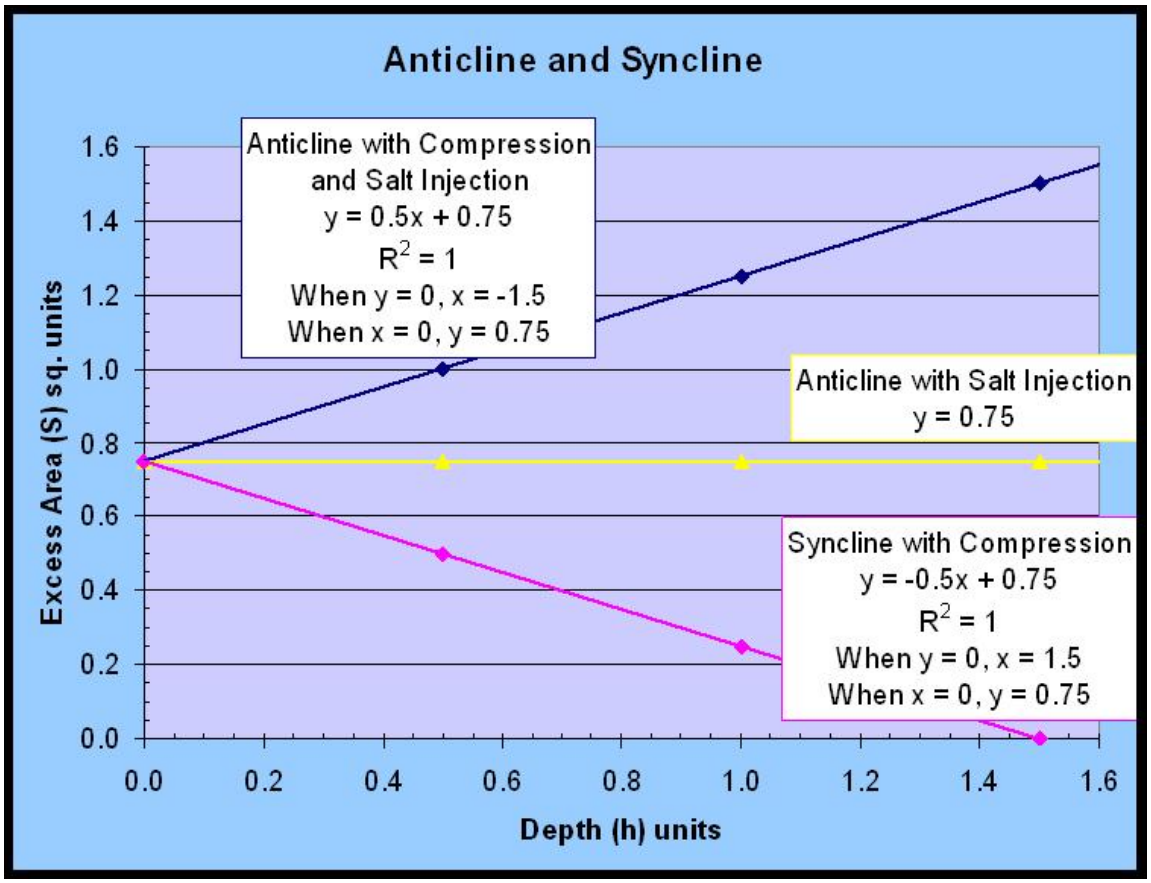

Figure 19: Excess area versus depth to detachment graph from new models. Displays: (1) an anticline with influences from both compression and salt injection (blue data points), (2) an anticline with only influences from salt injection (yellow), and (3) a "falling" compressed syncline (pink). The different data sets intersect at x = 0, and y = 0.75, which represents the amount of material that has migrated out from under the syncline into the core of the anticline.

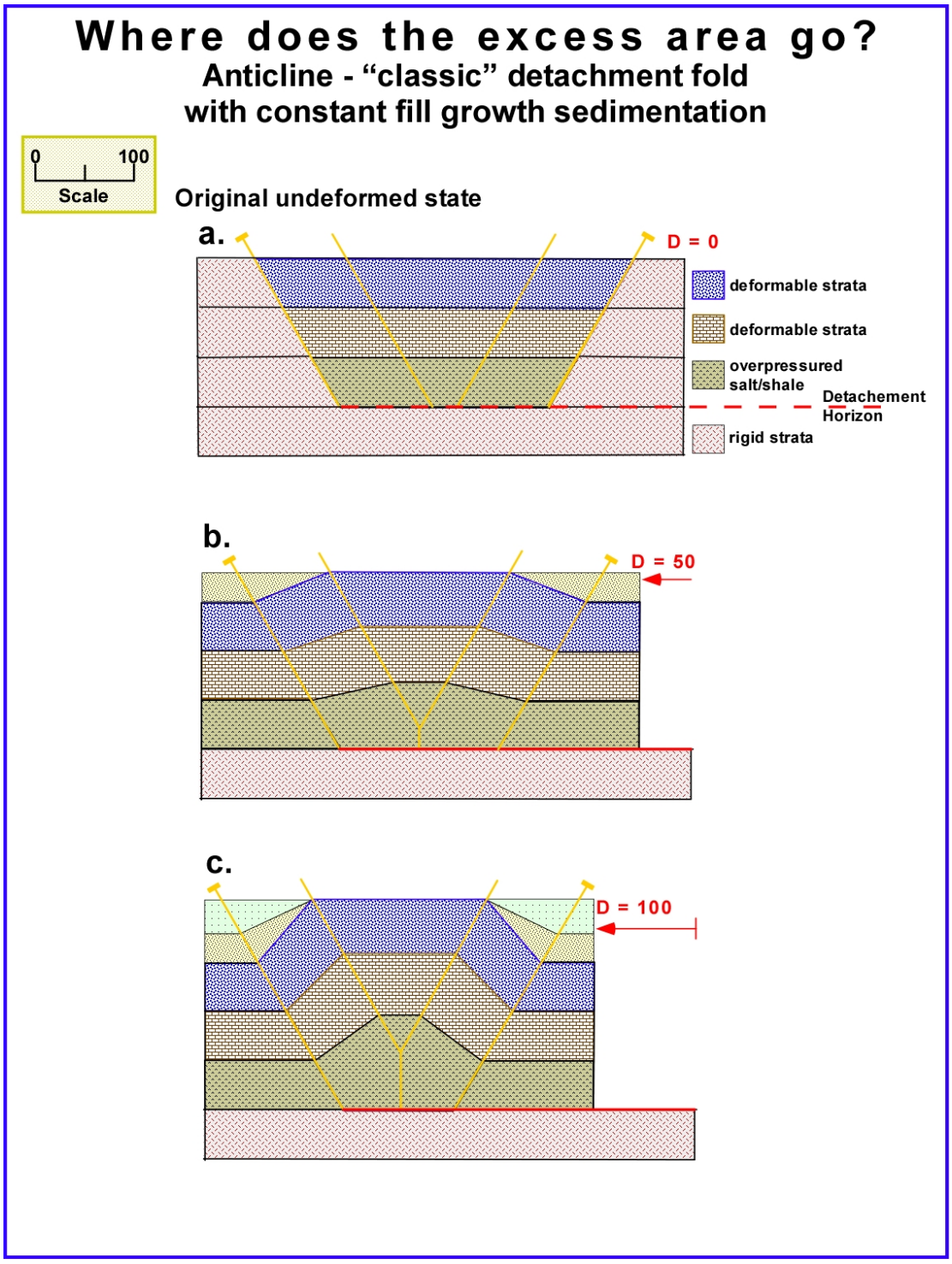

Figure 20: Geometric model of a classic box-type detachment anticline with constant over-fill growth sediments. Displacements = 0 (a.), 50 (b.), and 100 units (c.). Notice how each subsequent layer gains additional amplitude as it is folded.

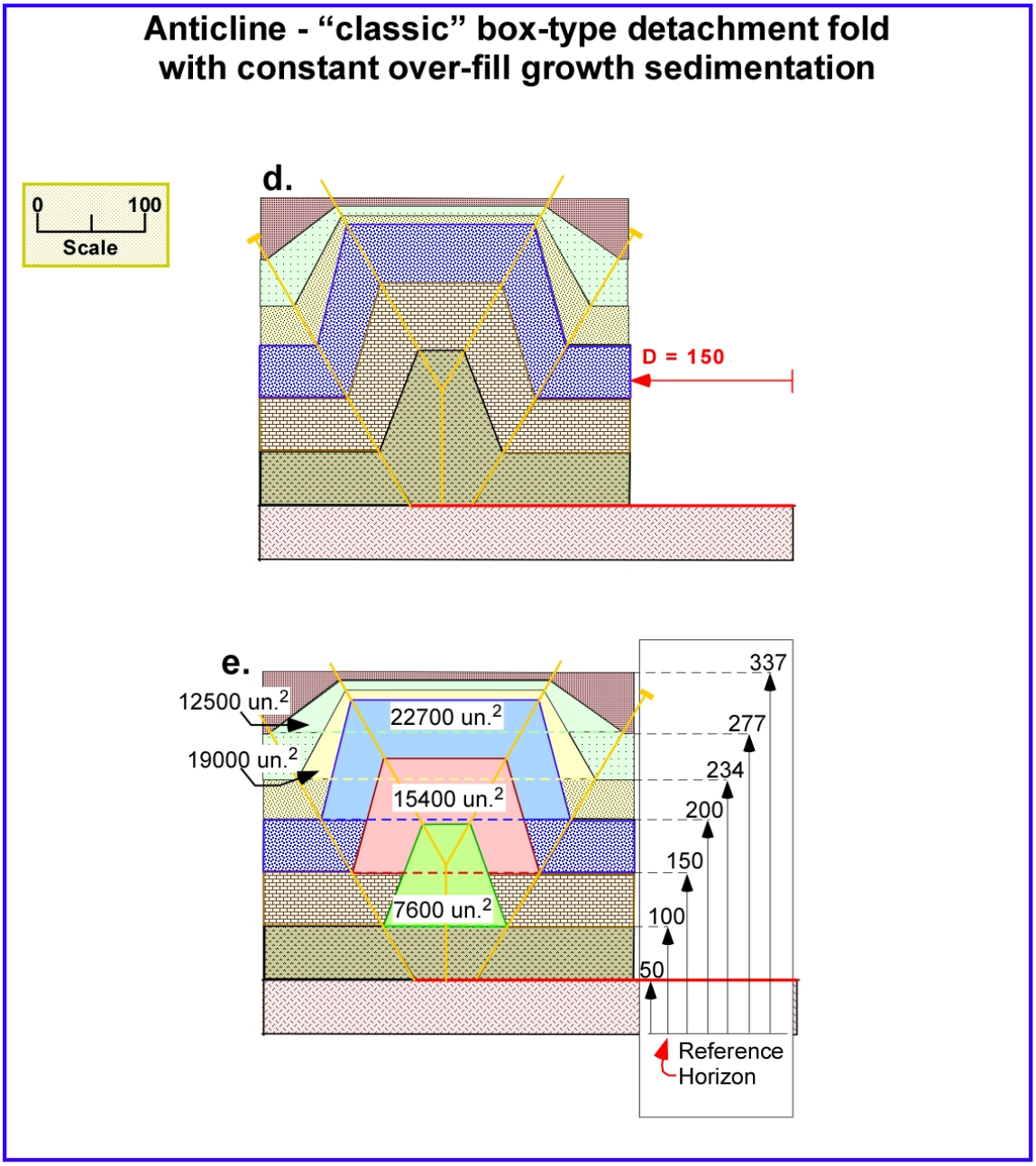

Figure 21: Geometric model of a classic box-type detachment anticline with constant over-fill growth sediments, with marked excess areas and depths. Displacement = 150 units, plus the excess area for each horizon identified. Continuation from figure 20. To the right of the figure is the marked amount of units to the top of each horizon above the reference horizon, along with the square units of excess area in each level.

displacement (b.), and (c.) represents a second layer of over-fill growth sediments after 100 units of displacement. With each amount of displacement, the subsequent growth layer(s) is folded. Figure 21 depicts step (d.), where a third layer of growth sediments have been added after 150 units of displacement. Part (e.) shows the same figure as in (d.), but with the amounts of material labeled that is elevated above regional for each horizon in square units. When the excess area data is plotted against the depth to the reference horizon, a graph is produced that shows the pre-growth and growth sediments (Figure 22). In this graph, the blue data points represent the pre-growth sediment, which shows a positive sloping line, and a perfect line of fit of the data ($R^2 = 1$). Also, this line intersects the depth intercept at 50 units, which is the location of the true detachment horizon. The pink data points represent growth sediments, and portray a negative sloping line. This variability shown in this data set is probably due to errors in rounding, along with difficulties presented by line widths and such. This small amount of error in a perfect model illustrates that the method still works when there are small errors introduced when interpreting non-perfect (seismic) data. The correct answer can easily be calculated in these models since these are perfect geometric shapes. The two lines, pre-growth and growth sediments, should intersect at the on-set of deformation, and the growth sediments should intersect the depth intercept (where excess area equals zero) at the point where folding stops.

The excess area method works perfectly with ideal (or perfect geometric) models. In this thesis I have attempted to take those concepts and apply them to the real data of the

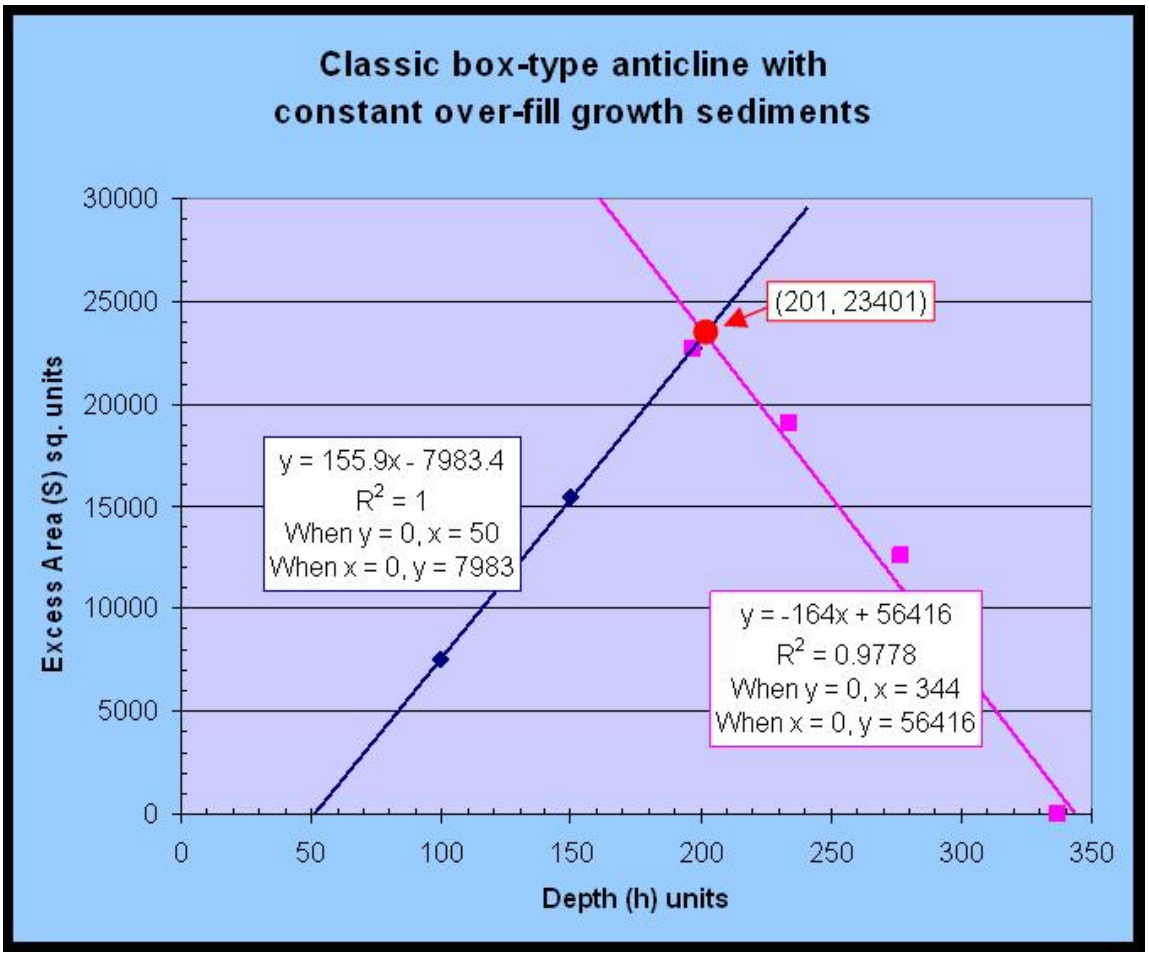

Figure 22: Excess area versus depth to detachment graph of a classic box-type detachment anticline with constant over-fill growth sediments. The blue data set represents pre-growth strata, which intersects the depth axis (where excess area = 0) at 50 units, which corresponds to the true depth of detachment found in figure 21. The pink data set represent growth sediments, and also intersects the depth intercept at approximately 340 units, which corresponds to the cessation of folding. The intersection of the pre-growth and growth sediment lines represents the onset of folding.

Perdido fold belt. Since the displacement is not known, an arbitrary reference horizon has been selected parallel to that of the “rail-road track” sedimentation of the abyssal plain in order to test the models for the known depth to detachment. In doing this, there is a built in assumption that the reference horizon and the lower detachment horizon are parallel. This may prove to be invalid in this study since units may thin basinward, and a new reference horizon might need to be determined.

In order to do these calculations, all data are acquired using Canvas Illustrator software. When evaluating a seismic line, I first find and mark a reference horizon that is parallel to the regional abyssal plain. I then mark the appropriate kink-band boundary/axial surfaces for each anticline and syncline. After this is completed, I interpret several horizons, and determine the excess area above or below regional associated with each, along with its relative distance from the arbitrary reference horizon. Each horizon is hidden from the others when being interpreted in order to reduce operator bias in the interpretation. The seismic background can then be removed, in order to look only at the excess area polygons. Since the excess areas and heights above the arbitrary reference horizon are marked in square inches and inches, respectively, on the computer screen, rather than that of miles or kilometers, each excess area display shows the appropriate conversion for one square unit into square miles. Once the data is collected, it is then put into Microsoft Excel, where it is graphed, fitted with a straight line and displayed with the equation for the line and R-value. Once in this setting, the data is available for interpretation.

Requisite Strain and Line Length Changes

An additional calculation that will be helpful in determining the timing and evolution of the PFB is that of requisite strain. Groshong and Epard (1994) define requisite strain (*e*) to be the amount of layer parallel strain required for the given cross-section to be area constant. However, layer-parallel strain is not required for area balance in all beds or in all folds. If bed length is constant ($L_0 = L_1$), then $e = 0$. The product of reorganizing equation (2) is (see Figure 13):

$$L_0 = W + D \tag{5}$$

where the original bed length (L_0) equals the width of the fold at regional for the stratigraphic unit of interest (W) plus the displacement (D). Groshong and Epard (1994) show that the layer-parallel strain is calculated from

$$e = (L_1 - L_0) / L_0. \tag{6}$$

An engineering convention is used when evaluating the layer-parallel strain. Positive values for *e* equate to original line length extension (tension) and negative values for *e* equal original line length shortening (compression). Figure 16 shows how the layer parallel strain changes as you move up section, in scenarios with differing amounts of displacements.

In summary, the methods defined by Groshong and Epard (1994) were used to determine layer-parallel and requisite strains within the individually interpreted horizons. Once the

data are acquired from the excess-area to depth of detachment calculations and plotted on a graph, D can determine by examining the slope of the pre-growth sediments. Values for h and S can also be read straight off of the plot. W can be determined by measuring the cross-sectional view of the fold in the seismic profile, along with L_1.

CHAPTER III

OBSERVATIONS

SEISMIC

Fold initiation can be seen by examining the growth strata and on-lapping reflectors using the extensive seismic interpretations. The following will outline the seismic profiles of these detachment folds, which are post-Jurassic in age (i.e. sediments overlying the Louann salt), along with identifying any other important aspects of the sediments. A composite line was created (Figures 23A, 23B) by splicing together four seismic lines that generally show the maximum compression in each of the folds. This composite generically summarizes the attributes of the PFB, but individual seismic lines where analyzed and compared in order to provide a more detailed and accurate interpretation.

Cretaceous (145 – 65.0 Ma)

Throughout the entire fold belt and basinward, Cretaceous sediments remain constant thickness. Seismically, this package of reflectors is outlined by a set of bold, regionally continuous, high amplitude reflectors (Figure 10). In the crests and troughs of folds the reflectors appear to be less clear and may be highly faulted and chaotic on a small (but seismic) scale, whereas, the reflectors elsewhere are parallel with generally good continuity.

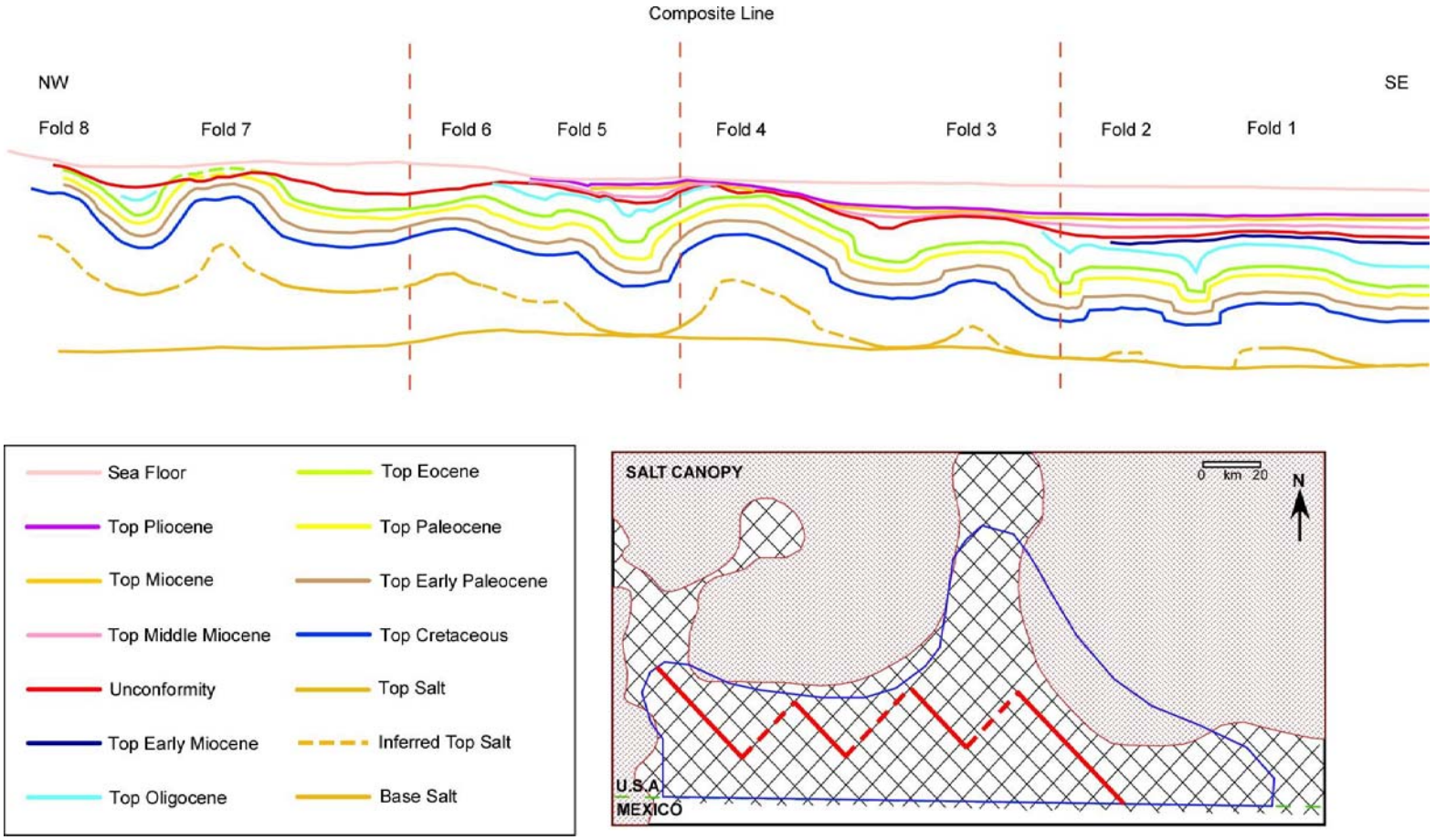

Figure 23A: Composite line of Perdido folds 1-8. Exhibits maximum shortening throughout fold belt, and was composed of four different TGS seismic lines which were spliced together and interpreted on age dated reflectors. At the boundaries between seismic lines, some modification was done in order to have one continuous line. This composite profile provides a general overview of deposition of sediments across the fold belt, and partially into abyssal plain. The map provided shows the locations of the seismic lines used in this composite; the bold red portion represent actual interpreted lines, the dashed red lines are the connections between the lines.

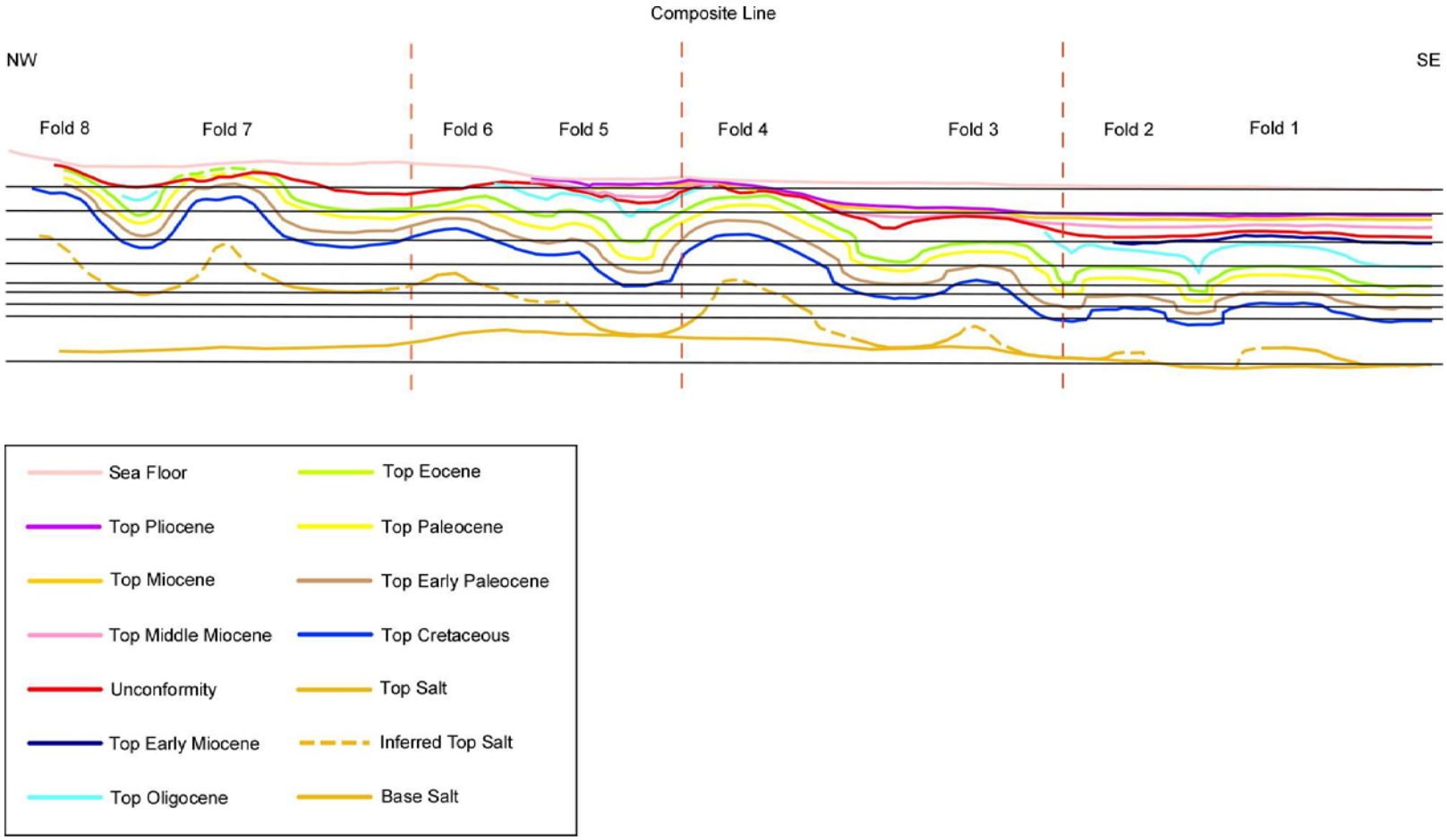

Figure 23B: Composite line of Perdido folds 1-8 compared to regional elevation. As described in figure 23A, along with the regional markers leveled with reflectors in the abyssal plain

Early Paleocene (65.0 – 60.9 Ma)

Overlaying the Cretaceous sediment is a package of sub-parallel reflections (Figure 10). The distinction between early Paleocene and Paleocene strata is not as clearly defined as the boundaries between that of the Cretaceous. Across fold 8 there are observed on-laps of early Paleocene sediments onto the flanks. The entire package thins over fold 8 and is highly faulted.

Paleocene (60.9 – 54.7 Ma)

Similar to that of early Paleocene reflectors, the Paleocene strata on-lap and thin over fold 8. This package also contains hummocky to sub-parallel reflectors, which are generally moderate to low amplitude. The package is bounded at the top by a high amplitude reflector.

Eocene (54.7 – 33.7 Ma)

Rocks deposited between 54.7 and 33.7 million years ago thin greatly over folds 7 and 8, and remain constant thickness elsewhere, with possible thinning to the east. Located in the synclines between folds 1 and 2, 2 and 3, 3 and 4, and 4 and 5, there is a detachment of sediment (presumably on the Jackson shale) at the top of the section, which results in an undulated and thrusted bed out of the synclines, and occasionally an additional box type fold on top of the previous structure (Figure 24). In general, the reflectors are discontinuous with moderate to high amplitudes with parallel to hummocky beds. This stratum appears similar in structure to that of Paleocene strata.

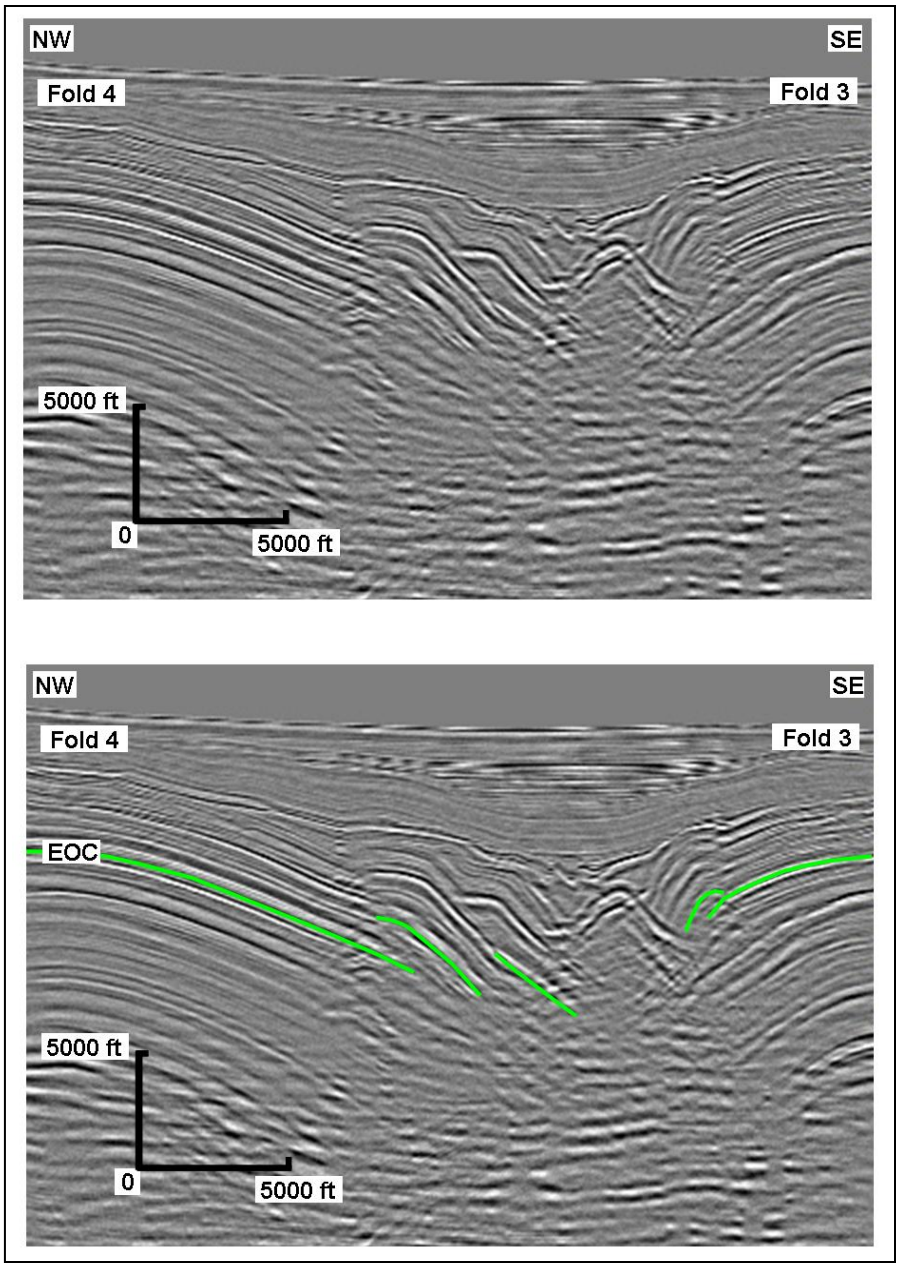

Figure 24: An uninterpreted and interpreted seismic profile displaying a detachment upon Eocene strata. Green marker represents the top of the Eocene strata, which thrust out of the tight syncline between folds 3 and 4. Similar features found in syncline between folds 1 and 2, 2 and 3, 4 and 5. Seismic data are owned by TGS-NOPEC, all images of the data have been reproduced with their written permission.

Oligocene (33.7 – 23.8 Ma)

Oligocene strata on-laps onto the flanks of folds 7 and 8, thin substantially over fold 6, and are constant thickness over folds 1 through 5. Similar to Eocene strata, in the synclines between folds 1 and 2, 2 and 3, 3 and 4, and 4 and 5, there is a detachment of sediment at the top of the section (possibly on the Anahuac shale), which results also in an undulated and thrusted bed out of the synclines. However, there is not as much deformation here as in that of the Eocene. The reflectors are mostly moderate to high amplitudes, parallel and laterally continuous. Occasionally the reflectors become hummocky and chaotic.

Early Miocene (23.8 – 15.6 Ma)

Due to a regionally extensive unconformity, only the most basinward limits of early Miocene strata can be easily observed, and are not seen west of fold 4. This package of sediment thins substantially over and on-laps folds 3 and 4, along with thinning over fold 1, and in some places on-laps fold 2 (Figure 10). This package of sediment appears to thicken to the east, which is the opposite of all prior sediments which appear to thin to the east. These rocks not only thicken in the synclines between folds 3 and 4 but also over the crest of fold 2. The reflectors are generally low amplitude, parallel and laterally continuous.

Middle Miocene (15.6 – 11.0 Ma)

At some point between the early and middle Miocene, a regional unconformity occurred that eroded down through the Eocene strata on fold 8, possibly down through the early Paleocene at fold 7, through Oligocene west of the crest of fold 6, and removed all of the early Miocene west of fold 4 (Figure 25). This unconformity was then deformed due to continued folding and compression in the area. It was then followed by an episode of deposition which on-laps the unconformity on the basinward (east) flanks of fold 6 and both flanks of fold 4. Middle Miocene sediment can then be traced basinward of fold 4 out into the flat parallel reflectors in the basin. In general, the reflectors are low amplitude, parallel and laterally continuous, but there are areas where hummocky to chaotic reflectors are observed, along with several slump features off of the crest of some of the anticlines.

Late Miocene (11.0 – 5.8 Ma)

Late Miocene strata are not as regionally extensive as some of the preceding strata. These sediments are observed to on-lap fold 5 from the east and on-lap the unconformity on both flanks at fold 4. It then continues basinward, thinning greatly over fold 3, and remains constant thickness over folds 1 and 2. The reflectors are low amplitude, parallel and laterally continuous.

Pliocene (5.8 – 2.85 Ma)

The typical reflector observed is moderate to low amplitude and parallel to sub-parallel.

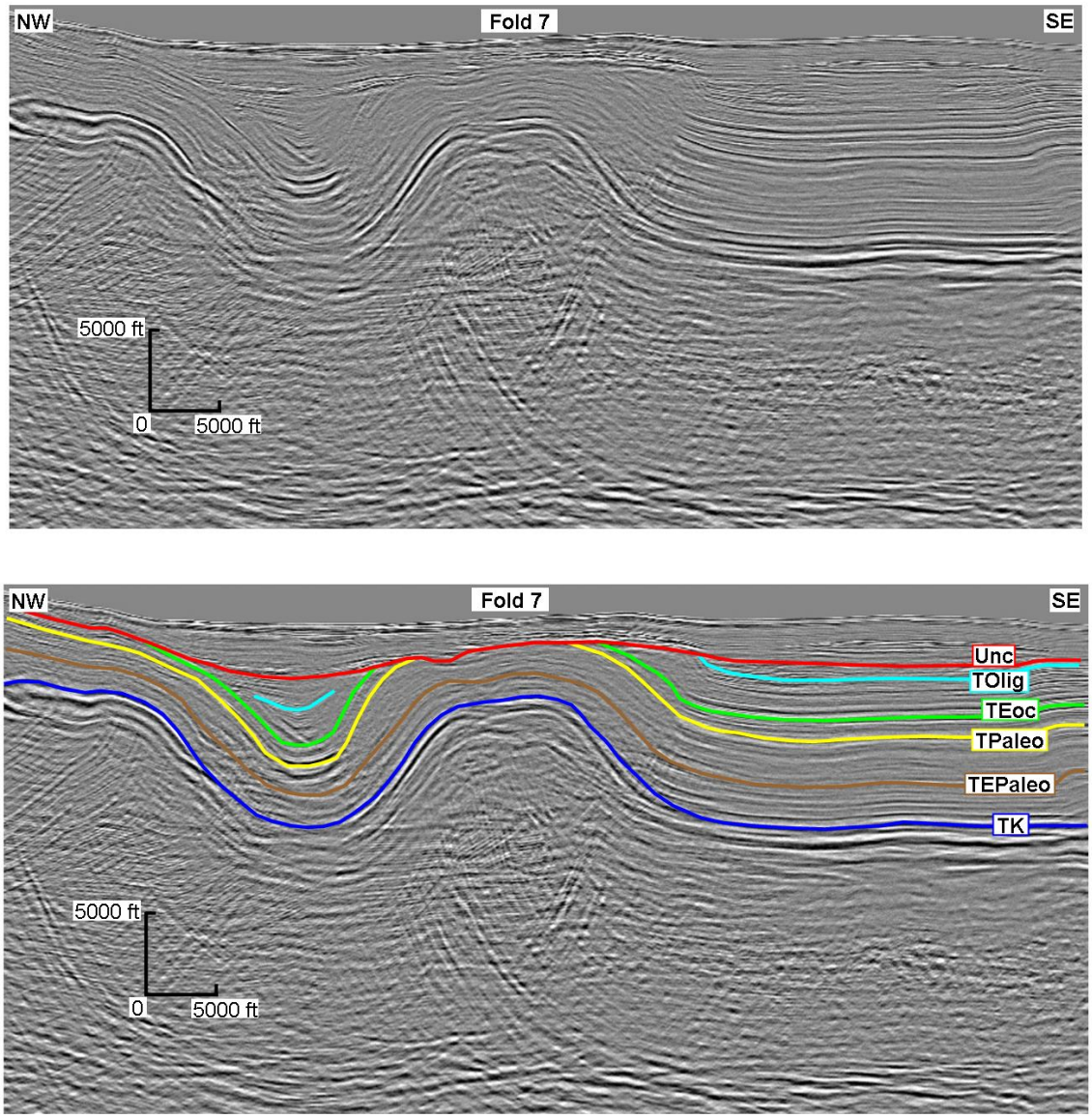

Figure 25: Uninterpreted and interpreted seismic profile displaying a regional unconformity. This unconformity has been folded by subsequent compression. All horizons are labeled. Seismic data are owned by TGS-NOPEC, all images of the data have been reproduced with their written permission.

Besides thinning some over fold 5 and on-lapping the basinward flank of fold 6, Pliocene strata seem to be constant thickness over folds 1 through 4. Due to the occasional infiltration of allochthonous salt and the low amplitude reflectors over folds 5 through 8, Pliocene strata are difficult to interpret.

Water bottom (2.85 Ma – Present)

Sediments between the water bottom and the top of the Pliocene thin over the crest of folds 3 through 8, with bathymetric expressions of the anticlines clearly visible above folds 4 through 8. The sediment over folds 1 and 2 are regionally flat and maintain a constant thickness. The variably continuous reflectors are mostly moderate to low amplitude, hummocky to chaotic, with interspersed parallel reflectors.

GEOMETRIC MODELS

Excess Area vs. Depth to Detachment

As mentioned in the methods chapter (Chapter II), the depth to detachment (h) and excess area (S) data are plotted on an x-y graph, respectively. The excess area data has been acquired for folds 1, 2, 3, 4 and 7, along with the synclines between folds 1 and 2 (labeled syncline 1), and also between folds 2 and 3 (labeled syncline 2). The more extensive evaluations and model building have revolved around folds 1 and 2, and the inclusive syncline. Folds 3 and 4 were attempted, but due to their shapes, which have been tilted and partially elevated above regional strata, estimating regional becomes

difficult. The more westward folds (6-8) are also elevated well above regional. Similarly, fold 7 was attempted, but difficulties arise when regional is estimated for the folds. This data is presented below.

Due to the large unconformity above early Miocene sediments and several non-continuous reflectors that do not cover the fold crest, many strata reflectors are not interpreted between the upper pregrowth and lower growth strata sections. However, the intersection between the upper pregrowth (late Oligocene) and lower growth (up to middle Miocene) sections on the excess area plot still constrains the time of fold initiation, and based on the interpretation of the on-lap relationships, it actually gives the correct time of fold initiation. Many of the late stage growth sediments are easily interpreted, and can be followed for great distances. These reflectors are interpreted as late stage growth sediments, and the early growth phase was interpolated with the use of a linear line that was fit to this data.

Fold 1

Two non-adjacent seismic lines where interpreted to include fold 1 (Figures 26, 27). Although the details of the results vary slightly, the overall conclusions are the same. Initially, in seismic profile (A), the curves are positively sloping from the lower levels of sediment (Cretaceous) up to a particular point in the sediment column located near the Oligocene marker, with some significant scatter that results in 2 different scenarios. In seismic profile (A), scenario (1) employs a single linear line of fit (R^2) to these data

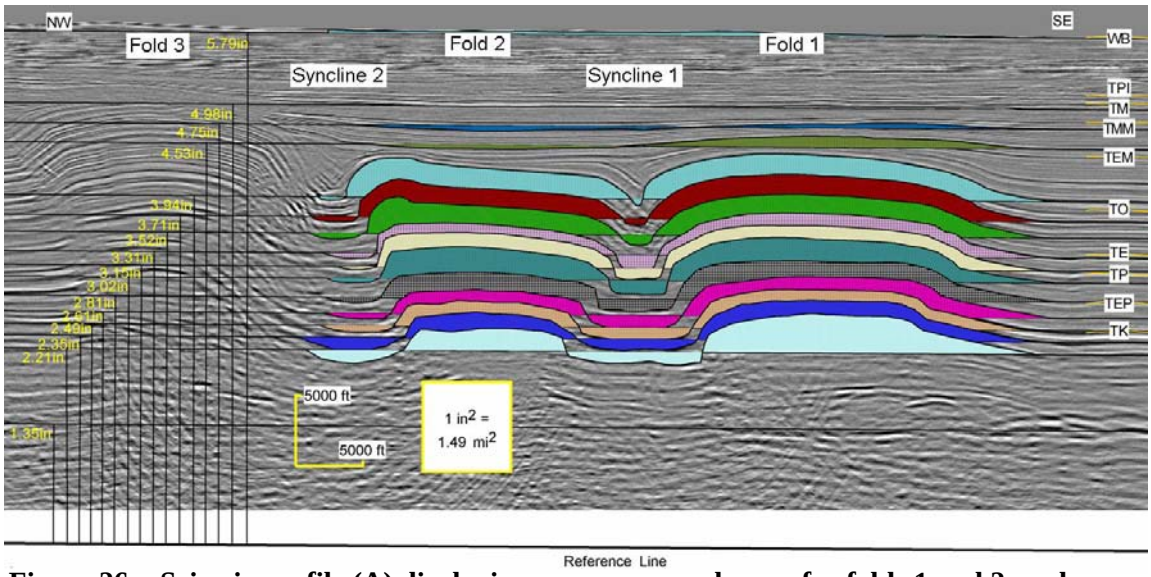

Figure 26a: Seismic profile (A) displaying excess area polygons for folds 1 and 2, and syncline 1 and 2. The right hand border displays the reflectors corresponding to identified horizons (orange). The leftward portion of the diagram displays the units above the arbitrary reference horizon (labeled in yellow). Seismic data are owned by TGS-NOPEC, all images of the data have been reproduced with their written permission.

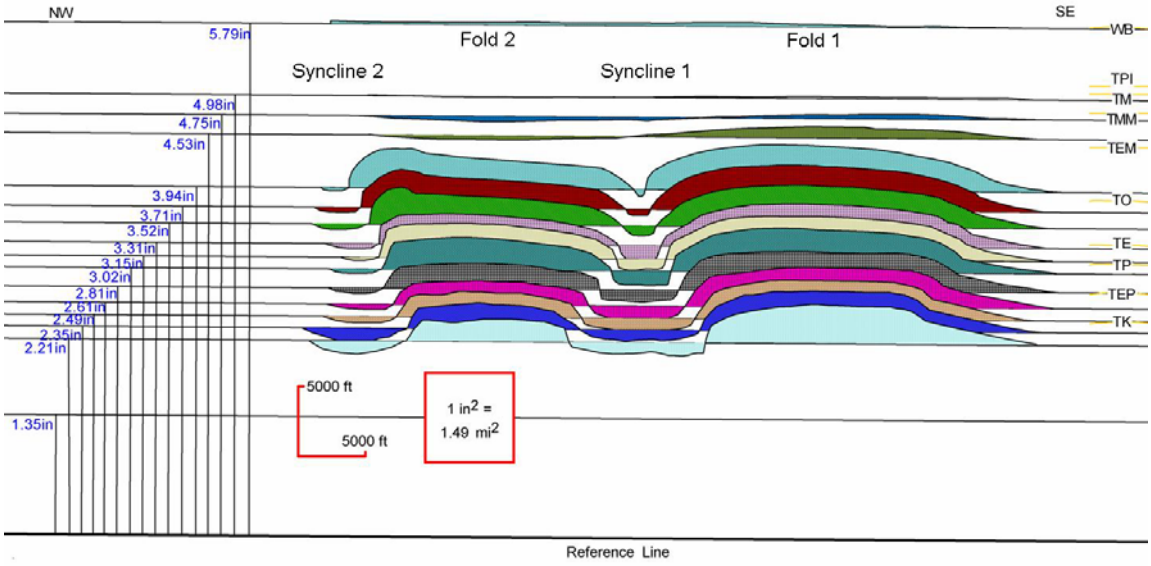

Figure 26b: Profile (A) displaying excess area polygons for folds 1 and 2, and syncline 1 and 2, without the seismic background. The right hand border displays the reflectors corresponding to identified horizons (orange). The leftward portion of the diagram displays the units above the arbitrary reference horizon (labeled in blue).

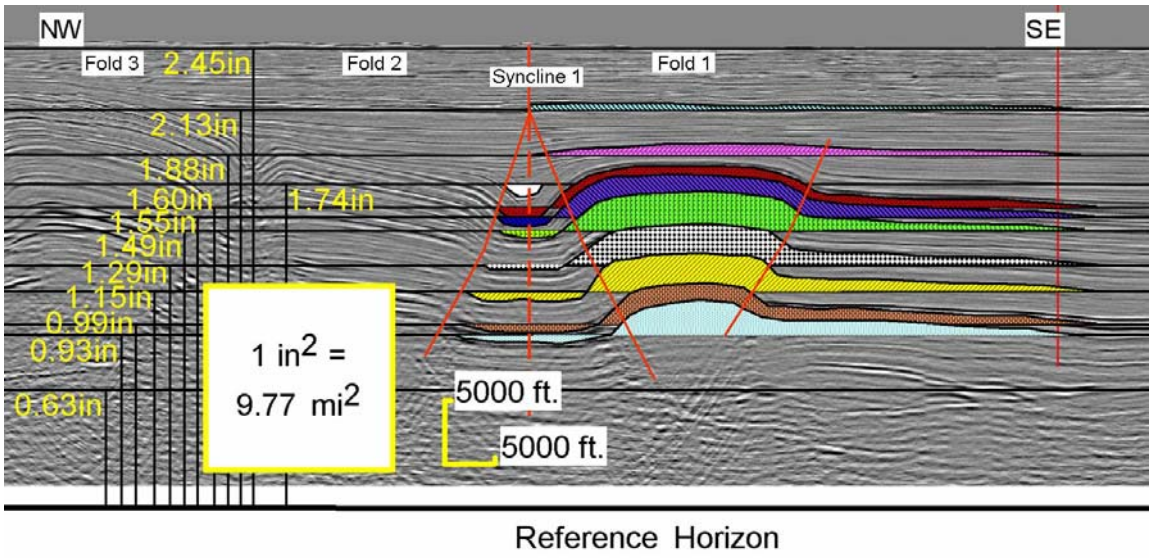

Figure 27a: Seismic profile (B) displaying excess area polygons for fold 1 and syncline 1. The leftward portion of the diagram displays the units above the arbitrary reference horizon (labeled in yellow). Seismic data are owned by TGS-NOPEC, all images of the data have been reproduced with their written permission.

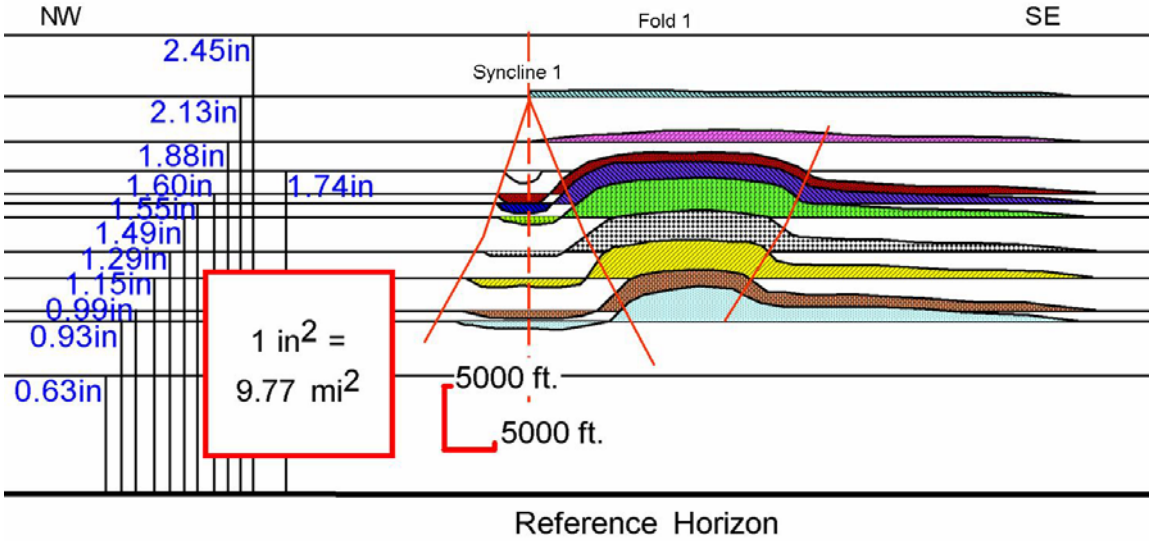

Figure 27b: Profile (B) displaying excess area polygons for fold 1 and syncline 1, without the seismic background. The leftward portion of the diagram displays the units above the arbitrary reference horizon (labeled in blue).

points which equals 0.9264, with an equation of y = 0.2697x + 0.4804 (Figure 28). When y = 0, x = -1.530, and when x = 0, y = 0.462. The displacement of the sediment (D), gathered from the slope of the line, is 0.3019. In this scenario (1), where the data is fit with one linear line, strata around the Paleocene marker seem to have more area than expected, and layers in the early Oligocene have slightly less. If the same points in seismic profile (A) are fit with two linear lines (scenario 2), then R^2 = 0.9744 for the deeper sediments (older than Eocene) and an equation of y = 0.4323x + 0.1303 (when y = 0, x = -0.301, and when x = 0, y = 0.1303) is obtained (Figure 29). For the younger sediments (Eocene through early Miocene), R^2 = 0.9075 and y = 0.349x + 0.264, which can be solved for x when y = 0 (x = -0.756) and when x = 0, y = 0.264 (Figure 29). Due to the differing slopes of these two lines, there are two different displacements. The older sediments appear to have shortened more with D = 0.4323, and the younger sediments less with D = 0.349. The line of fit is not perfect (where R^2 = 1) for either, and there is some scatter between the data points as previously mentioned. After reevaluating some of these anomalies, I noticed that most of these incidences occur near the same locations in relation to the strata. This location is the dividing measure between scenarios (1) and (2). After going back and carefully reviewing the seismic data, it has been determined that at around this stratigraphic level there is a definite change in fold axial surface style. Rather than there being one single, linear fold limb, which was the initial thinking when making these interpretations, there are a minimum of two fold axial surfaces on each limb. The upper units coincide with consistently steeper fold axial surfaces, while the lower units fit less steeply dipping axial surfaces (Figure 30). This

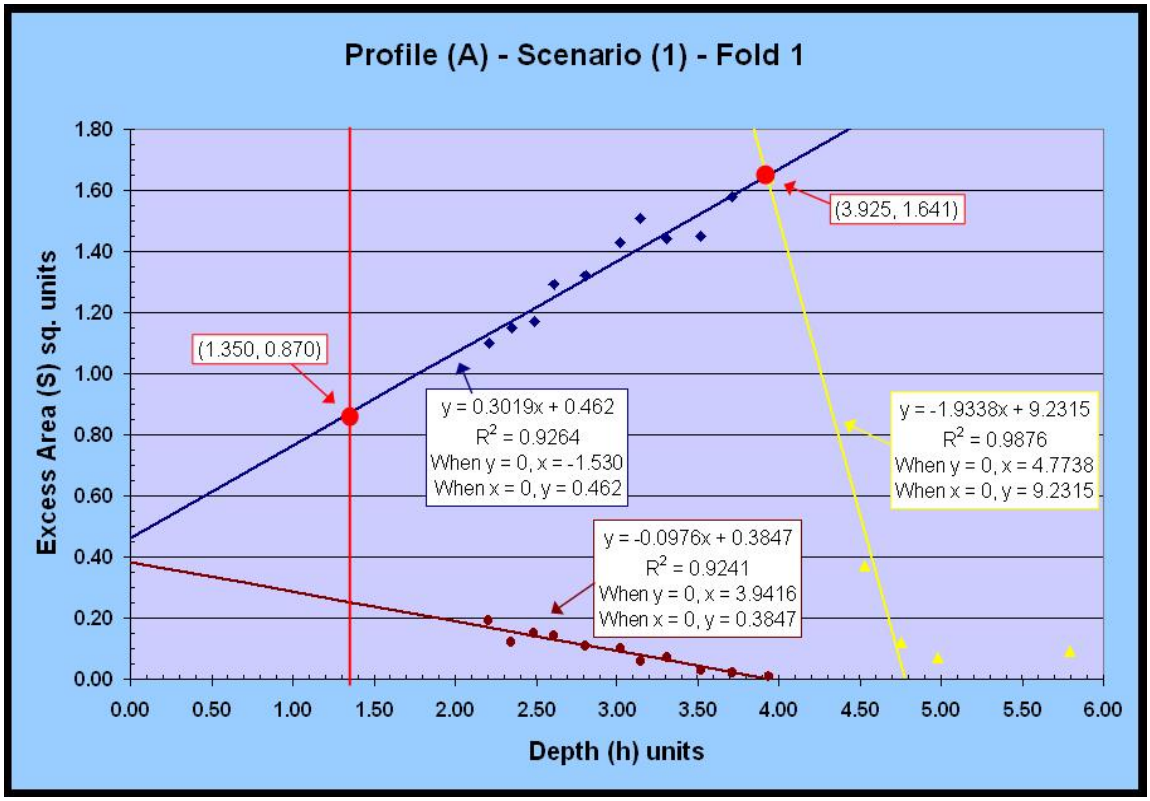

Figure 28: Excess area vs. Depth to detachment graph for seismic profile (A), scenario (1), fold 1. Blue data points represent pre-growth sediments, yellow represent growth sediments, and the maroon represents data points for syncline 1. The known depth to detachment is 1.35 units above the arbitrary reference horizon, shown with a red vertical line.

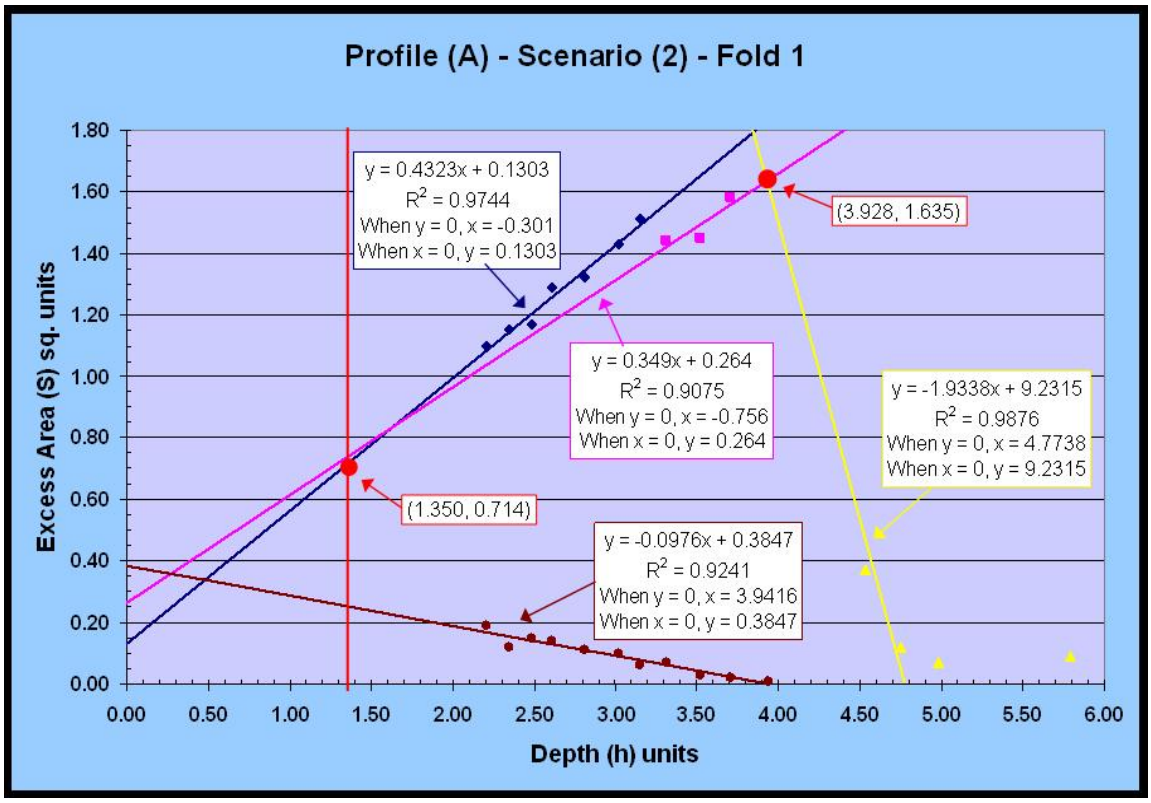

Figure 29: Excess area vs. Depth to detachment graph for seismic profile (A), scenario (2), fold 1. Blue data points represent pre-growth sediments Cretaceous to Eocene in age, pink points represent pre-growth sediments from Eocene to early Miocene, yellow represent growth sediments, and the maroon represents data points for syncline 1. The known depth to detachment is 1.35 units above the arbitrary reference horizon, shown with a red vertical line.

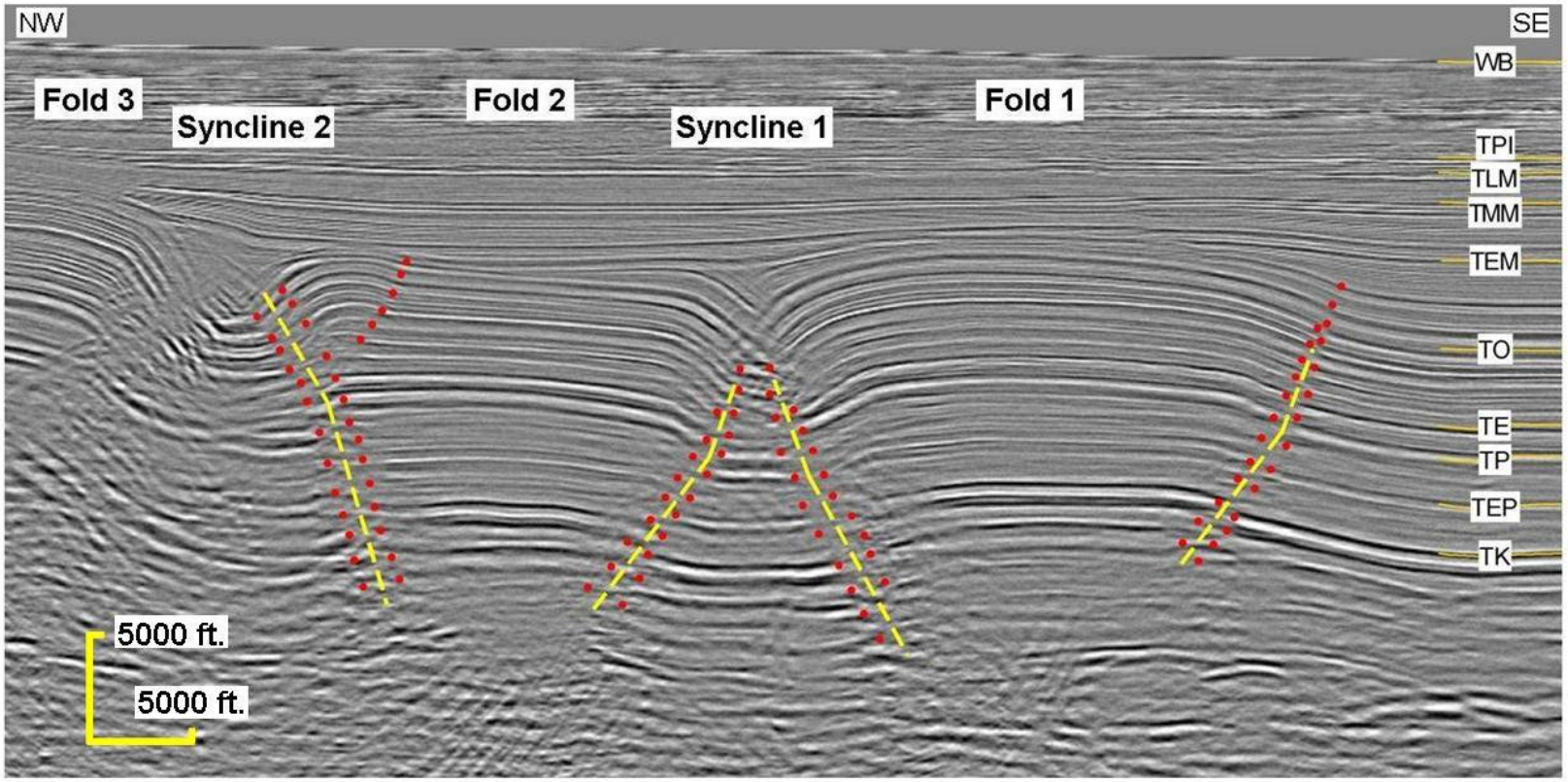

Figure 30: Seismic profile displaying kinked fold axial surface geometry. Red dots represent the limits of the tabular kink bands on seismic, and the yellow dashed line shows the approximate location and shape of the fold axial surfaces. Seismic data are owned by TGS-NOPEC, all images of the data have been reproduced with their written permission.

new found data was compared against the stratigraphic columns (Figures 4A, 4B), which shows that this abrupt change in style corresponds to a difference in sediment type. The lower units, which has less steeply dipping fold limbs, corresponds to mostly marine origin carbonates, a majority of which are deep water deposits (previously described as carbonate dominated, fine grained and muddy). The upper units correspond to channelized turbidites and other deep-water deposits, composed of mostly fine grained siliciclastic sands.

The depth to detachment should be shown as the point on the depth intercept where excess area equals zero. However, in this case, the depth to detachment is known to be at approximately 1.35 units. At this location on the graphs (Figures 28, 29), there is still approximately an area of 0.870 square units in scenario (1), and for scenario (2), 0.714 square units. An explanation for this will be given in the following chapter: Interpretations and Discussions (Chapter IV).

Next, the excess area of sediments younger than Oligocene are plotted on the graph, which exhibit a different behavior. These sediments, up to near water bottom, correspond to a steeply dipping negative sloping line (Figures 28, 29). As previously mentioned, due to the unconformity and the large amount of on-lapping strata, only three major data points are plotted between the Oligocene and late Miocene in seismic profile (A). When a straight line is fit to this data, $R^2 = 0.9876$, with $y = -1.9338x + 9.2315$. The intersection of this line with the one described in scenario (1) give (x, y) coordinates of

(3.925, 1.641), which is located at roughly the bottom of the Oligocene stratum. When scenario (2) is solved for the intersection, the intersection point between the negative sloping line and the positive sloping line associated with the younger sediments equals (3.928, 1.635). These values are very similar to that found in scenario (1), and also correspond to that of early Oligocene strata. Also, this negative sloping line terminates against the depth intercept at roughly the end of the early Miocene, or just at the beginning of the middle Miocene strata.

Figure 27 exhibits seismic profile (B), which gives results that are only slightly different from profile (A). Due to seismic resolution and data quality, the excess area data for fold 1 on this line is a little more difficult to interpret since there is more scatter in the plot (Figure 31). The positive sloping line of fit has an $R^2 = 0.7908$, and an equation yielding $y = 0.1142x + 0.1292$. It is hard to determine from the data if there is a second possible line that could be fit to the data, as in profile (A). Thus, only a single scenario or a single line is fit to the data. When $y = 0$, $x = -1.313$ and when $x = 0$, $y = 0.1292$, also giving the displacement to equal 0.1142. The negative sloping line is composed of only two data points, thus giving an $R^2 = 1$. The equation for this line is $y = -0.8929x + 1.7486$, so when $y = 0$, $x = 1.958$ and when $x = 0$, $y = 1.7486$. In the same way as calculated in profile (A), the intersection of the positive and negative sloping lines equals (1.608, 0.313), which corresponds to sediments early Miocene in age.

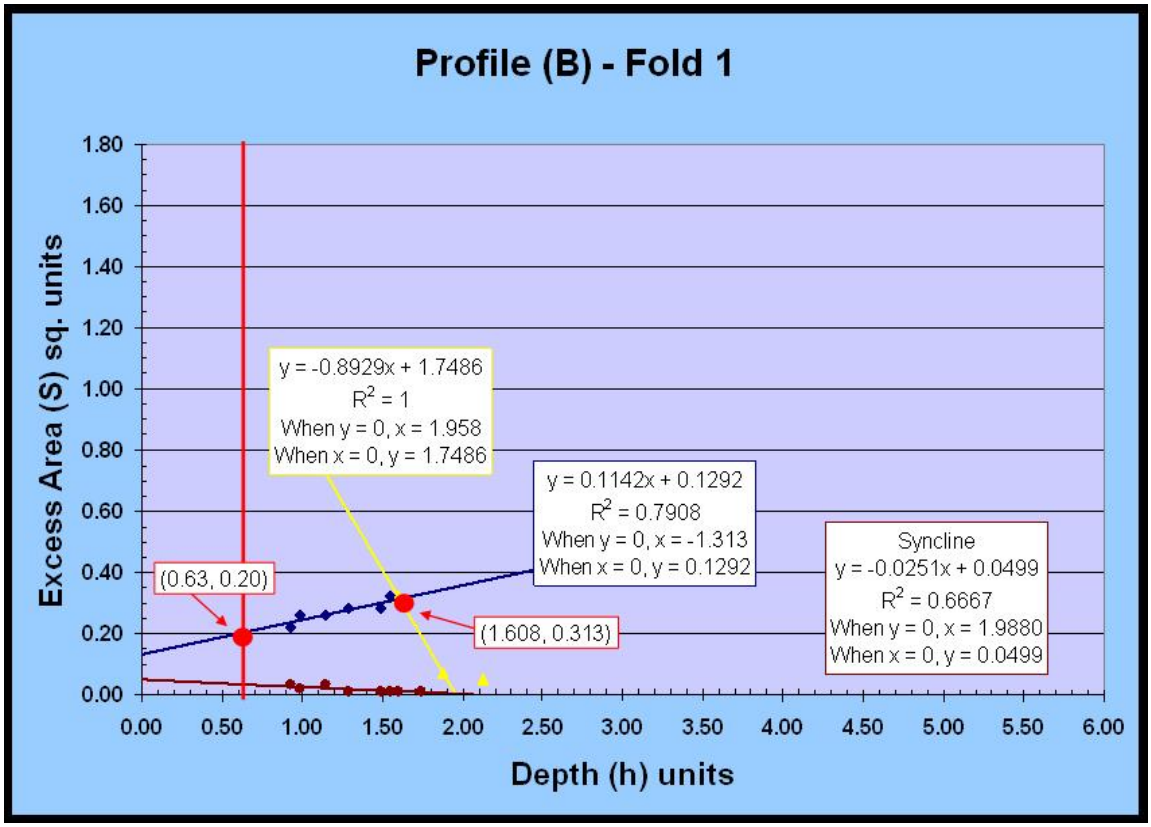

Figure 31: Excess area vs. Depth to detachment graph for seismic profile (B), fold 1. Blue data points represent pre-growth sediments, yellow represent growth sediments, and the maroon represents data points for syncline 1. The known depth to detachment is 0.63 units above the arbitrary reference horizon, shown with a red vertical line. The same graphical scale is used as in Profile (A).

Fold 2

Seismic profile (A) was again used in the determinations of excess area in fold 2, and similarly has two different scenarios (Figure 26). Scenario (1) uses a single linear line to fit the data, yielding in $R^2 = 0.9196$, and $y = 0.345x – 0.3596$ (Figure 32). When $y = 0$, $x = 1.042$, and when $x = 0$, $y = -0.3596$. The displacement calculated in scenario (1) equals 0.345. Scenario (2) employs the technique of two lines to fit the data, similar to fold 1 (Figure 33). In this case, the older sediment, Cretaceous to Eocene has an $R^2 = 0.9415$, and an equation $y = 0.4852x – 0.7148$. Thus, when $y = 0$, $x = 1.4732$ and when $x = 0$, $y = -0.7148$, and $D = 0.4852$. The younger sediment, Eocene through early Miocene, has a displacement of 0.4381, an $R^2 = 0.9743$ and an equation of $y = 0.4381x – 0.7285$. Solving for $y = 0$ results in $x = 1.6629$, and $x = 0$ yields $y = -0.7285$.

Syncline between folds 1 and 2 – Syncline 1

Data points collected from the syncline between folds 1 and 2 are plotted on the same graph as fold 1, and are plotted as positive values (Figures 28, 29, 31). Even though these excess areas are below regional and should be negative values, plotting them as positive values creates a line with a negative slope that intersects the pre-growth sediment line of the folds. This technique also displays the amount of material which has been displaced from underneath the syncline. Similar to fold 1, data has been acquired from the syncline from two non adjacent seismic lines: the same ones used in the analysis of fold 1 (Figure 26, 27). The analysis of seismic profile (A) offers a line of fit to be 0.9248, and gives the equation $y = -0.0976x + 0.3847$. When $y = 0$, $x = 3.9416$, and

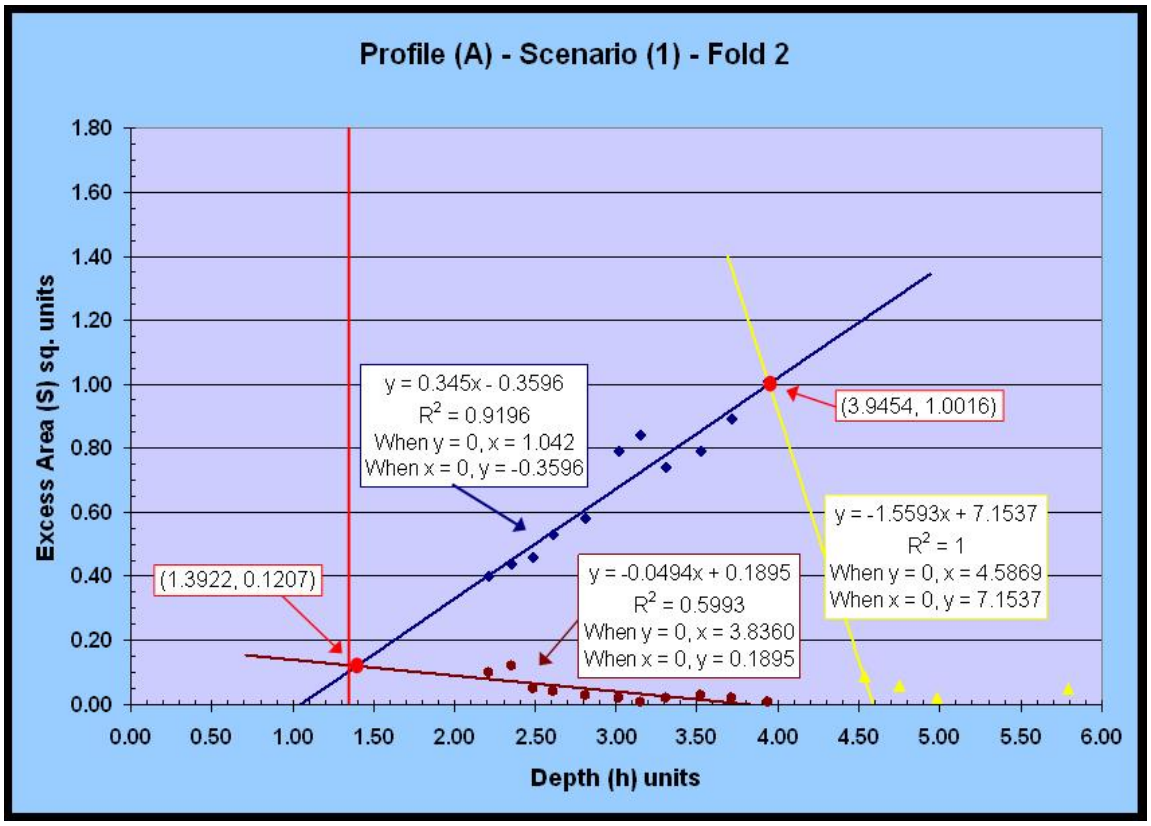

Figure 32: Excess area vs. Depth to detachment graph for seismic profile (A), scenario (1), fold 2. Blue data points represent pre-growth sediments, yellow represent growth sediments, and the maroon represents data points for syncline 2. The known depth to detachment is 1.35 units above the arbitrary reference horizon, shown with a red vertical line.

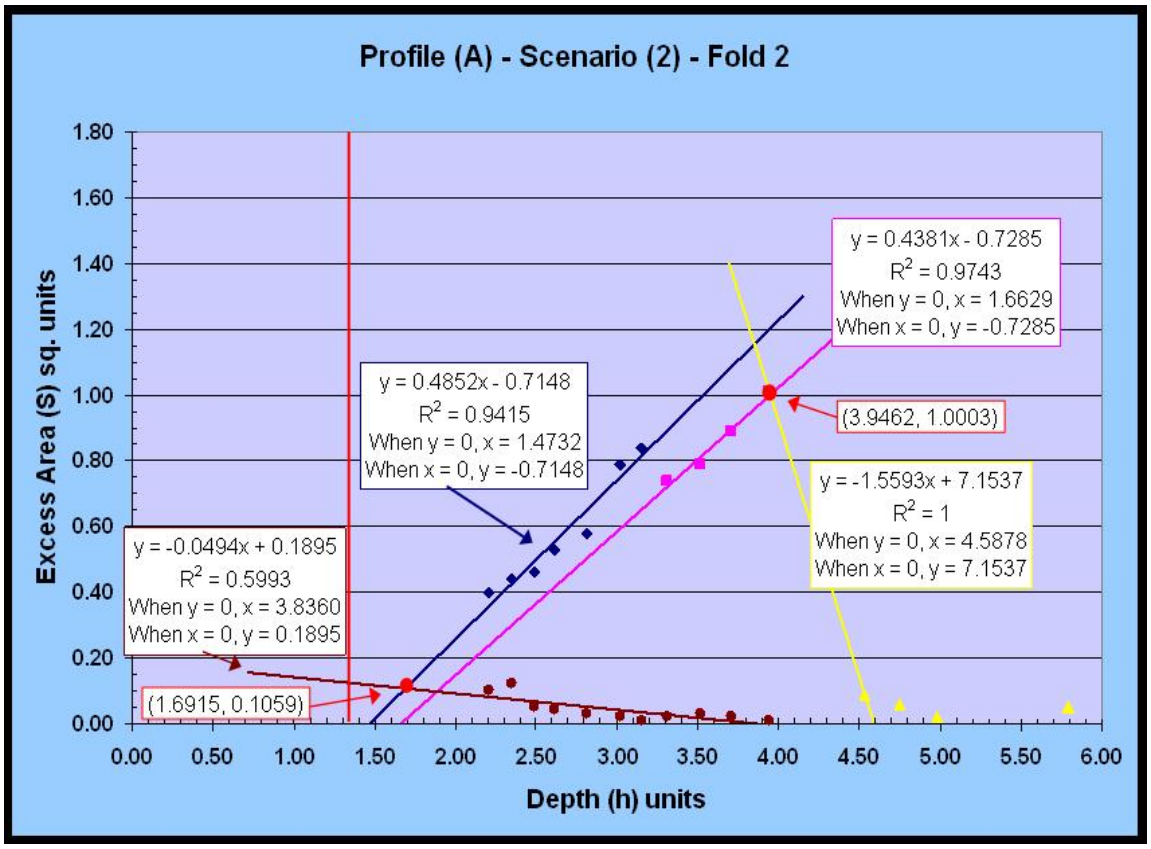

Figure 33: Excess area vs. Depth to detachment graph for seismic profile (A), scenario (2), fold 2. Blue data points represent pre-growth sediments Cretaceous to Eocene in age, pink points represent pre-growth sediments from Eocene to early Miocene, yellow represent growth sediments, and the maroon represents data points for syncline 2. The known depth to detachment is 1.35 units above the arbitrary reference horizon, shown with a red vertical line.

when x = 0, y = 0.3847. Seismic profile (B) has a lot more scatter, yielding R^2 = 0.6667, and an equation of y = -0.0251x + 0.0499. When y = 0, x = 1.9880, and when x = 0, y = 0.0499.

Fold 3

Fold 3 is analyzed on a third seismic profile, (C), which is not long enough to accurately represent regional (Figure 34). Regional for this profile was set to the bottom of the synclines, rather than the abyssal plain sediments. Because of this, the area added to this anticline can not be accurately assessed without further work to determine a true value for regional. This data only uses the line of fit for a singular event (Figure 35). This line fits the data well, with R^2 = 0.9561 and an equation of y = 0.666x – 0.229. When this equation is solved for the x and y intercepts, x = 0.3438 when y = 0, and when x = 0, y = -0.229. The growth sediments also display a line with a steeper negative slope, as seen in folds 1 and 2. Only three excess areas could be determined on this profile, but when fit to a line, the data give R^2 = 0.9916 and y = -1.2977x + 3.6711. When y = 0, x = 2.8290, and when x = 0, y = 3.6711. The (x, y) intersection of these two lines is (1.986, 1.094).

Syncline between folds 2 and 3 – Syncline 2

Data points collected from the syncline between folds 2 and 3 are plotted on the same graph as fold 2, and are plotted as positive values (Figures 32, 33) similar to syncline 1. As described with syncline 1, the line created has a negative slope that intersects the pre-growth sediment line of the folds. Data has been acquired from the syncline from

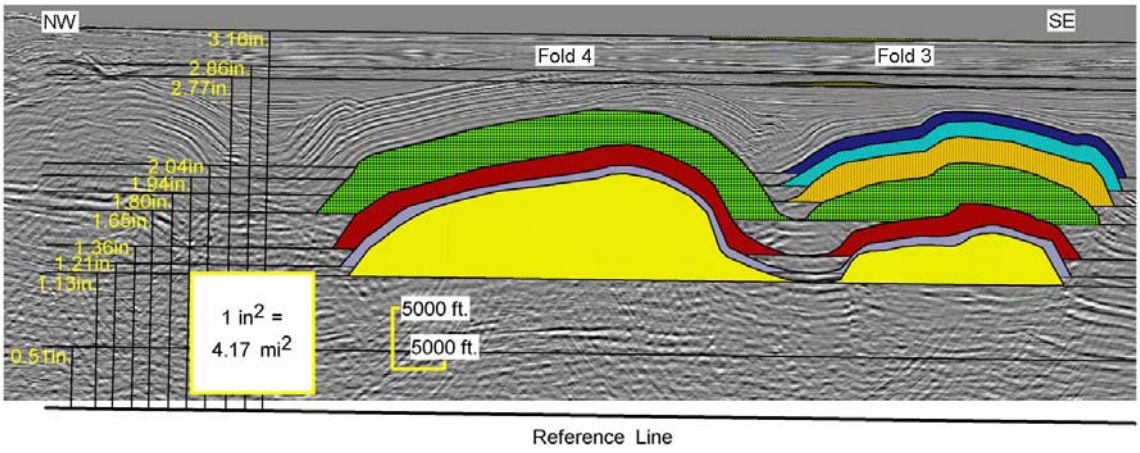

Figure 34a: Seismic profile (C) displaying excess area polygons for folds 3 and 4. The leftward portion of the diagram displays the units above the arbitrary reference horizon to the base of the syncline (labeled in yellow). Seismic data are owned by TGS-NOPEC, all images of the data have been reproduced with their written permission.

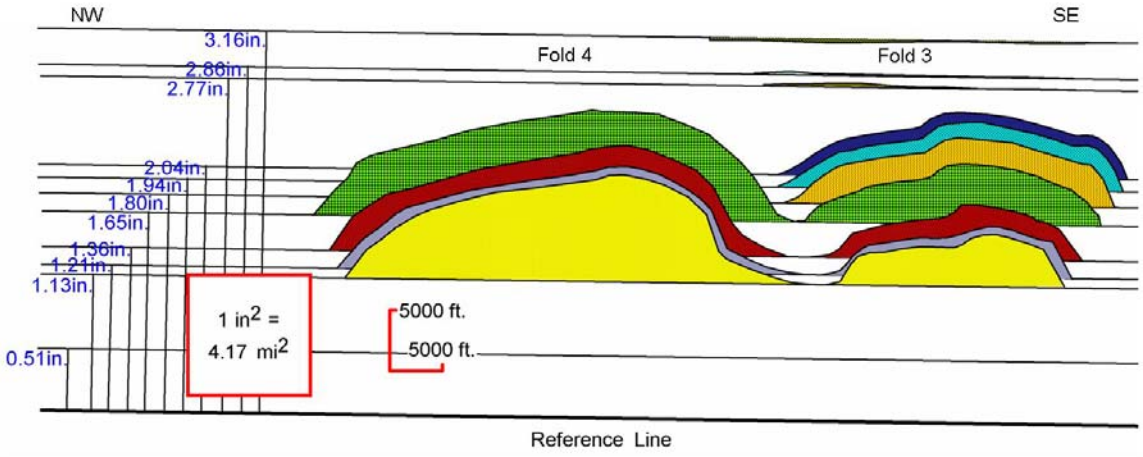

Figure 34b: Profile (C) displaying excess area polygons for folds 3 and 4, without the seismic background. The leftward portion of the diagram displays the units above the arbitrary reference horizon to the base of the syncline (labeled in blue).

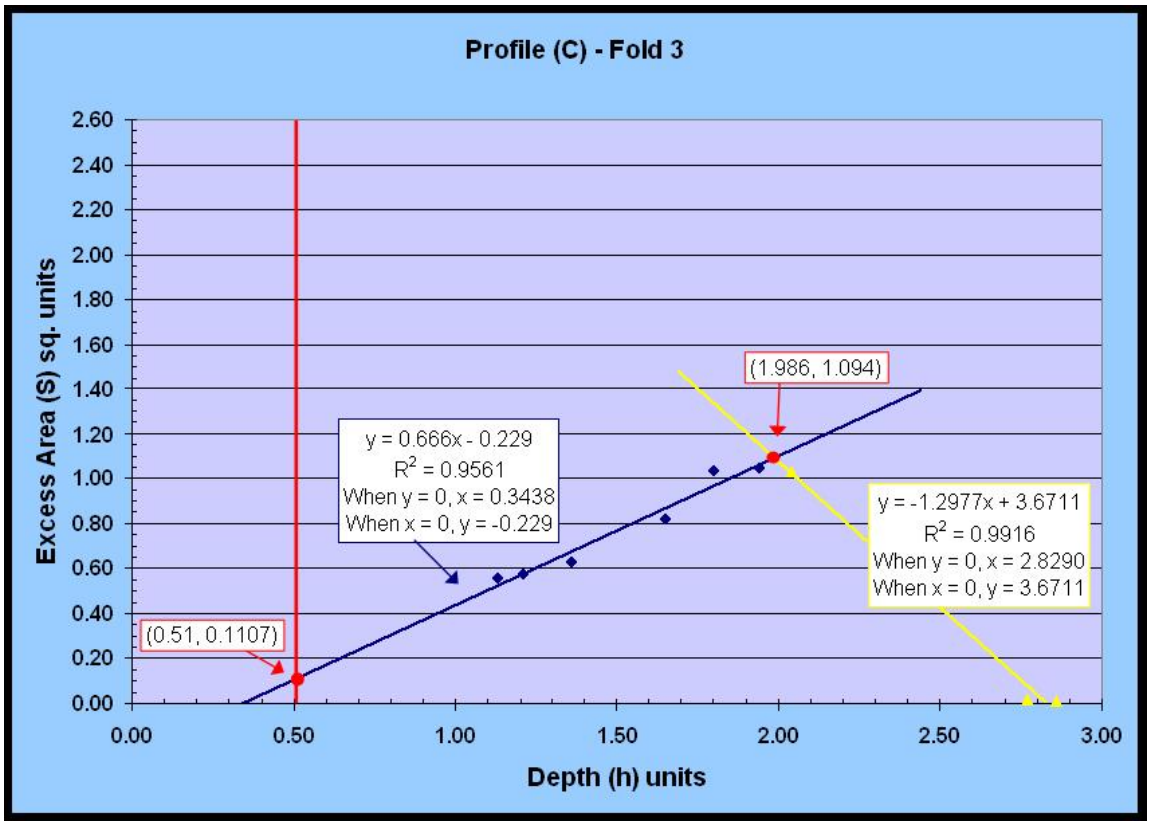

Figure 35: Excess area vs. Depth to detachment graph for seismic profile (C), fold 3. Blue data points represent pre-growth sediments, yellow represent growth sediments. The known depth to detachment is 0.51 units above the arbitrary reference horizon, shown with a red vertical line.

seismic profile (A) only, and not from any other profile due to seismic resolution (Figure 26). The analysis offers a line of fit to be 0.5993, and gives the equation y = -0.0494x + 0.1895. When y = 0, x = 3.8360, and when x = 0, y = 0.1895.

Fold 4

Data from fold 4 is much less conclusive than that taken from the previous sets of folds. Figure 34 shows fold 4 in seismic profile. Four layers were interpreted, all of which are pregrowth sediments. No growth sediments were mapped due to the fact that most of the reflectors are on-lapping fold 4 up until the Pliocene. The four points that were graphed give an $R^2 = 0.9601$ and y = 0.8492x + 1.0767 (Figure 36). This equation yields x = -1.2679 when y = 0, and when x = 0, y = 1.0767.

Fold 7

Seismic profile (D) was used to interpret fold 7 (Figure 37). This fold was analyzed under the assumption that regional was set at the bottom of the synclines, rather than that of the flat lying abyssal plain sediments. In reality, true regional for each of these layers is much lower stratigraphically, but regional is difficult to locate within the scope of this study. Due to limitations in seismic resolution within the core of the fold, only six layers were interpreted. Three points fit a line with a positive slope, so that $R^2 = 0.9381$ and y = 1.7072x – 2.9556 (Figure 38). When y = 0, x = 1.7313 and when x = 0, y = -2.9556. Correspondingly, the additional three points fit a negative sloping line with $R^2 = 0.9908$ and y = -1.2422x + 5.1259. When y = 0, x = -4.1265 and when x = 0, y = 5.1259. These

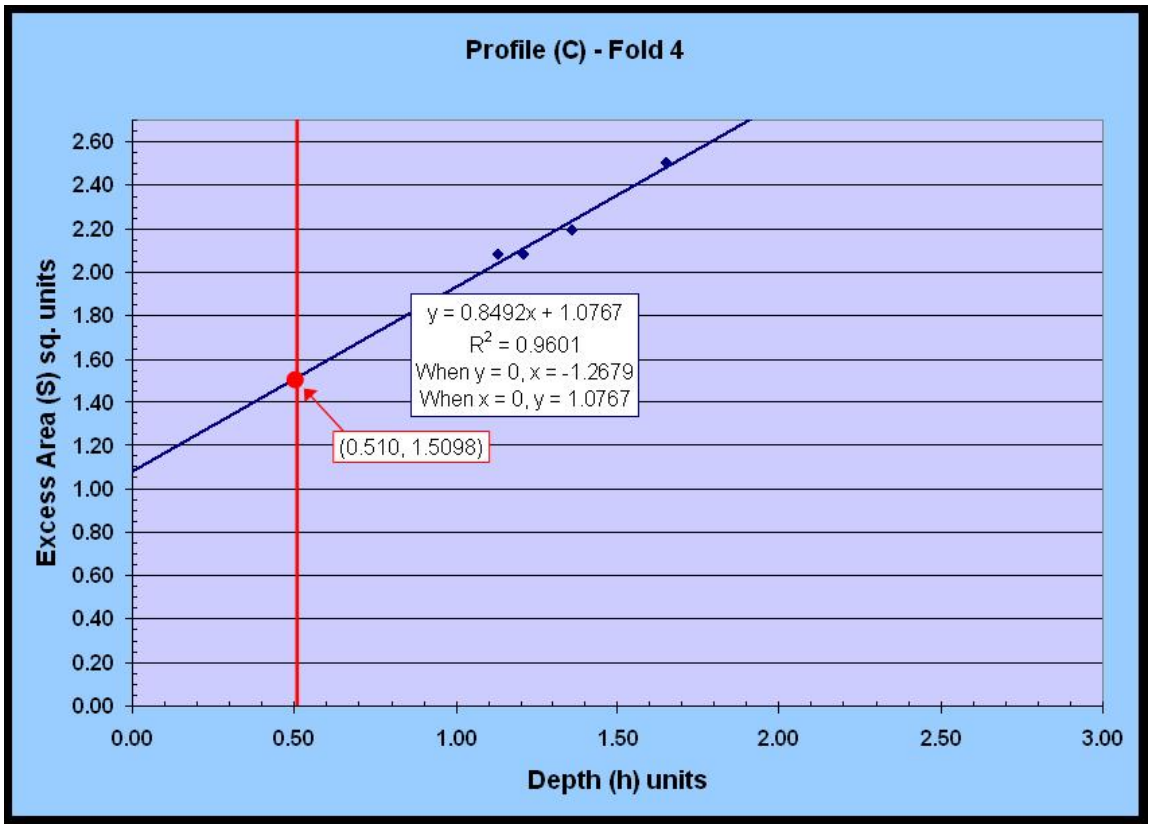

Figure 36: Excess area vs. Depth to detachment graph for seismic profile (C), fold 4. Blue data points represent pre-growth sediments. Due to poor seismic resolution, no other sediments were mapped. The known depth to detachment is 0.51 units above the arbitrary reference horizon, shown with a red vertical line.

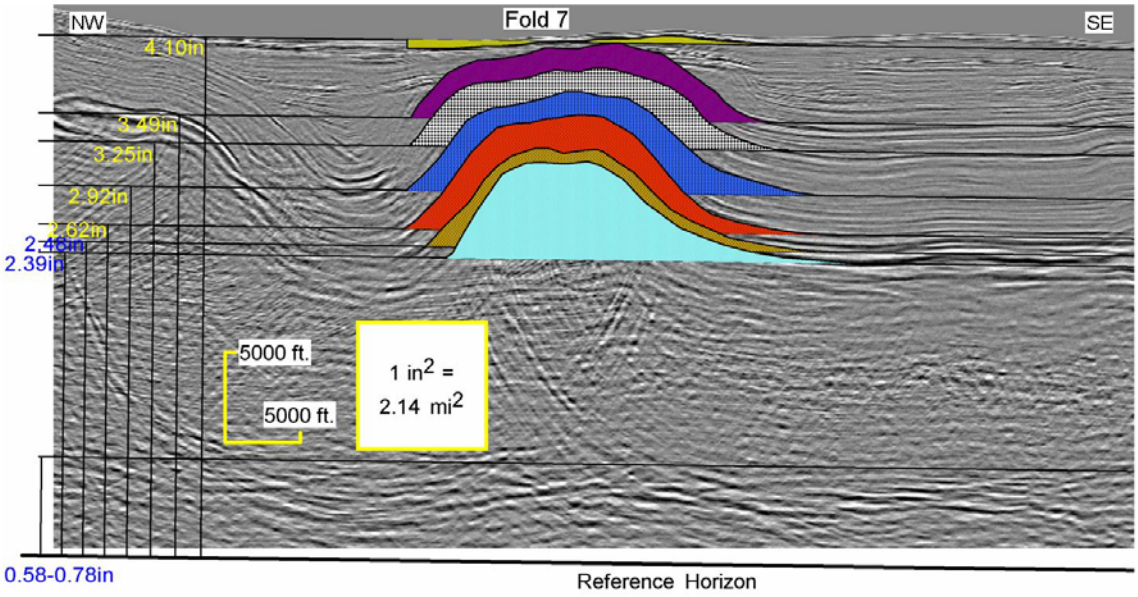

Figure 37a: Seismic profile (D) displaying excess area polygons for fold 7. The leftward portion of the diagram displays the units above the arbitrary reference horizon (labeled in yellow and blue). Seismic data are owned by TGS-NOPEC, all images of the data have been reproduced with their written permission.

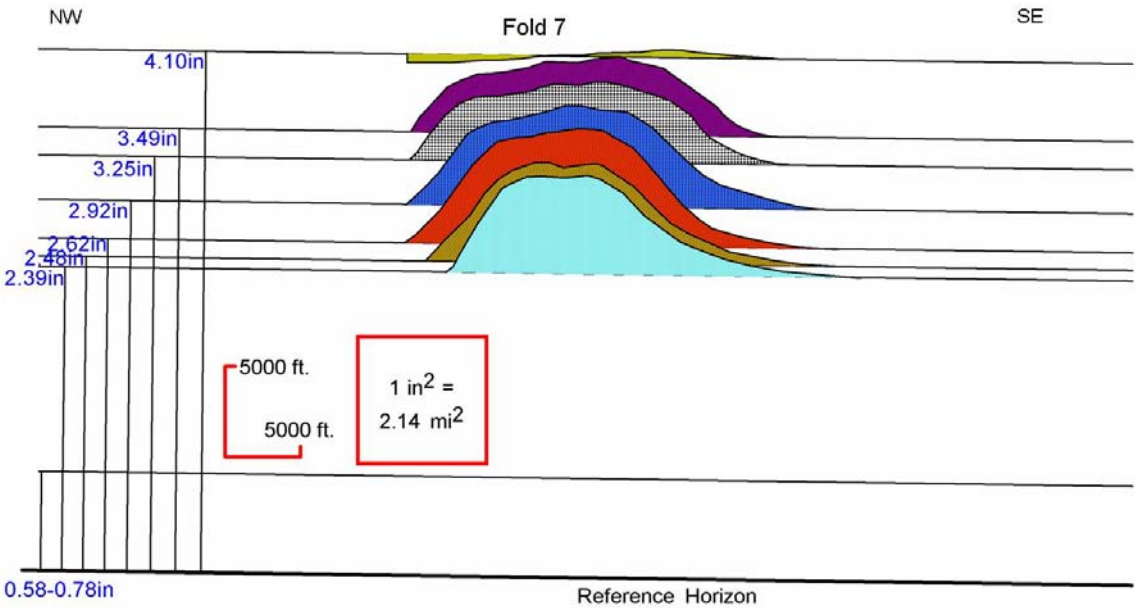

Figure 37b: Profile (D) displaying excess area polygons for fold 7, without seismic background. The leftward portion of the diagram displays the units above the arbitrary reference horizon (labeled in yellow and blue).

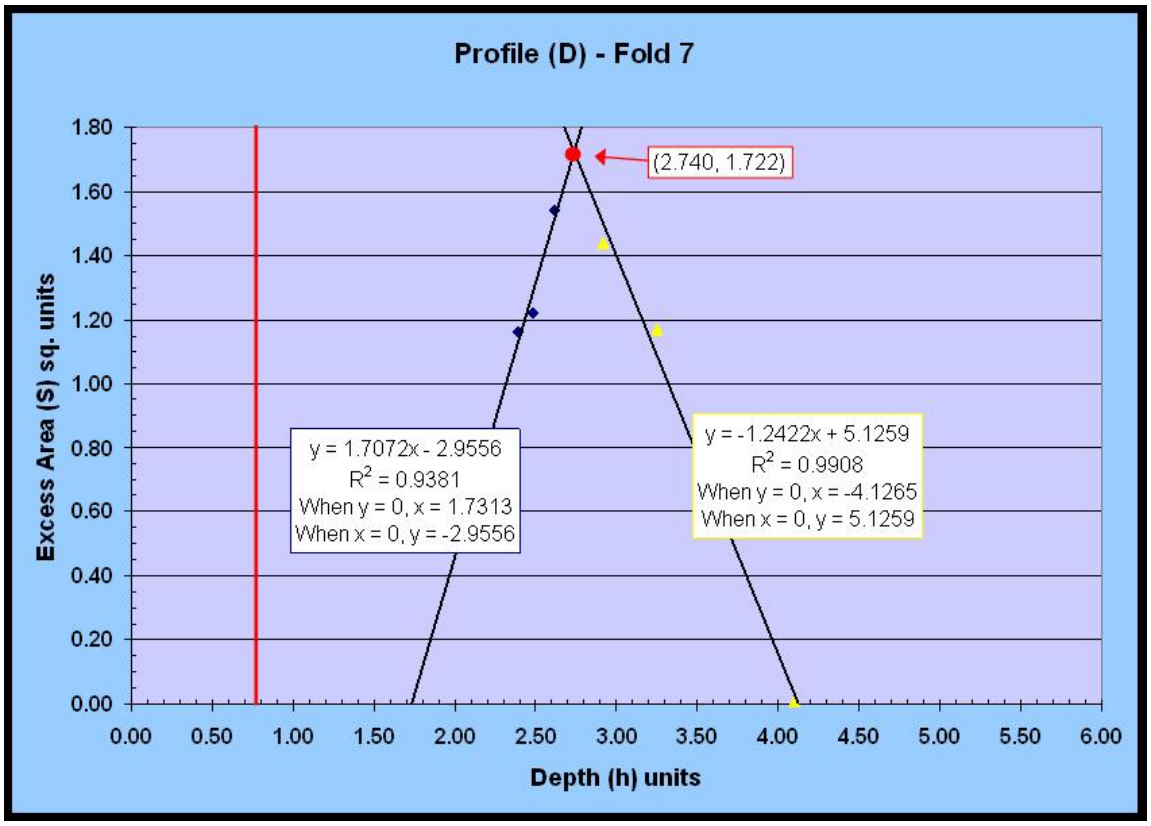

Figure 38: Excess area vs. Depth to detachment graph for seismic profile (D), fold 7. Blue data points represent pre-growth sediments, yellow represent growth sediments. The known depth to detachment is 0.78 units above the arbitrary reference horizon, shown with a red vertical line.

two lines intersect at the (x, y) coordinates (2.740, 1.722).

Requisite/Layer Parallel Strain

Measurements for the requisite/layer parallel strain follow engineering convention, with shortening being a negative value, and elongation being positive values. All of the figures have had the seismic removed from the background in order to focus on the excess area polygons. Please see subsequent figures to observe the seismic profiles. All of the following tables display the depth above the arbitrary reference horizon (h), the excess area (S), the final width of the fold (W), final bed length (L_1), original bed length (L_0), the displacement (D) and the layer parallel strain of each interpreted layer (in percent).

Fold 1

Layer parallel strain was evaluated on seismic profile (A) for scenarios (1) and (2) in fold 1, and is displayed on figure 39, and the results in table 1. Considering scenario (1), at the bottom of the section there is the expected strain represented with -1.5%. The amount the layers were strained up the section decreases until the top of the early Paleocene, were there is some elongation. The layers above this horizon continue to be shortened. The maximum shortening occurs during the Eocene, with very little to almost no line length change during the late Paleocene. The earliest of early Miocene sediments also appear to elongate. In scenario (2), which implements two different line fits for the data set, the maximum amount of layer shortening is found at the bottom of the section,

Table 1: Layer-parallel strain: Seismic profile (A), scenarios (1) and (2), fold 1. Displays the parameters of the seismic profile. Values calculated using the equations described in chapter II: Methods. Negative value for layer parallel strain represents shortening, and a positive value represents elongation. Scenario (1) represents data points fit to one linear line, and scenario (2) displays the same data points fit to 2 different lines. The tops of horizons are shown in their approximate locations: TK=Top Cretaceous, TEPal=Top Early Paleocene, TPal=Top Paleocene, TE=Top Eocene, TO=Top Oligocene

	Profile A - Fold 1									
	h	S	W	L_1	L_0 (Sc.1)	D (Sc.1)	Layer Par (Sc.1)	L_0 (Sc.2)	D (Sc.2)	Layer Par. (Sc.2)
	2.21	1.1	3.72	3.96	4.0219	0.3019	-1.5%	4.1523	0.4323	-4.6%
	2.35	1.15	3.85	4.09	4.1519	0.3019	-1.5%	4.2823	0.4323	-4.5%
TK-	2.49	1.17	3.85	4.13	4.1519	0.3019	-0.5%	4.2823	0.4323	-3.6%
	2.61	1.29	4.12	4.41	4.4219	0.3019	-0.3%	4.5523	0.4323	-3.1%
TEPal-	2.81	1.32	4.18	4.52	4.4819	0.3019	+0.9%	4.6123	0.4323	-2.0%
	3.02	1.43	4.38	4.64	4.6819	0.3019	-0.9%	4.8123	0.4323	-3.6%
TPal-	3.15	1.51	4.38	4.68	4.6819	0.3019	-0.0%	4.8123	0.4323	-2.8%
TE-	3.31	1.44	4.38	4.53	4.6819	0.3019	-3.2%	4.7290	0.3490	-4.2%
	3.52	1.45	4.41	4.61	4.7119	0.3019	-2.7%	4.7590	0.3490	-3.1%
TO-	3.71	1.58	4.43	4.69	4.7319	0.3019	-0.9%	4.7790	0.3490	-1.9%
	3.94	1.64	4.58	4.90	4.8819	0.3019	+0.4%	4.9290	0.3490	-0.6%

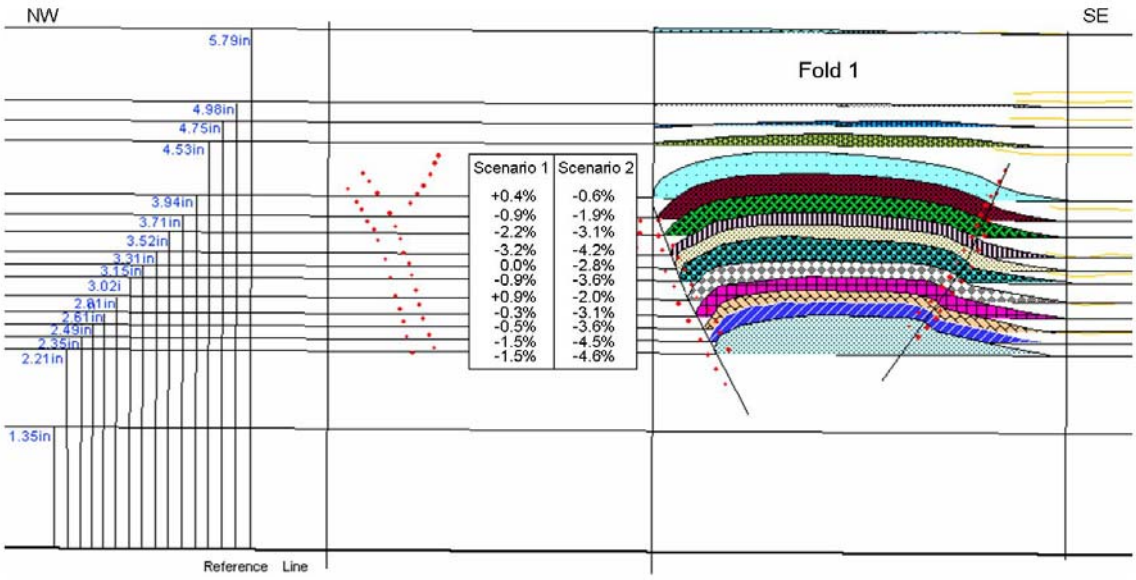

Figure 39: Layer parallel strain shown relative to corresponding layers for seismic profile (A), scenarios (1) and (2), fold 1.

and generally decreases up section. At both the late Paleocene and top of the Eocene, there is a small spike of elongation.

Fold 2

Figure 40 and table 2 displays layer parallel strain scenarios (1) and (2) of fold 2 in profile (A), and exhibits a behavior very similar to that in fold 1, with a few exceptions. In scenario (1), the bottom three interpreted layers appear to shorten, increasingly as you move up section, until the fourth layer when the strain begins to decrease. At 3.15 units above the arbitrary detachment (top Paleocene), there is a minor amount of elongation of the original line length, followed by continued shortening which decreases up section. Scenario (2) generally has the maximum shortening at the bottom of the section, with decreasing amounts up section.

Syncline between folds 1 and 2 – Syncline 1

Layer parallel strain for syncline 1 is shown in figure 41, which was interpreted on seismic profile (A). As previously mentioned, there are possibly two different scenarios, (1) and (2) that can be used to describe the little bit of scatter of the plotted data points. Table 3 displays all of the data collected from the syncline.

In scenario (1), the lower most unit shows some stretching, denoted with a positive value, followed by a time during mostly the early Paleocene of decreasing amounts of shortening. At the top of the early Paleocene, the line lengths again seem to be longer

Table 2: Layer-parallel strain: Seismic profile (A), scenarios (1) and (2), fold 2. Displays the parameters of the seismic profile. Values calculated using the equations described in chapter II: Methods. Negative value for layer parallel strain represents shortening, and a positive value represents elongation. Scenario (1) represents data points fit to one linear line; and scenario (2) displays the same data points fit to 2 different lines.

	Profile A - Fold 2									
	h	S	W	L_1	L_0 (Sc.1)	D (Sc.1)	Layer Par (Sc.1)	L_0 (Sc.2)	D (Sc.2)	Layer Par (Sc.2)
	2.21	0.40	1.82	2.09	2.1650	0.3450	-3.5%	2.3052	0.4852	-9.3%
	2.35	0.44	1.94	2.16	2.2850	0.3450	-5.5%	2.4252	0.4852	-10.9%
TK-	2.49	0.46	2.08	2.29	2.4250	0.3450	-5.6%	2.5652	0.4852	-10.7%
	2.61	0.53	2.22	2.44	2.5650	0.3450	-4.9%	2.7052	0.4852	-9.8%
TEPal-	2.81	0.58	2.41	2.67	2.7550	0.3450	-3.1%	2.8952	0.4852	-7.8%
	3.02	0.79	2.59	2.91	2.9350	0.3450	-0.9%	3.0752	0.4852	-5.4%
TPal-	3.15	0.84	2.66	3.01	3.0050	0.3450	+0.2%	3.1452	0.4852	-4.3%
TE-	3.31	0.74	2.69	2.99	3.0350	0.3450	-1.5%	3.1281	0.4381	-4.4%
	3.52	0.79	2.84	3.17	3.1850	0.3450	-0.5%	3.2781	0.4381	-3.3%
	3.71	0.89	2.99	3.31	3.3350	0.3450	-0.8%	3.4281	0.4381	-3.5%
TO-	3.94	1.01	3.20	3.54	3.5450	0.3450	-0.1%	3.6381	0.4381	-2.7%

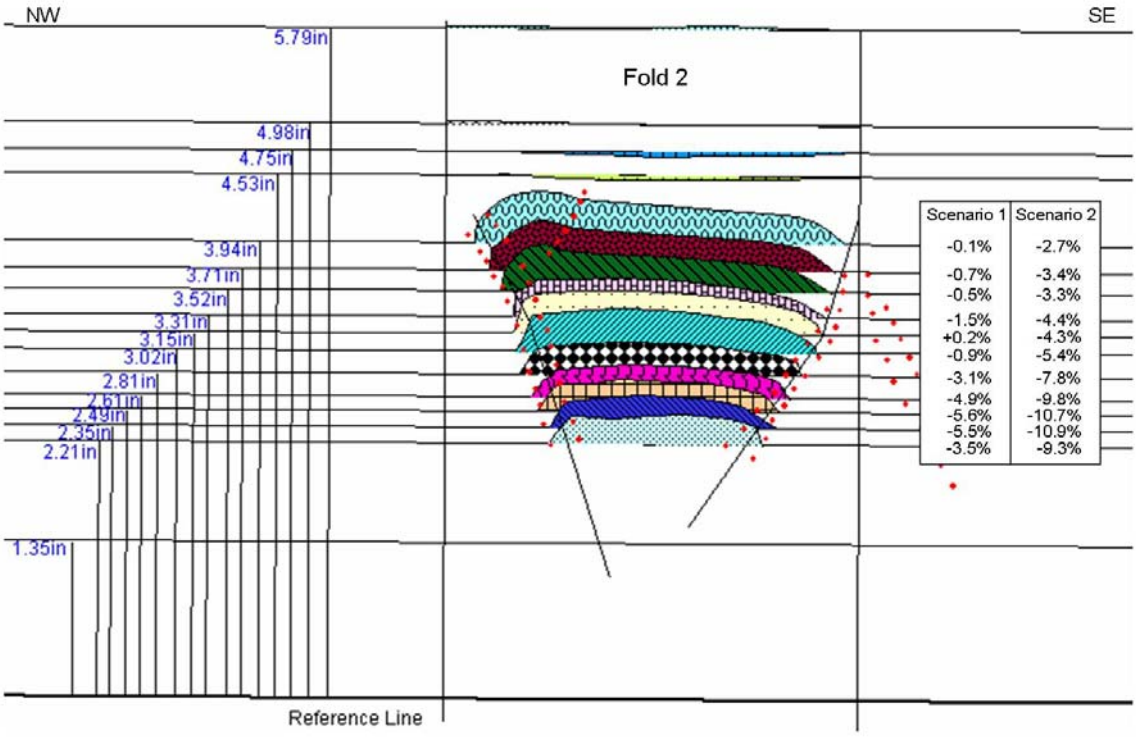

Figure 40: Layer parallel strain shown relative to corresponding layers for seismic profile (A), scenarios (1) and (2), fold 2.

Table 3: Layer-parallel strain: Seismic profile (A), syncline 1. Displays the parameters of the seismic profile. Values calculated using the equations described in chapter II: Methods. Negative value for layer parallel strain represents shortening, and a positive value represents elongation. Scenario (1) represents data points fit to one linear line, and scenario (2) displays the same data points fit to 2 different lines.

	Profile A - Syncline 1									
	h	S	W	L1	L0 (Sc.1)	D (Sc.1)	Layer Par (Sc.1)	L0 (Sc.2)	D (Sc.2)	Layer Par. (Sc.2)
	2.21	0.19	1.55	1.68	1.6476	0.0976	+1.5%	1.6549	0.1049	+2.0%
	2.35	0.12	1.34	1.37	1.4376	0.0976	-5.2%	1.4449	0.1049	-4.7%
TK-	2.49	0.15	1.27	1.36	1.3676	0.0976	-1.1%	1.3749	0.1049	-0.6%
	2.61	0.14	1.06	1.16	1.1576	0.0976	-0.4%	1.1649	0.1049	+0.2%
TEPal-	2.81	0.11	0.88	1.02	0.9776	0.0976	+3.6%	0.9849	0.1049	+4.3%
	3.02	0.10	0.67	0.88	0.7676	0.0976	+13.6%	0.7749	0.1049	+14.6%
TPal-	3.15	0.06	0.55	0.70	0.6476	0.0976	+6.9%	0.6549	0.1049	+8.1%
TE-	3.31	0.07	0.47	0.69	0.5676	0.0976	+23.0%	0.5610	0.0910	+21.6%
	3.52	0.03	0.36	0.46	0.4576	0.0976	+2.0%	0.4510	0.0910	+0.5%
TO-	3.71	0.02	0.26	0.37	0.3576	0.0976	+5.4%	0.3510	0.0910	+3.5%
	3.94	0.01	0.13	0.21	0.2276	0.0976	-5.0%	0.2210	0.0910	-7.7%

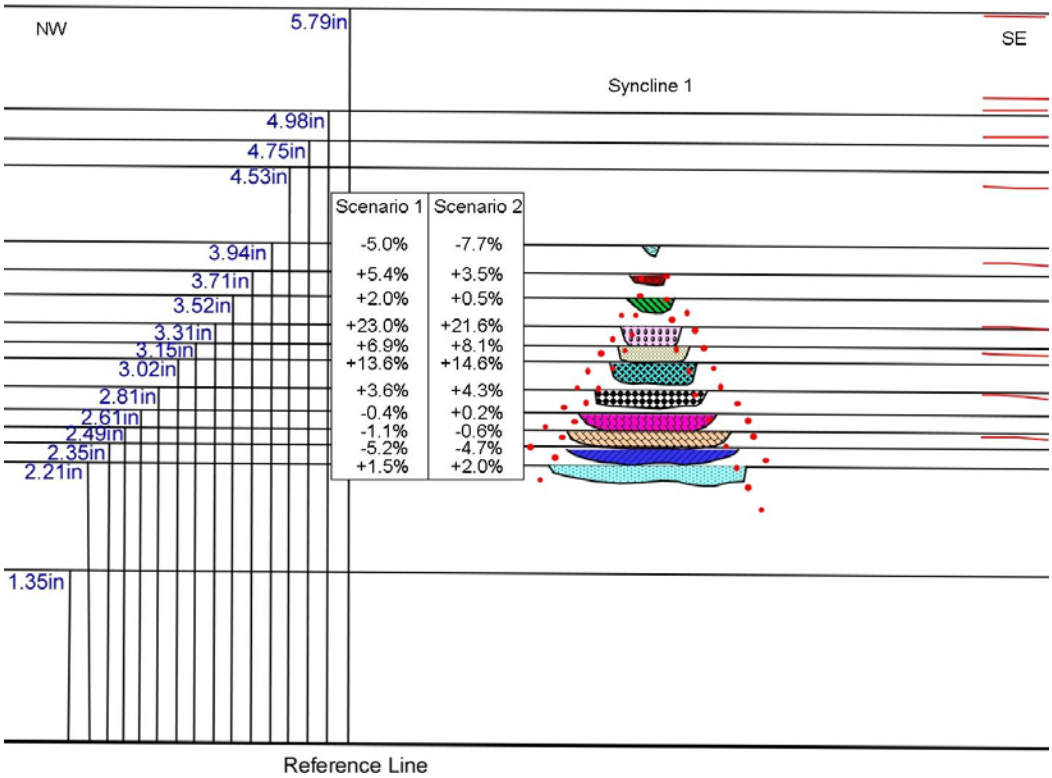

Figure 41: Layer parallel strain shown relative to corresponding layers for seismic profile (A), scenarios (1) and (2), syncline 1.

than originally deposited, and this continues up section in no particular fashion until nearly the top of the Oligocene. Maximum elongation of the line is shown at the top of the Eocene, with a value of +23.0%. The top layer that was interpreted shows some amount of shortening of the original line length. Scenario (2) employs the technique of two distinct lines to fit the data set. Similar to scenario (1), there is a small amount of elongation in the lower most interpreted line, followed by to layers with shortening up section. At this point, the above layers elongate up-section until the earliest early Miocene. Also similar to scenario (1), the layer with maximum elongation is the one that corresponds to the top of the Eocene, with a value of +21.6%.

Fold 3

Fold three again is analyzed on profile (C), and the results for layer parallel strains shown in figure 42 and on table 4. As expected, the layers at the bottom of the section have the most amount of layer shortening, and that amounts decreases up section, with the exception of the top layer, which increase slightly.

Syncline between folds 2 and 3 – Syncline 2

Syncline 2 was interpreted on seismic profile (A). View figure 26 (seismic profile A) for a longer line showing a fold train with interpreted folds 1 and 2, along with synclines 1 and 2. Similar to syncline 1, syncline 2 is interpreted using 2 different scenarios (1 and 2). The results for this are displayed in table 5. In scenario (1), the bottom five layers display elongation, typically increasing up section. At around the Paleocene, the line

Table 4: Layer-parallel strain: Seismic profile (C), fold 3. Displays the parameters of the seismic profile. Values calculated using the equations described in chapter II: Methods. Negative value for layer parallel strain represents shortening, and a positive value represents elongation.

Profile C - Fold 3						
h	**S**	**W**	**L_1**	**L_0**	**D**	**Layer Para.**
1.13	0.56	1.95	2.32	2.6160	0.6660	-11.3%
1.21	0.58	2.08	2.36	2.7460	0.6660	-14.1%
1.36	0.63	2.22	2.53	2.8860	0.6660	-12.3%
1.65	0.82	2.46	2.81	3.1260	0.6660	-10.1%
1.80	1.04	2.72	3.10	3.3860	0.6660	-8.5%
1.94	1.05	2.85	3.21	3.5160	0.6660	-8.7%
2.04	1.03	2.92	3.22	3.5860	0.6660	-10.2%

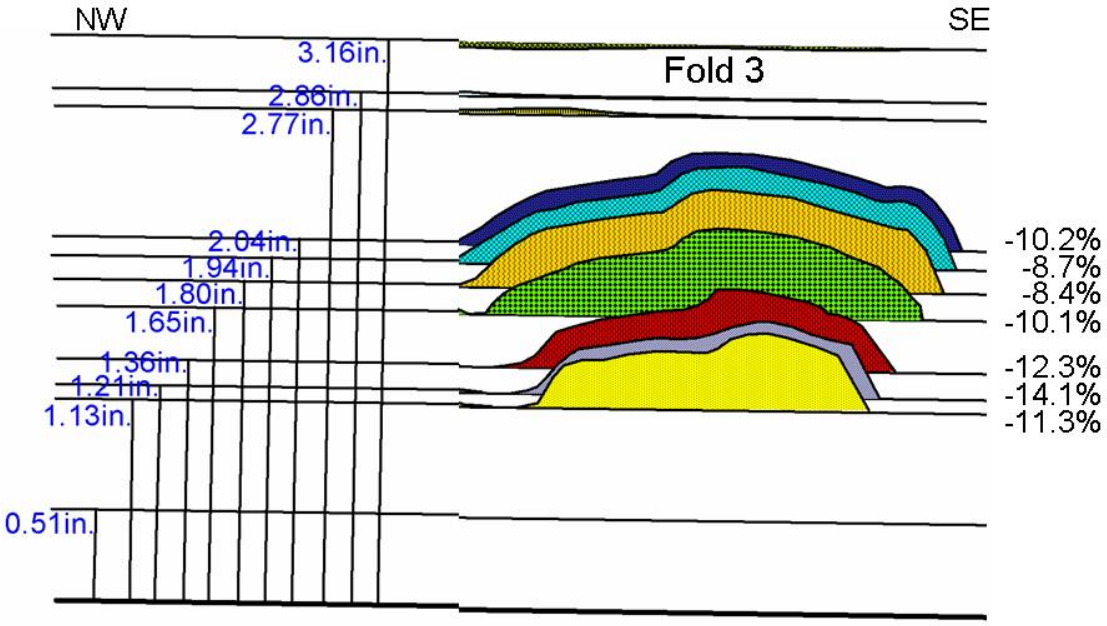

Figure 42: Layer parallel strain shown relative to corresponding layers for seismic profile (C), fold 3.

lengths are compressed and again decreasing amounts up section afterwards. The top two layers, late Oligocene and earliest early Miocene, show slight elongation followed by shortening, respectively.

In scenario (2), the results appear nearly opposite that of scenario (1). Interpreted in the bottom seven layers is shortening, with increasing amounts up section from Cretaceous to early Eocene. By the top of the Eocene, the slope of the line has changed, causing a different displacement, yielding a more or less constant elongation from the top of the Eocene to the earliest early Miocene.

Fold 4

Table 6 and figure 43 display the layer parallel strains for fold 4, which was interpreted in profile (C). This fold acts opposite of the preceding ones, as the maximum compressive layer parallel strain is observed in the upper most units, with values decreasing down section.

Fold 7

Fold 7 behaves similarly to fold 4 in that the maximum compressive layer parallel strain is observed in the upper most units, with values decreasing down section. This can be observed on figure 44 and table 7.

Table 5: Layer-parallel strain: Seismic profile (A), syncline 2. Displays the parameters of the seismic profile. Values calculated using the equations described in chapter II: Methods. Negative value for layer parallel strain represents shortening, and a positive value represents elongation. Scenario (1) represents data points fit to one linear line; and scenario (2) displays the same data points fit to 2 different lines.

	Profile A - Syncline 2									
	h	**S**	**W**	**L1**	**L0 (Sc.1)**	**D (Sc.1)**	**Layer Par (Sc.1)**	**L0 (Sc.2)**	**D (Sc.2)**	**Layer Par (Sc.2)**
	2.21	0.10	1.07	1.12	1.1194	0.0494	+0.1%	1.1768	0.1068	-4.8%
	2.35	0.12	1.16	1.24	1.2094	0.0494	+2.5%	1.2668	0.1068	-2.1%
TK-	2.49	0.05	0.83	0.88	0.8794	0.0494	+0.1%	0.9368	0.1068	-6.1%
	2.61	0.04	0.75	0.80	0.7994	0.0494	+0.1%	0.8568	0.1068	-6.6%
TEPal-	2.81	0.03	0.60	0.66	0.6494	0.0494	+1.6%	0.7068	0.1068	-6.6%
	3.02	0.02	0.58	0.61	0.6294	0.0494	-3.1%	0.6868	0.1068	-1.2%
TPal-	3.15	0.01	0.41	0.44	0.4594	0.0494	-4.2%	0.5168	0.1068	-4.9%
TE-	3.31	0.02	0.58	0.62	0.6294	0.0494	-1.5%	0.5994	0.0194	+3.4%
	3.52	0.03	0.63	0.67	0.6794	0.0494	-1.4%	0.6494	0.0194	+3.2%
	3.71	0.02	0.51	0.56	0.5594	0.0494	+0.1%	0.5294	0.0194	+5.8%
TO-	3.94	0.01	0.30	0.33	0.3494	0.0494	-5.6%	0.3194	0.0194	+3.3%

Table 6: Layer-parallel strain: Seismic profile (C), fold 4. Displays the parameters of the seismic profile. Values calculated using the equations described in chapter II: Methods. Negative value for layer parallel strain represents shortening, and a positive value represents elongation.

Profile C - Fold 4						
h	**S**	**W**	**L_1**	**L_0**	**D**	**Layer Para.**
1.13	2.08	3.67	4.45	4.5192	0.8492	-1.5%
1.21	2.08	3.74	4.42	4.5892	0.8492	-3.7%
1.36	2.20	3.80	4.38	4.6492	0.8492	-5.8%
1.65	2.50	3.97	4.59	4.8192	0.8492	-4.8%

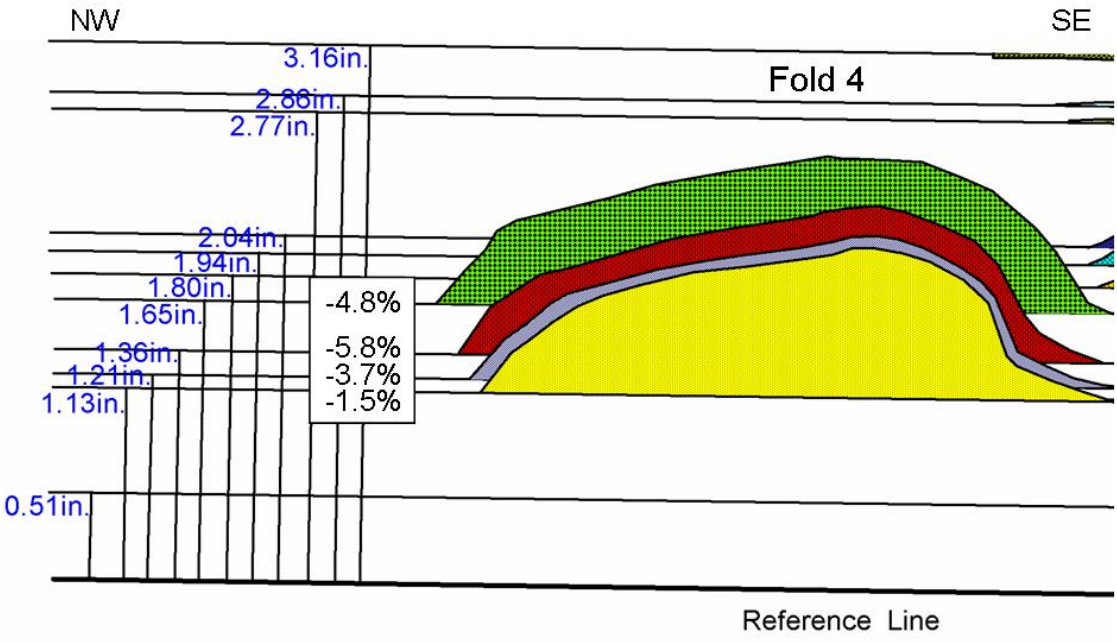

Figure 43: Layer parallel strain shown relative to corresponding layers for seismic profile (C), fold 4.

Table 7: Layer-parallel strain: Seismic profile (D), fold 7. Displays the parameters of the seismic profile. Values calculated using the equations described in chapter II: Methods. Negative value for layer parallel strain represents shortening, and a positive value represents elongation.

Profile D - Fold 7						
h	**S**	**W**	**L_1**	**L_0**	**D**	**Layer Para.**
2.39	1.16	3.11	3.85	4.8172	1.7072	-20.1%
2.48	1.22	3.18	3.82	4.8872	1.7072	-21.8%
2.62	1.54	3.32	4.08	5.0272	1.7072	-18.8%
2.92	1.44	3.25	3.77	4.9572	1.7072	-24.0%
3.25	1.17	2.88	3.36	4.5872	1.7072	-26.8%
3.49	1.14	2.83	3.22	4.5372	1.7072	-29.0%

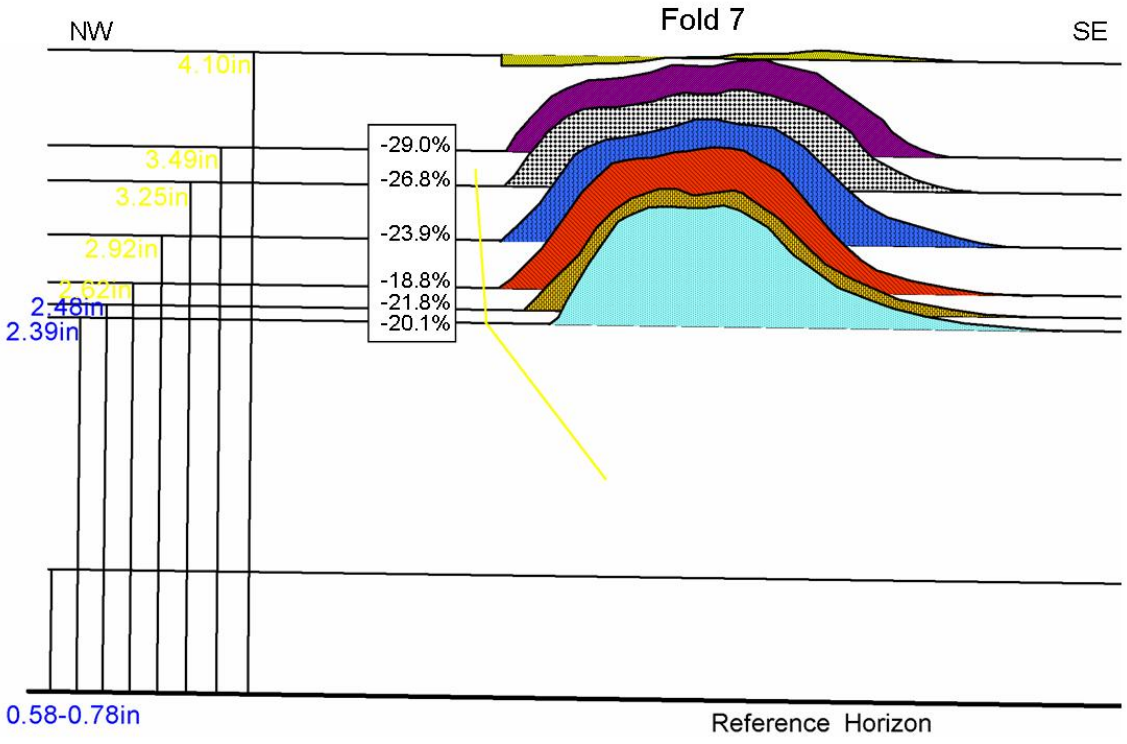

Figure 44: Layer parallel strain shown relative to corresponding layers for seismic profile (D), fold 7.

CHAPTER IV

INTERPRETATION AND DISCUSSION

SEISMIC

Through evaluating the seismic data, timing and evolution of the fold belts can be inferred. Figure 23A and 23B displays a composite line that was created by splicing together four individual seismic profiles. These figures, as previously explained, exhibit the maximum shortening of the folds, and as a result, the composite lines presents a somewhat misleading picture of the folds. In map view, the folds gain and lose displacement in a pattern similar to thin skinned fold and thrust belts. As one fold or thrust fault loses shortening or displacement, adjacent folds or faults gain displacement. However, the observations laid out in chapter III, and hence the following interpretations, were made from individual seismic profiles, not the composite profile. The below described will show that in general, the fold belt appears to have originated in the west, and then propagated east through time, with the first fold starting as early as the early Paleocene.

Additionally, the seismic interpretation has lead to the identification of two different fold axial surface dips on each fold limb (Figure 30). The change in dip occurs nearly every time at the same level stratigraphically on each fold, leading to the assumption that the change in fold style is rock type dependant.

Cretaceous (145 – 65.0 Ma)

After rifting, the opening of the Gulf of Mexico and the deposition of Jurassic age Louann salt, the seafloor at the now Perdido fold belt was presumably flat. This comes from the more or less flat, parallel and laterally continues reflectors of the overlying Cretaceous. None of these reflectors seem to thin or on-lap any of the folds, which implies that these were pregrowth sediments for the entire fold belt.

Early Paleocene (65.0 – 60.9 Ma)

In a couple of the seismic profiles, there is evidence of thinning and on-lap of reflectors onto the flanks of fold 8, the most westward fold observed in this study. This is presumably the onset of deformation for this fold, therefore considered at least partial or early growth sediments. Early Paleocene reflectors elsewhere appear to be parallel to sub-parallel, and do not thin over any of the other folds, thus remaining pregrowth sediments. Different than the other folds, with the exceptions of folds 4c and 7, fold 8 in map view is more domal in nature, rather than exhibiting an elongate, anticlinal fold axis. This might be due to salt withdrawal from nearby this fold (presumably north or west) and injection into the core.

Paleocene (60.9 – 54.7 Ma)

Based on the observations of seismic reflectors, the story for this package of sediment is similar to that of the early Paleocene. Through out the entire fold belt, the reflectors are

sub-parallel to hummocky, but constant thickness over every fold with the exception of fold 8, which several seismic profiles show this layer to thin and on-lap the flanks of this fold. Fold 8 was still growing at this time, but without the company of any of the other folds; however, it is not long until the other folds are activated.

Eocene (54.7 – 33.7 Ma)

By the end of the Eocene a new fold has emerged, fold 7. The Eocene reflectors thin over both folds 7 and 8, but remains constant thickness elsewhere. Many on-laps are visible in conjunction with these two folds, demonstrating the continuing growth of such. Even though a later unconformity will remove much of this sediment, the on-lapping and thinning is observed on the flanks of the folds. The Eocene strata are considered growth sediments over folds 7 and 8, and pregrowth sediments elsewhere.

Oligocene (33.7 – 23.8 Ma)

During the Oligocene, fold 6 forms causing Oligocene reflectors to thin over this anticline. Due to the unconformity, it is difficult to determine if the Oligocene strata make it over folds 7 and 8. Presumably, it does not, but on-laps these folds as they have gained a large amount of amplitude. The Oligocene strata are observed and thicken within the syncline between these two folds. Basinward of fold 6, the reflectors are as described: parallel and laterally continuous. From the evaluations of these reflectors along with those of early Miocene, the time of fold initiation for most of the rest of the folds occurs near the end of the Oligocene, or shortly there after during the earliest

stages of early Miocene. Oligocene strata are mostly considered pregrowth sediments over folds 1-5, and considered growth sediments over folds 6-8.

Early Miocene (23.8 – 15.6 Ma)

As previously mentioned in chapter III, due to the regionally extensive unconformity, only the most basinward sediments of early Miocene can be observed on seismic. This limits the interpretation to sediments east (basinward) of fold 4. By this time, folds 6 through 8 have already formed as seen by the previously on-lapping reflectors, and are continually gaining amplitude. The early Miocene reflectors are shown to thin over and on-lap at times folds 1, 3 and 4. Most of the on-laps are that of the earliest Miocene, which infers that fold initiation of folds 1, 2, 3 and 4 were after the Oligocene, but before the end of the early Miocene. Most of the lower reflectors in this time interval on-lap a smaller fault propagation fold that originates out of the syncline between folds 3 and 4. Similar subsequent folds are found thrusting out of the synclines between folds 2 and 3, and 4 and 5.

In chapter III, there were described two additional detachments, ones other than the main fold forming detachment upon the Louann salt. The two other detachments occur stratigraphically during the late Eocene and late Oligocene (presumably on Jackson and Anahuac shales, respectively). These detachments are activated during the earliest Miocene. This is concluded due to the observed late early Miocene reflectors that on-lap or truncate against the fault propagation folds above these smaller thrust, and the folded,

constant thickness Oligocene sediments. These folds occur due to the tight nature of the synclines. The working hypothesis is that these main synclines formed with the fold axes intersecting nearly at the surface of the sea bottom. The synclines probably bottom out against the base of the mobile salt layer (presumably basement rock) around this time, displacing all of the salt that was located below them into one or either of the adjacent anticlines. Since the synclines can no longer move downward, continued compression is taken up within the syncline, which causes the upper sediments to detach upon the above mentioned layers.

Fold 2 appears different in nature than any of the subsequent folds. Since the early Miocene reflectors appear to thicken eastward over the present crest of fold 2, this fold presumably began to uplift on the westward side, and subside on the east throughout the early portions of this interval, and ceased well before the end of the early Miocene.

Middle Miocene (15.6 – 11.0 Ma)

During the beginning of the middle Miocene there was a large regional unconformity that occurred. As previously described, this unconformity eroded down to possibly sediments of early Paleocene in some places (i.e. fold 7), and has since been folded and deformed. This is proof of continued uplift of the more westward anticlines, at least through the middle Miocene.

Due to poor seismic resolution caused from over-riding allochthonous salt, it is difficult to determine the placement, if any, of middle Miocene sediment west of fold 6. The visible reflectors are observed to on-lap the east (basinward) flank of fold 6, and both flanks of fold 4, and thin over fold 5. As previously described, basinward of fold 4 middle Miocene reflectors thicken through the syncline between folds 3 and 4, thin greatly over fold 3, thicken slightly over fold 2, and is followed by some amount of thinning over fold 1. Because the top of the middle Miocene is folded over fold 3, and appears to have been uplifted above regional onto fold 4, it is assumed that those folds west of and including fold 3 were still substantially gaining amplitude, while folds 1 and 2 have nearly ceased.

Late Miocene through Pliocene (11.0 – 2.85 Ma)

Only a few of the reflectors between the time interval of 11.0 and 2.85 Ma appear to on-lap any of the structures, however, the reflectors do appear to thin substantially. Due to folded sediments of late Miocene to present, along with bathymetric expressions on the sea bottom, folds 4 through 8 were still actively growing through this time. Folds 1 through 3 have since ceased and are overlain by flat and parallel reflectors (growth sediments). Reflectors ranging in age from 2.85 Ma to present day are nearly equal thickness and parallel, but also are folded over many of the western folds, indicating that the folds were actively growing up until (and possibly include) the present. The sediment package thins greatly to the west, over much of the regionally elevated folds (i.e. folds 4-8).

GEOMETRIC MODELS

The change in fold axial surface style has been shown to be sediment, or rock type dependant, conveying that the upper most sections of the folds, which correspond to more steeply dipping fold axial surfaces are composed of deepwater siliciclastic sands, where as the lower portions are less steeply dipping and correlate to deepwater carbonate sequences. When this is applied to the geometric models, the excess areas versus depths to detachment calculations are not greatly affected. However, the difference can be observed in the layer parallel strain calculations within the folds.

Excess Area vs. Depth to Detachment

Fold 1

As described in chapter III, excess area techniques were applied to fold 1 on two non-adjacent seismic lines. In profile (A), using scenario (1) where the pregrowth excess area data points are fit to a single linear line, the excess area versus depth to detachment graph shows the pre-growth sediment line to intersect the known depth to detachment at the coordinates (1.350, 0.870), implying that about 0.870 square units of material has been added to the core of this anticline (Figure 28). This material that has been added is that of the mobile salt layer, which has migrated out from under the positively downward moving synclines into the core of the anticlines. Also, the pre-growth sediments line intersects that of the growth sediments at (3.925, 1.641), insinuating that the time of fold origination began at 3.925 units above the reference horizon, which corresponds to the

latest Oligocene, which is consistent with the seismic reflector observations. Also, the curves suggest that folding ceased around 4.77 units above the reference horizon, which is equivalent to early late Miocene strata, which in fact also corresponds to the observed seismic interpretation. In profile (A), as the excess area data points are fit with two different linear lines, as in scenario (2), similar results are offered: excess area added to the core of the syncline equals 0.714 square units, fold initiation at approximately 3.928 units above the reference horizon (also near latest Oligocene) and cessation at 4.77 units (early late Miocene) above the reference horizon (Figure 29). This data fits very well with the seismic, and confirms the seismic interpretations. In profile (B), approximately 0.2 square units of material was added to the core of the anticline, and fold initiation began at 1.608 units above the reference line, which again equals the time of latest Oligocene. Fold cessation occurred at 1.958 units above the reference line, equal to that of near late middle Miocene sediments, slightly younger than in profile (A). The slight difference in timing is partially due to the 2-D seismic resolution and quality. The new geometric models developed in this study fits with the gathered seismic data near perfectly.

Fold 2

Fold 2 was additionally interpreted within 2 different scenarios on one seismic line. In seismic profile (A), scenario (1) shows that much less material was added to the core of the anticline than in fold 1, with approximately 0.1207 square units added (Figure 32). This is not surprising since the time of fold growth for fold 2 was short lived. This fold,

determined from evaluating the seismic both appears and behaves differently than the other folds. It appears that it is more of an “after-thought” of the fold belt. The observations made justify an interpretation that the westward side moved up slightly over a very brief interval, and the more eastern side seems to have moved down within the same time frame. The time of fold initiation equals 3.9454 units above the reference line, which equates to the top of the Oligocene. This is a little earlier than reported in the seismic analysis, but I feel that if more lines were interpreted between the Oligocene and middle Miocene, a time of folding around the earliest of early Miocene would be observed. Also, profile (A) shows that the fold stopped growing at approximately 4.587 units above the reference line, which is equivalent to early middle Miocene. This data also fits within the realms of the seismic profiles. Scenario (2) gives nearly comparable results (Figure 33). The excess area added to the core of the anticline is 0.1059 square units, and the time of fold initiation is nearly at the same level (3.946 units). The time of fold cessation from this scenario uses the same excess area data points as in scenario (1), which provide the same results.

Syncline 1

Through evaluating the synclines, especially syncline 1, it can be observed that the synclines move down below the regionally identified stratigraphic level of each horizon. The examination of the excess area curves reveal that as you move up section, the amount of excess area decreases, until a point where the excess area equals zero. At this location, where excess area equals zero, the initiation of folding is marked. When these

synclines formed, the fold axial surfaces intersected at nearly the sea floor, allowing almost no excess area to accumulate. The sediments above the synclines (i.e. growth sediments) thicken through the syncline, which is expected of the growth sediments. Also, these synclines are presumably bottoming out at the base of the mobile salt layer (i.e. basement rock). If this is so, then as excess area is accumulated with continued shorting, this area will be transferred up section, rather than down. With enough shortening through the syncline, some of the layers, rather than moving down below regional, will actually move up above regional. Profile (A) displays all of the above mentioned traits, with the excess area equaling zero right near the point of fold initiation. Profile (B) shows slightly similar results, with the excess area curve equaling zero well into the growth phase. However, the quality of the data acquired from profile (B) is somewhat poor due to difficulties with seismic resolution.

Fold 3

Due to the fact that regional can not be established on seismic profile (C) without further work, the amount of material that has migrated out from under neighboring synclines and into the core of this fold can not be determined. However, the timing information should still be relevant. At 1.986 units above the reference horizon, the intersection of the pregrowth and growth sediments occurs on the graph, which correlates to the time of fold initiation being in the late Oligocene. This again correlates well with the seismic interpretation. There is a slight difference in the age of fold initiation, but not a large amount, with the models predicting initiation to be a little earlier than observed on the

seismic. Fold cessation is approximately located at 2.8 units above the reference horizon, which is equivalent to Pliocene age strata, again correlating well with the seismic interpretation on profile (C).

Syncline 2

The syncline between folds 2 and 3 (labeled syncline 2) behave very similar to that of syncline 1. The excess area values decrease as you go up section through the syncline, and go to zero presumably at the onset of folding. This is due to the fact that when folding commenced, the fold axial surfaces for the synclines intersected (or at least nearly did) at the sea floor. The trend line for these excess area data points go to zero at 3.84 units above the arbitrary reference horizon, which is equivalent to near the top of the Oligocene, stratigraphically.

Fold 4

The data gathered from this fold is inconclusive, with the onset of deformation and the cessation of the folding not determinable without further work. Interpreting several more lines or evaluating the growth strata in more detail would prove useful in an additional study.

Fold 7

Similar to the previous two folds (3 and 4), regional can not be easily established on seismic profile (D) without further work being performed. Therefore, neither the amount

of material added to the core of the fold from the displacement of mobile salt from under the falling synclines, nor the true depth to detachment can be calculated. However, the intersection of the pregrowth and growth sediment excess area curves does give a valid interpretation for the onset of folding. The two above mentioned curves intersect at 2.740 units above the arbitrary reference level, which is equivalent to near late early Paleocene or the early middle Paleocene stratigraphically, which once again is comparable to the seismic interpretation.

Layer Parallel Strain

Fold 1

In fold 1, seismic profile (A) incorporated the results from two different scenarios. Scenario (1) used one single linear line to fit the data, and it shows original line length elongation in the lower section of sediment, up until the Eocene. There are some variations throughout, but the general trend fits the models. At the Eocene, there is slightly more shortening, followed by lesser amounts up-section. This abrupt change corresponds to the change in sediment (rock) types. The lower section (carbonate sediments) behaves somewhat independently than that of the upper section (siliciclastic sandstone). Scenario (2), which was fit with two different lines, follows the same pattern as scenario (1). In both scenarios, there are a few slight variations, for example at the top of the early Paleocene, or during the Paleocene there is an abrupt elongation in scenario (1) and slightly more shortening in scenario (2). The slight variation in the data is a probable result of errors in the seismic interpretation.

Fold 2

Fold 2 was also interpreted having two different scenarios (1 and 2) in profile (A). Scenario (1) shows maximum shortening near the bottom, and the amount decreases as you move up section, until the Paleocene, where there is a slight elongation. This package is conclusive of the carbonate rocks, with the Paleocene being the transition between carbonates to siliciclastics. At the onset of siliciclastic sediments (from the Eocene on) there is some amount of shortening, with a decreasing amount up section. This scenario shows that there is an effect of sediment (rock) type on the folds. Scenario (2), however, does not show any evidence of this. The lower levels have the most shortening, and the amounts decreases fairly systematically up-section.

Syncline 1

The synclines should present similar results to that of the anticlines, but opposite. The top most layers stratigraphically should be shortened, and the lower most units should have the least amount of shortening, or elongating. Using profile (A), syncline 1 is evaluated with the possibility of two different scenarios (1 and 2), the same as folds 1 and 2. In scenario (1), the upper most units is shortened, and is immediately followed by varying amounts of elongation as you move down section, until you reach the top of the early Paleocene. From here, there is some shortening, with increasing amounts until the lowest section, which elongates. At the Eocene, there is the maximum amount elongation, which could be a result of a change is fold axial surface style. With scenario

(2), the upper most unit is shortened, but similar to scenario (1), is followed by elongation of the original line length. Only until the top Cretaceous is there another episode of shortening, with increased shortening the next layer down, but then again the bottom most layer is elongated. The layer with maximum elongation corresponds to the Eocene.

Fold 3

Seismic profile (C) was used in the layer parallel strain analysis of fold 3. The bottom most layer is shortened, and that shortening decreases systematically up section, until the top layer. At this point, the shortening increases slightly. The observation of a change in strain at the Eocene or Paleocene boundaries is not noticed in this line. Perhaps, additional seismic profiles need to be interpreted in order to see this effect.

Syncline 2

When the two different scenarios for syncline 2 are used, results are given that are nearly contradictory to each other. In scenario (1), we have maximum shortening in the top most layer, and varying amounts of shortening, which are generally decreasing, down section, until the top of the early Paleocene. At the early Paleocene, the line lengths are lengthened, and vary in amounts as you move down section. In scenario (2), the upper most units (early Miocene down to top Eocene) show nearly the same amounts of elongation. With continued movement down section, the line lengths are shortening, with decreasing amounts down. These are not what I would have expected in the

syncline, and feel that scenario (1) gives a more accurate assessment of the layer parallel strains.

Fold 4

Only four horizons were interpreted on seismic profile (C) for fold 4, which gives layer parallel strain values that are opposite than what is expected. The bottom layer only slightly shortens, with increase shortening of layers up section. Based on the models created, the line lengths should decrease in the amounts that are shortened as you move up-section, until some point were the line lengths begin to elongate. Additional seismic profiles needed to be interpreted in order to investigate this fold further.

Fold 7

Seismic profile (D) was used in the interpretation of the fold 7. Similar to that of fold 4, as you move up section, there is incrementally more shortening within the individual layers. One possible reason for this, on this fold, is that in map view, fold 7 is more domal in nature. This could be due to a different mechanism of folding. Rather than purely compression, there might have been a large influence of salt injection into the core of this fold, which would add the same amount of excess area to each layer up section. In order to verify this as the cause for the contrast of the layer parallel strains demonstrated in the models, further investigation is required.

CHAPTER V

SUMMARY AND CONCLUSIONS

In this study, new appropriate methods for excess area to depth of detachment models were developed to describe deformation in the Perdido fold belt area, where the location of regional undeformed bedding can be identified. Data were interpreted and models were developed to explain the structural evolution of the fold belt. The results are summarized below.

1. The timing of deformation is confirmed, and modified some from the literature. The timing in the literature appears to be a little earlier than found here, with the major onset of deformation evident near the late Oligocene/early Miocene for most folds. However, this is not true for every fold, especially for the more proximal (westward) folds, which began as early as the early Paleocene. Figure 45 summarizes the timing of deformation of all 8 folds in the fold belt, by identifying the time periods in which folding occurred.
2. Defining evidence of fold geometry supports the hypothesis and interpretation that the steeply dipping seismic reflectors are in fact kink bands, rather than high-angle reverse faults
3. The evolution of the fold belt is easily identifiable by evaluating either the onset of growth sedimentation, or the lack thereof in both the excess area

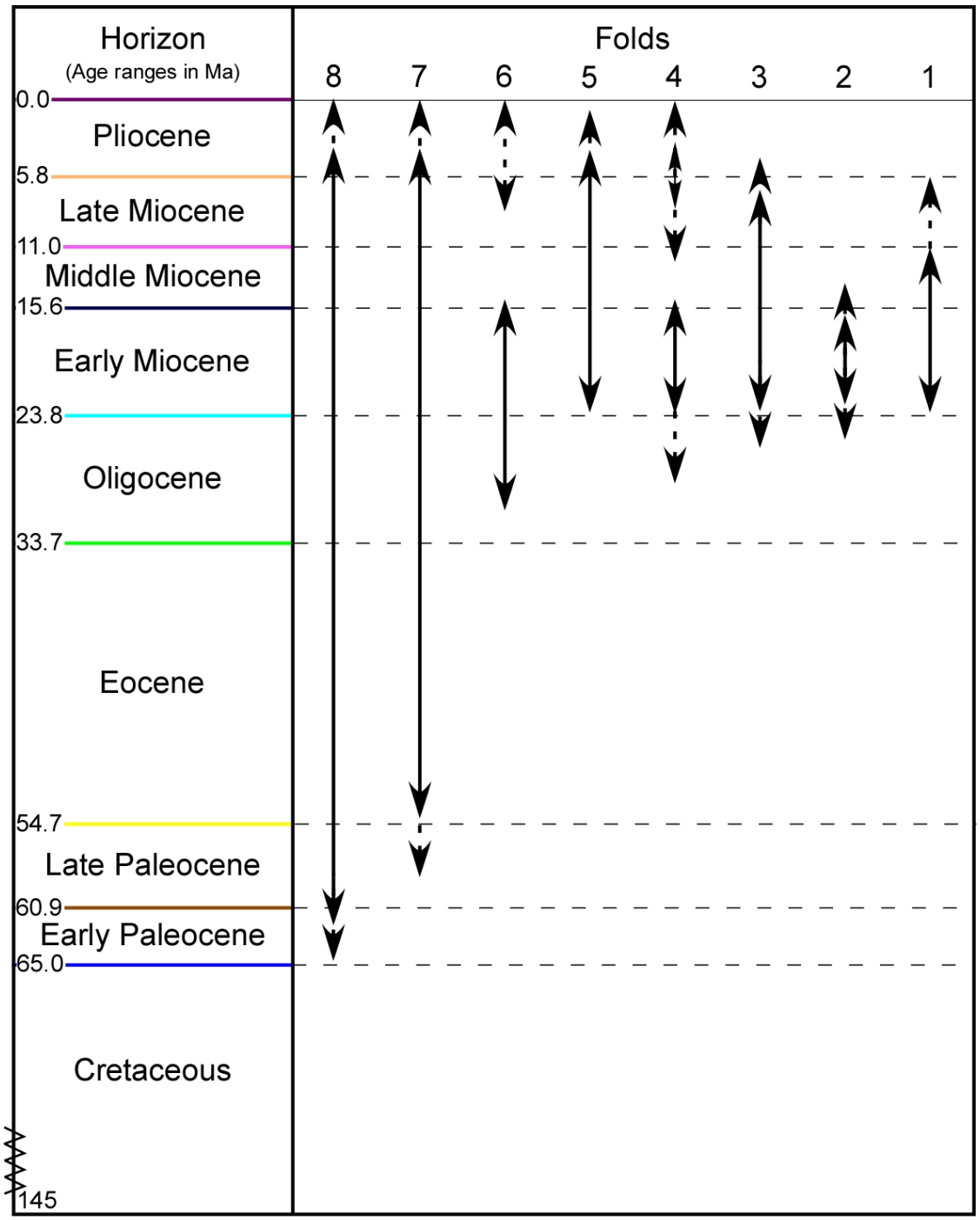

Figure 45: Fold history for the Perdido fold belt. This chart shows the progression of folds 1-8, and their relevance to each other. The bold arrows represent confident ages for the folds based upon seismic interpretation and excess area techniques, and the dashed arrows represent possible extensions in time. The colored boundaries correspond to the colored stratigraphic boundaries marked on the seismic interpretations (Figure 10).

curves and the seismic data. This analysis indicates that the more westward folds, starting with fold 8, originated first, and as a general rule, development of the folds progressed basinward/eastward (Figure 45).

4. The structural styles composing the fold belt changes according to sediment (rock) type. Dips of the fold axial surfaces are sediment, or rock-type dependent. The lower strata (Cretaceous to Paleocene) are deep-water carbonate rocks and coincide with less steeply dipping fold axial surfaces. The upper strata (Paleocene to early Miocene) are deepwater turbidity siliciclastics that commonly have more steeply dipping fold axial surfaces than do the carbonates.
5. In the excess area versus depth to detachment curves where abyssal plain regional stratigraphy is known, the amount of material added to the cores of the anticline from the sediments displaced from under the downward moving syncline can be observed.
6. The synclines move positively down until all of the mobile salt has evacuated, and a salt “weld” is formed between the trough of the syncline and the basement. It is a salt weld in the sense that all of the salt has been “squeezed” out as the trough of the syncline moves down until it reaches the base of the salt. However, this is not a true weld, since with additional shortening the folds continue to translate along this horizon. Since the detachment horizon can be observed in most areas of the seismic profiles, the

true depth to detachment is known, and the excess area that has been added is determined from the excess area plots.

Much more work is possible with this data set, and studies should be continued to further evaluate the folds. Also, more detail and time should be spent in looking at the synclines, and creating more accurate geometric models to depict the behavior of these positively downward moving bodies of rock.

REFERENCES CITED

Bryant, W. R., J. Antoine, M. Ewing, and B. Jones, 1968, Structure of Mexican continental shelf and slope, Gulf of Mexico: AAPG Bulletin, v. 52, no. 7, p. 1204-1228.

Camerlo, R. H., D. Meyer, and R. E. Meltz, 2005, Shale tectonics in the northern Port Isabel fold belt trend, deepwater Gulf of Mexico: Houston Geological Society General Luncheon, 23, Feb, 2005.

Camerlo, R. H., and E. F. Benson, 2001, Geometric analysis of the Perdido fold belt, northwestern Gulf of Mexico (abs.): AAPG Annual Convention Program Book, p. A32.

Camerlo, R. H., and E. F. Benson, 2006, Geometric and seismic interpretation of the Perdido fold belt: northwestern deep-water Gulf of Mexico: AAPG Bulletin, v. 90, no.3, p. 363-386.

Chamberlain, R. T., 1910, The Appalachian folds of central Pennsylvania: Journal of Geology, v. 18, p. 228-251.

Dahlstrom, C. D. A., 1990, Geometric constraints derived from the law of conservation of volume and applied to evolutionary models for detachment folding: AAPG Bulletin, v. 74, no. 3, p. 336-344.

Davies, R. K., and R. C. Fletcher, 1990, Shear bands in a plastic layer at yield under combined shortening and shear: a model for the fault array in a duplex, *in* R. J. Knipe, and E. H. Rutter, eds., Deformation mechanisms, rheology and tectonics: Geological Society Special Publication, no. 54, p. 123-131.

Epard, J.-L., and R. H. Groshong, Jr., 1993, Excess area and depth to detachment: AAPG Bulletin, v. 77, no. 8, p. 1291-1302.

Epard, J.-L., and R. H. Groshong, Jr., 1995, Kinematic model of detachment folding including limb rotation, fixed hinges and layer-parallel strain: Tectonophysics, 247, p. 85-103.

Feng, J. and R. T. Buffler, 1996, Post mid-Cretaceous depositional history, Gulf of Mexico basin: structural frame work of the northern Gulf of Mexico: Gulf Coast Association of Geological Societies Special Publication in conjunction with Transactions, v. 46, p. 9-25.

Fiduk, J. C., 1999, Comparing two models of source rock potential in the Perdido fold belt area, northwestern deep Gulf of Mexico: Gulf Coast Association of Geological Societies Transactions, v. 49, p. 212-222

Fiduk, J. C., P. Weimer, B. D. Trudgill, M. G. Rowan, P. E. Gale, R. L. Phair, B. E. Korn, G. R. Roberts, W. T. Gafford, R. S. Lowe, and T. A. Queffelec, 1997, Seismic interpretation of Mesozoic-Cenozoic strata, Perdido fold belt area (Alaminos Canyon), northwestern deep Gulf of Mexico: Gulf Coast Association of Geological Societies Transactions, v. 47, p. 159-168.

Fiduk, J. C., P. Weimer, B. D. Trudgill, M. G. Rowan, P. E. Gale, R. L. Phair, B. E. Korn, G. R. Roberts, W. T. Gafford, R. S. Lowe, and T. A. Queffelec, 1999, The Perdido fold belt, northwestern deep Gulf of Mexico: Part 2 – seismic stratigraphy and petroleum systems: AAPG Bulletin, v. 83, no. 4, p. 578-612.

Galloway, W. E., 1989, Genetic stratigraphic sequences in basin analysis II: application to northwest Gulf of Mexico Cenozoic basin: AAPG Bulletin, v. 73, no. 2, p. 143-154.

Groshong, R. H., Jr., and J.-L. Epard, 1994, The role of strain in area-constant detachment folding: Journal of Structural Geology, v. 16, no. 5, p. 613-618.

Haq, B. U., J. Hardenbol, and P. R. Vail, 1987, Chronology of fluctuating sea levels since the Triassic: Science, v. 235, p. 1156-1166.

Hazzard, R. T., W. C. Spooner, and Blanpied, 1947, Notes on the stratigraphy of the formations that underlie the Smackover Limestone in south Arkansas, northeast Texas, and northern Louisiana: Shreveport Geological Society 1954 Reference Report, v. 2, p. 483-503.

Huh, S., J. S. Watkins, R. Kasande, J. C. Fiduk, S. Bryant, K. E. Silver, B. E. Bradshaw, F. Xue, and J. Xi, 1996, Regional structure and tectonics of the Texas shelf: Gulf Coast Association of Geological Societies Special Publication in conjunction with Transactions, v. 46, p. 39-51.

Jackson, M. P. A., and S. J. Seni, 1983, Geometry and evolution of salt structures in a marginal rift basin in the Gulf of Mexico, east Texas: Geology, v. 11, p. 131-135.

Mitra, S., 2002, Structural models of faulted detachment folds: AAPG Bulletin, v. 86, no. 9, p. 1673-1694.

Mount, V. S., J. Suppe, and S. C. Hook, 1990, A forward modeling strategy for balancing cross sections: AAPG Bulletin, v. 74, no. 5, p. 521-531

Peel, F.J., C.J. Travis, and J. R. Hossack, 1995, Genetic structural provinces and salt tectonics of the Cenozoic offshore U.S. Gulf of Mexico: a preliminary analysis, *in* M. P. A. Jackson, D. G. Roberts, and S. Snelson, eds., Salt tectonics: a global perspective: AAPG Memoir 65, p. 153-175

Rowan, M. G., B. D. Trudgill, and J. C. Fiduk, 2000, Deep-water, salt-cored foldbelts: Lessons from the Mississippi Fan and Perdido fold belts, northern Gulf of Mexico, *in* W. Mohriak and M. Talwani, eds., Atlantic rifts and continental margins: American Geophysical Union Geophysical Monograph, 115, p. 173-191.

Rowan, M. G., F. J. Peel, and B. C. Vendeville, 2004, Gravity-driven fold belts on passive margins, *in* K. R. McClay, ed., Thrust tectonics and hydrocarbon systems: AAPG Memoir 82, p. 157-182.

Salvador, A., 1987, Late Triassic-Jurassic paleogeography and origin of Gulf of Mexico basin: AAPG Bulletin, v. 71, no. 4, p. 419-451.

Spang, J. H., 1999, New models for the origin of shale/salt-cored anticlines in the Gulf of Mexico using a modified area-constant detachment fold model: Gulf Coast Association of Geological Societies Transaction, v. 49, p. 470-477.

Trudgill, B. D., J. C. Fiduk, M. G. Rowan, P. Weimer, P. E. Gale, B. E. Korn, R. L. Phair, W. T. Gafford, J. B. Dischinger, G. R. Roberts, and L. F. Henage, 1995, The geological evolution of petroleum potential of the deep water Perdido fold belt, Alaminos Canyon, northwestern deep Gulf of Mexico: Gulf Coast Association of Geological Societies Transaction, v. 45, p. 573-579.

Trudgill, B. D., M. G. Rowan, J. C. Fiduk, P. Weimer, P. E. Gale, B. E. Korn, R. L. Phair, W. T. Gafford, G. R. Roberts, and S. W. Dobbs, 1999, The Perdido fold belt, northwestern deep Gulf of Mexico: Part 1 – structural geometry, evolution, and regional implications: AAPG Bulletin, v. 83, no. 1, p. 88-113.

Watkins, J. S., B. E. Bradshaw, S. Huh, R. Li, and J. Zhang, 1996, Structure and distribution of growth faults in the northern Gulf of Mexico OCS: Gulf Coast Association of Geological Societies Special Publication in conjunction with Transactions, v. 46, p. 63-77.

Watkins, J. S., and R. T. Buffler, 1996, Gulf of Mexico deepwater frontier exploration potential: Gulf Coast Association of Geological Societies Special Publication in conjunction with Transactions, v. 46, p. 79-92.

Wiltschko, D. V., and W. M. Chapple, 1977, Flow of weak rocks in Appalachian Plateau folds: AAPG Bulletin, v. 61, no. 5, p. 653-670.

Winker, C. D., 1982, Cenozoic shelf margins, northwestern Gulf of Mexico: Gulf Coast Association of Geological Societies Transaction, v. 32, p. 427-448.

Winker, C. D., and R. T. Buffler, 1988, Paleogeographic evolution of early deep-water Gulf of Mexico and margins, Jurassic to Middle Cretaceous (Comanchean): AAPG Bulletin, v. 72, no. 3, p. 318-346.

Winker, C. D., 2004, Stratigraphy and structural timing of the Perdido fold belt, an emerging toe-of-slope play in the northwestern Deep-Water Gulf of Mexico (abs.): Gulf Coast Association of Geological Societies Transactions, v. 54, p. 765.

Worrall, D. M., and S. Snelson, 1989, Evolution of the northern Gulf of Mexico, with emphasis on Cenozoic growth faulting and the role of salt, *in* A. W. Bally and A. R. Palmer, eds., The geology of North America: An overview: Geological Society of America Decade of North American Geology, v. A, p. 97-138.

VITA

Name:	Troy Dale Waller, II
Address:	Hess Corporation, 500 Dallas Street, Houston, TX 77002
Email Address:	tjwaller@tamu.edu
Education:	M.S., Geology, Texas A&M University, 2007
	B.S., Geology with Engineering Option, Texas A&M University, 2005
Works:	Almeida, R., J. S. Chester, F. M. Chester, D. L. Kirschner, T. D. Waller, D. E. Moore, 2005, Mesoscale structure and lithology of the SAFOD Phase I and II core samples, Eos Trans. AGU, v. 86, no. 52, Fall Meet. Suppl., Abstract T21A-0454.
	Waller, T. D., II, J. H. Spang, 2007, New geometric model for detachment folds in the deepwater, western Gulf of Mexico, GSA Abstracts with Programs v. 39, no. 3, Abstract 120289.